Optimal Passive Sonar Signal Processing Using the Waveguide Invariant

by

Andrew Young

Department of Electrical and Computer Engineering
Duke University

Date: _____

Approved:

_____
Jeffrey Krolik, Supervisor

_____
Jeffrey Rogers

_____
Loren Nolte

_____
Steven Cummer

_____
William Joines

_____
Mathieu Kemp

Dissertation submitted in partial fulfillment of
the requirements for the degree of Doctor of Philosophy in the Department of
Electrical and Computer Engineering in the Graduate School
of Duke University

2019

ABSTRACT

Optimal Passive Sonar Signal Processing Using the Waveguide Invariant

by

Andrew Young

Department of Electrical and Computer Engineering
Duke University

Date: _____

Approved:

_____
Jeffrey Krolik, Supervisor

_____
Jeffrey Rogers

_____
Loren Nolte

_____
Steven Cummer

_____
William Joines

_____
Mathieu Kemp

An abstract of a dissertation submitted in partial fulfillment of the requirements for the degree of Doctor of Philosophy in the Department of Electrical and Computer Engineering in the Graduate School of Duke University

2019

Abstract

This dissertation presents optimal signal processing methods and performance analysis for passive, waveguide invariant (WI)-based acoustic source range estimation in shallow water marine environments. The WI, commonly denoted by β, characterizes the range- and frequency-varying channel fading pattern that can be observed in the time-frequency spectrum of hydrophone data. The structure of the fading pattern is governed by the physics of ducted acoustic propagation and can be exploited to estimate source range using a variety of methods; this work focuses on model-based, single-hydrophone techniques for both narrowband (tonal) as well as broadband sources.

Maximum likelihood (ML) estimators are presented for both β and source range for the case of tonal sources. Estimator performance is analyzed for various signal-to-noise ratios (SNRs) and numbers of tones processed in both Pekeris and complex environments using the KRAKEN normal mode program. Acoustic data from the SWellEx-96 experiment is analyzed, and source range is estimated with root-mean-square error (RMSE) under 3% of source range using knowledge of β for the local environment and 6% using an estimate β obtained from an area several kilometers away.

The Cramér-Rao lower bound (CRLB) on achievable variance of unbiased range and β estimates is derived for the case of a broadband source in an ideal waveguide and is seen to exhibit similar trends as the performance curves for the ML estimators

derived for tonal sources. Additionally, an example is provided showing how the framework for derivation of the bounds can be extended to a complex environment modeled after the SWellEx-96 experiment.

Receiver localization can be performed by combining the time-varying WI-based range estimates with knowledge of the source track, and this has a potentially significant application to autonomous underwater vehicle (AUV) navigation. To this end, three receiver localization methods are presented that use either the Doppler effect, WI-based range estimates, or both. Results from Monte Carlo simulations as well as from processing experimental data demonstrate the potential to localize AUVs with an error on the order of a few hundred meters under realistic assumptions regarding source and environmental parameters.

This dissertation is dedicated to the U.S. taxpayers who have funded my graduate research; it has been an honor to work on your behalf.

Contents

List of Figures

List of Abbreviations and Symbols

Notation

Unless otherwise noted, scalar quantities are denoted in this work by italics, as in x, while vector quantities are denoted using bold-faced symbols, as in $\mathbf{x}$. A particular index of a vector quantity is a scalar and is given in italics, as in x_n. All vectors are column vectors unless otherwise noted, for example $\mathbf{x} = [x_1\ x_2\ ...\ x_N]^T$, where $(\cdot)^T$ indicates the transpose operator. Matrices are generally represented by capital, bold-faced letters, as in $\hat{\mathbf{R}} = \frac{1}{N}\mathbf{x}\mathbf{x}^H$, where $(\cdot)^H$ indicates the Hermitian, or conjugate transpose.

The various symbols used throughout this text are defined upon first usage within each chapter and are generally consistent among chapters (e.g. ω for radial frequency or r for source range), though some variables used for indexing purposes are different (e.g. p indicates a particular propagating mode in Chapter 3 and a particular striation in Chapter 4). A listing of abbreviations used throughout the text is provided below, with each abbreviation being defined on first use.

Abbreviations

2D-DFT	2-Dimensional discrete Fourier transform
AIS	Automatic identification system
AUV	Autonomous underwater vehicle
CPA	Closest point of approach
CRLB	Cramér-Rao lower bound

CSAC	Chip-scale atomic clock
CTD	Conductivity, temperature, depth
DFT	Discrete Fourier transform
DVL	Doppler velocity logger
FFT	Fast Fourier transform
FIM	Fisher information matrix
FNN	Feed-forward neural network
GPS	Global positioning system
HLA	Horizontal line array
IMU	Inertial measurement unit
INS	Inertial navigation system
LBL	Long baseline
LS	Least squares
MC	Monte Carlo
MFP	Matched field processing
ML	Maximum likelihood
MSE	Mean-square error
MUSIC	Multiple signal classification
NLLS	Non-linear least squares
OWTT	One-way travel time
PRN	Pseudo-random noise
RMSE	Root-mean-square error
RF	Radio frequency
SBL	Short baseline
SNR	Signal-to-noise ratio
SOO	Source of opportunity

SSP	Sound speed profile
STFT	Short-time Fourier transform
SVM	Support vector machine
SWellEx-96	Shallow Water Experiment, 1996
TLA	Tilted line array
TWTT	Two-way travel time
USBL	Ultra-short baseline
VHF	Very high frequency
VLA	Vertical line array
WI	Waveguide invariant

Acknowledgements

I would like to thank my advisor, Dr. Jeffrey Krolik, as well as my supervisor at the Naval Research Laboratory, Dr. Jeffrey Rogers, for their guidance. I would also like to thank Dr. Andrew Harms and Dr. Granger Hickman for their many helpful technical discussions during the early and later stages of my graduate career, respectively. I would also like to acknowledge the invaluable support and friendship of many current and former lab members over the years, especially Dr. Jonathan Soli, who was a role model and mentor to several of us. Most importantly, I would like to thank my loving wife, Jenna, for her patient and unwaivering support during this journey.

Financial support for the work contained in this dissertation was provided by the Office of Naval Research (ONR).

1

Introduction

The oceanic waters of Earth are vast and cover the majority its surface, yet they remain largely under-explored relative to land due in no small part to the disparity in attenuation between electromagnetic and acoustic waves in that medium. Both RF signals, which are commonly used in terrestrial applications such as communications and navigation (e.g. GPS), and optical signals decay almost entirely within 1 km of propagation in the ocean, while acoustic signals have been experimentally transmitted and received at ranges of 18,000 km [1].

It is not surprising, then, that acoustics is the preferred modality for sensing in underwater environments, and a variety of inferences can be made about the environment using acoustics. For example, one can determine the presence, and number, of distant underwater objects or sources, as well as estimate various parameters about them such as speed or range. While relatively simple algorithms can often be satisfactorily employed to meet one's needs, it is often the case that significant performance increases can be obtained from incorporating knowledge about the environment, such as the speed of sound at various depths in the water column or layers of the bottom, into the processor. To this end, the approach taken in this disser-

tation is to let knowledge of the physics governing multipath acoustic propagation in shallow water environments drive the development of optimal, model-based signal processing algorithms for estimating parameters of interest.

The following example is provided to help convey the utility of physics-based signal processing methods without getting too involved in the specific details of their implementation: imagine that you are swimming through the ocean while listening carefully to the sounds you hear underwater. Amongst a diversity of sounds from biological sources, wind, waves, etc. you can also faintly hear the dull, rumbling sound of propellers and machinery from a distant cargo ship. You swim to the surface to look for the ship, but it is too far away to be heard, or even seen, from the surface. Without a good model for how sound propagates in the ocean, one might deduce from these observations merely that the distance to the ship is greater than visual range and less than the maximum range at which it could be heard underwater - in other words, somewhere between roughly 5 km and 18,000 km. However, the same acoustic signal provided as an input to an optimal signal processing algorithm that models multipath propagation may yield a range estimate that is accurate within tens of meters by exploiting a feature in the acoustic signal that would otherwise be discarded by an algorithm employing a simpler, free-space propagation model.

In this dissertation, amplitude fluctuations in the time-frequency spectra of received acoustic signals are used to estimate two parameters of interest: source range and the waveguide invariant (WI), which is commonly denoted as β. The WI is a scalar parameter that describes the structure of peaks and nulls in the channel fading pattern (referred to as striations) in terms of their trajectories through range and frequency. A thorough introduction to β is provided in Appendix A.1, but for now it is sufficient to note that the parameter can be used to estimate source range from hydrophone data.

While estimating range from the acoustic emissions of distant sources is interest-

ing in its own right, it is important from an engineering perspective to also consider applications that might benefit from such estimates. Doing so involves not only a characterization of the accuracy of the WI-based range estimates but also the development of algorithms that use the estimates for a particular purpose. To this end, the Cramér-Rao bounds for WI-based range estimation are derived and examined for a variety of realistic source and environmental parameters, and an algorithm is presented that can be used to augment autonomous underwater vehicle (AUV) navigation.

The remainder of this dissertation is organized as follows: first, an introduction to the challenges facing AUV navigation is provided in Section 1.1, followed by an overview of the author's vision for using WI-based signal processing algorithms to augment existing navigation methods. A variety of WI-based ranging methods for AUV localization are explored in greater detail in Chapter 2 and include a statistical characterization of results obtained using Monte Carlo (MC) methods. Next, the Cramér-Rao lower bounds (CRLBs) for range and β estimation from processing broadband acoustic data are presented in Chapter 3. Finally, maximum likelihood (ML) estimators for source range and β are presented in Chapter 4 for tonal sources along with simulated AUV localization results derived from experimental data. Conclusions and comments regarding future work are presented in Chapter 5. Appendix A.1 provides a more formal introduction and description of the waveguide invariant, β, which may be useful for readers who are unfamiliar with the topic, but it is not strictly required for understanding the work presented in the rest of the dissertation. Appendix A.2 provides an overview of automatic identification system (AIS) data, which is central to the proposed AUV localization methods presented in Chapters 2 and 4. Finally, Appendix A.3 provides a brief review of related passive ranging and localization work.

1.1 AUV navigation challenges

Undersea AUV navigation is a challenging problem with a variety of solutions tailored to specific mission parameters, system complexities, and budgets. It is largely an unsolved problem, unlike surface and aerial navigation for which GPS provides a low-cost, effective solution for most needs. While GPS is effective for use in locating AUVs at or near the ocean surface, and many AUVs are equipped with GPS antennas and receivers for this reason, the radio frequency GPS signals are rapidly attenuated as they propagate through the water column and cannot be effectively utilized by submerged vessels. Yet, AUV missions often require the vehicles to maintain a low position uncertainty while submerged for the data they collect to be useful, and this leads to frequent surfacing for GPS position updates [2]. However, surfacing is generally undesirable as it requires a significant expenditure of energy and also puts the AUVs at risk of both collision with surface vessels and detection by RF and optical methods.

Another impediment to AUV navigation is underwater currents, which can be difficult to predict and can exceed speeds of 1 m/s in many coastal areas, as shown in Figure 1.1. Even if an AUV were to simply descend in the water column for a few hours and then surface again, without having used propellers or other means of locomotion while submerged, it could emerge at the surface several miles from its initial position due to such currents. This necessitates the use of additional equipment to assist with localization while submerged, and the cost and complexity vary greatly depending on the application.

1.2 Conventional localization methods

At a high level, AUV navigation equipment and techniques can be separated into three main categories, as shown in Figure 1.2: inertial, acoustic transponders/modems,

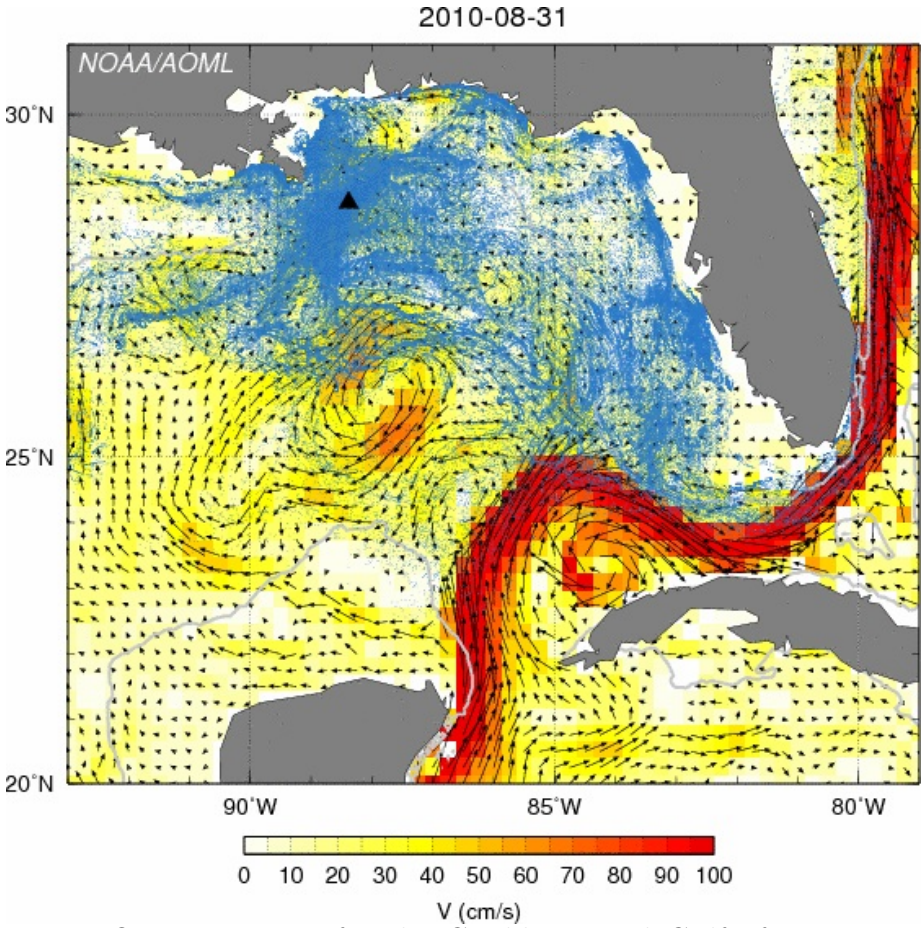

FIGURE 1.1: Ocean currents for the Caribbean and Gulf of Mexico, simulated using the Navy Coastal Ocean Model; dark red indicates currents approaching 1.25 m/s. Image credit: National Oceanic and Atmospheric Administration/Department of Commerce, https://www.aoml.noaa.gov/phod/dhos/lcs.php.

and geophysical. These categories will be briefly discussed and compared to the single-hydrophone, WI-based localization technique that is the focus of this dissertation.

1.2.1 Inertial methods

Inertial, or "dead reckoning," methods perform a time integration of the signals provided by equipment such as compasses, Doppler velocity loggers (DVLs), inertial measurement units (IMUs), and pressure sensors to estimate the change in position

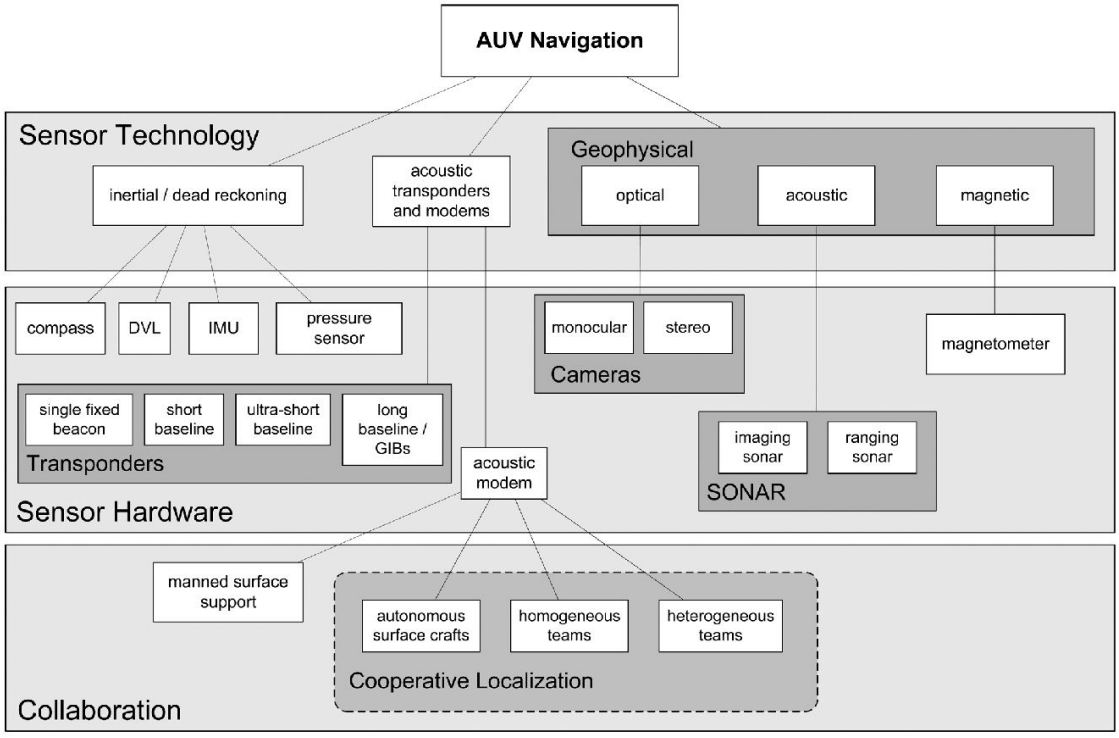

FIGURE 1.2: High-level overview of AUV navigation equipment and techniques. For brevity in this document, only IMUs, DVLs, and transponders are compared to the single-hydrophone, waveguide invariant-based technique. Reprinted with permission from Paull et al. [2]. Copyright 2014, IEEE.

since the last location update. DVLs exploit the Doppler effect measured from reflections of acoustically-transmitted signals off the ocean floor and can suffer degraded performance when the bottom is rapidly varying [2]. They estimate the speed of the AUV relative to the ground, and this can significantly mitigate the impact of drift due to unknown ocean currents. DVLs range in price from about $10,000 to over $100,000, which can make them prohibitively expensive for small, low-cost AUVs. Other drawbacks to DVLs include the requirement to remain within proximity of the ocean floor and the need for active transmission of acoustic signals.

1.2.2 Transponders and modems

Transponders generally fall into one of three categories based on the relative distance between the transponders and the AUV: short baseline (SBL), ultra-short baseline (USBL), and long baseline (LBL), as depicted in Figure 1.3. Transponders are very effective at localizing AUVs and can even achieve sub-meter accuracy [2]. Transponder-based localization involves what is referred to as a "time-of-flight" measurement in which the vehicle transmits a pulse that is repeated back by each transponder, and the distance to each transponder is then computed based on the time taken to receive the responses. In a recent development [3], a new type of one-way-travel-time USBL transponder has been used for AUV localization. The technique requires the AUV to be equipped with a chip-scale atomic clock (CSAC) for synchronization with a source that emits a periodic chirp waveform, enabling the AUV to remain in a passive (listen only) mode while still achieving good localization accuracy. Transponders generally work very well for AUV localization, but one of the main drawbacks to their use is the requirement for AUVs to remain within a limited range of the equipment. In an LBL setup, for instance, transponders are placed at known positions covering an area of operations, while SBL or USBL setups require a cooperative surface vessel to follow the AUV throughout its mission.

Acoustic modems are used to pass information between vessels by transmitted and receiving acoustic pressure signals, and the localization technique proposed in this dissertation requires AUVs to use this type of method to extract transmitted data from hydrophone recordings. The extracted data would be some form of re-packaged AIS data, which is initially transmitted via RF by surface vessels for collision avoidance purposes and contains information such as ship identification, heading, speed over ground, and GPS coordinates. The RF transmissions would be received by a surface buoy and relayed acoustically to a submerged AUV using an acoustic modem,

which could be performed periodically at low data rates. Like the CSAC method, this type of one-way communication is also passive from the perspective of the AUV. Using knowledge of the time-varying positions of transiting ships, combined with estimates of their range, the AUV position can be estimated in a similar manner to using transponders.

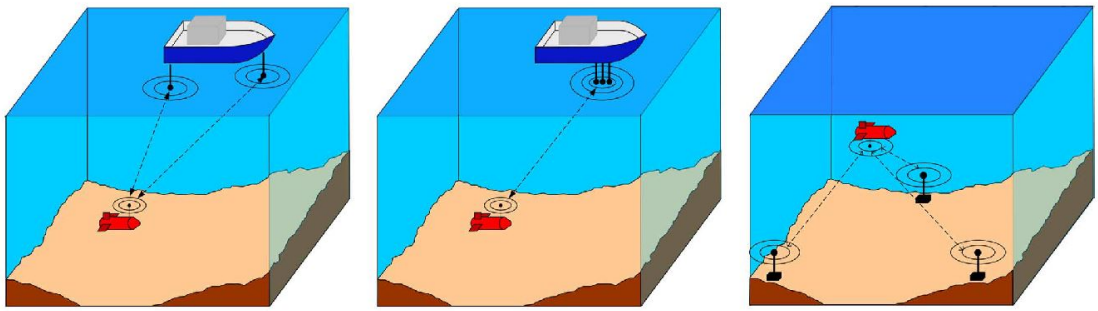

FIGURE 1.3: Various transponder setups: (a) SBL, (b) USBL, (c) LBL. Reprinted with permission from Paull et al. [2]. Copyright 2014, IEEE.

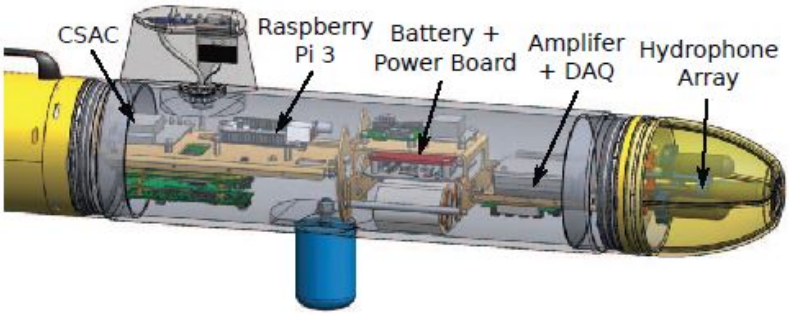

FIGURE 1.4: CAD model of the payload section of a low-cost Sandshark AUV, manufactured by Bluefin Robotics. The AUV is equipped with a CSAC for localization using one-way time-of-flight measurements in conjunction with an onboard, passive hydrophone array. Reprinted with permission via RightsLink from Rypkema et al. [3]. Copyright 2017, IEEE.

1.2.3 Geophysical navigation techniques

Geophysical techniques comprise optical, acoustic, and magnetic-based sensor modalities. Optical sensors include both monocular and stereo cameras, which can be used

for navigation when the AUV is within proximity of salient features in the seabed [2]. Active sonar includes imaging and ranging applications and can be used to estimate position relative to environmental features or to other AUVs, as shown in Figure 1.5, and it has also been noted that magnetic sensors can, in principle, be used for AUV navigation by utilizing prior knowledge of spatially-varying magnetic fields in the ocean. While these navigation methods can be advantageous in specific contexts, the requirement of precise, prior environmental knowledge can significantly limit the potential operating regions, as with acoustic transponders. By contrast, the WI-based navigation methods could be employed much more broadly through vast areas of the ocean in proximity to shipping lanes.

1.3 Using sources of opportunity for localization

The approach proposed in this dissertation uses a single hydrophone to listen to the acoustic emissions of a transiting source of opportunity (SOO), such as a cargo ship. The data is then used to estimate the channel fading pattern, leverage the physics of the waveguide invariant to estimate source range, and ultimately combine the range estimates with the AIS data to determine the location of the AUV. This technique falls primarily into the category of passive sonar but also requires low data rate acoustic communications from a cooperative vessel or buoy to convey the AIS data to the submerged AUV, such as was demonstrated experimentally in Petroccia et al. [5] and Ferreira et al. [6].

The proposed technique offers many benefits over the other localization methods covered in the previous sections. First, it is the lowest-cost technique, requiring only a single hydrophone to be equipped by the AUV at a cost of hundreds of dollars. In contrast, DVLs and high-grade IMUs can range from about \$10k to over \$1M, depending on performance. Second, it is entirely passive, enabling the AUV to execute its mission with minimal environmental acoustic footprint. DVLs and transponders,

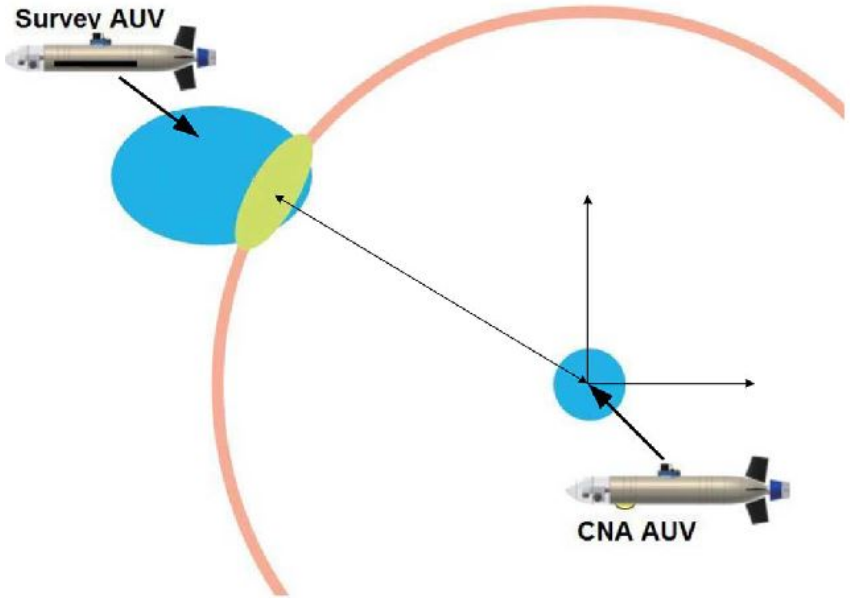

FIGURE 1.5: Depiction of ranging sonar used for cooperative AUV localization. A communication/navigation aid (CNA) AUV estimates the range to a survey AUV equipped with low-grade, low-cost navigation equipment. After estimating range, the CNA AUV transmits the estimate to the survey AUV using an acoustic modem. The blue ellipses represent the position uncertainty of each AUV, derived solely from their own measurements, while the lime green ellipse represents the updated uncertainty of the survey AUV after receiving and incorporating the range and position estimates transmitted by the CNA AUV. Reprinted with permission from Rui and Chitre [4]. Copyright 2010, IEEE.

on the other hand, require the AUV to transmit acoustic signals that can potentially be exploited by an adversary. Third, it does not require mission-specific equipment to be deployed in advance of AUV operations, as with most transponder-based techniques, though it would require some form of generalized AIS-relaying mechanism to be in place. Finally, it uses SOOs for localization instead of transponders, and the ship positions can be transmitted to many AUVs simultaneously throughout the ocean, with broadcast ranges from individual relaying nodes of approximately 7 km, as in [6]. An overview of the concept of operations for the proposed waveguide invariant-based localization technique for low-cost AUVs is now provided, with

reasonable assumptions made regarding a variety of relevant parameters.

1.3.1 Overview of WI-based localization

Consider an AUV that is operating in the vicinity of a coastal shipping lane. Its mission could involve a wide range of tasks such as monitoring marine life, characterizing surface vessel traffic, or recording data on ocean currents and temperatures. The AUV is operating at a depth that prevents it from receiving GPS signals, and it relies solely on a low-cost, low-grade IMU and a single hydrophone for navigation. Within an hour of its initial deployment, the AUV position uncertainty approaches one nautical mile, and it is desired to keep the uncertainty under that limit. Ordinarily, the AUV would come to the surface at this time, obtain a GPS-based position update, and then continue on its planned course with its position uncertainty being reset to just a few meters. However, this particular AUV is employing the WI-based localization method and can maintain an acceptable position uncertainty while remaining at its desired operating depth.

A cargo ship is approaching at a range of 5 km and a speed of 20 knots, though the precise range and speed are currently unknown to the AUV. The AUV processes a spectrogram of acoustic data captured by its on-board hydrophone, and a fading pattern (series of peaks and nulls) is observed. The time-varying range to the ship is continuously estimated using the technique described in Chapter 4 by processing the observed fading pattern. During this time, ship position information is received at one- to five-minute intervals from a distant AIS-relaying buoy, and the AUV estimates its location with an accuracy of a few hundred meters – a nearly ten-fold improvement over using the IMU alone. The IMU is re-calibrated using the WI-based position estimate, and the AUV continues with its mission as the ship passes by without ever needing to stop or come to the surface. Once the SOO is out of range, the AUV position uncertainty begins to increases until another ship approaches.

This process can be repeated many times throughout the course of the mission, eliminating the need for the AUV to periodically come to the surface for position updates. In principle, the AUV can remain submerged indefinitely in this manner while maintaining a bounded position uncertainty. The position error depends not only on the accuracy of the WI-based ranging method and of the IMU equipment but also on the shipping density in the area. For an AUV equipped with a low-grade IMU operating near a typical coastal shipping lane with a traffic density of one or two ships per hour [7], this technique could potentially allow an AUV to remain submerged with an upper bound on position uncertainty of hundreds of meters.

1.3.2 Technical overview of proposed localization technique

As mentioned in the previous section, the proposed localization technique makes extensive use of the time-frequency spectrum of the received acoustic signal. In this section, a more detailed view of the signal processing is provided, beginning with a brief definition of some commonly-used terminology.

Throughout this paper, the term "$I(r, \omega)$ surface" refers to the squared magnitude of a spectrogram of the pressure signal received by a single hydrophone due to a tonal source at range r, where the time axis of the spectrogram has been mapped to range. The mapping of time to range is done with the aid of AIS data, which includes the time-varying source GPS coordinates. The isolines that appear across $I(r, \omega)$ are central to the proposed localization technique and are referred to as "striations." The slopes of these striations, $\frac{\delta\omega}{\delta r}$, are governed by the waveguide invariant through equation (A.6). The reader is referred to Appendix A.1 for a more thorough treatment of the waveguide invariant, although it is not strictly necessary for understanding the signal processing methods presented later in this work.

If the value of β is known for an environment, then equation A.5 can be used to estimate source range by exploiting striations in the $I(r, \omega)$ surface. Once the time-

varying source range is estimated, the source location can be estimated by using a nonlinear least squares (NLLS)-based technique. This is equivalent to finding the point (latitude, longitude) that minimizes the sum of squared distances to a series of circles centered at the reported GPS positions along the ship track and having radii equal to the estimated time-varying range to the ship. The localization technique is an iterative process in which the position estimate is used to calculate source range rate, which is used to estimate time-varying source range, which is used to determine the location of the AUV. The range estimation and proposed localization techniques are described in detail in Chapter 4.

1.4 Potential benefits of WI-based ranging

Optimal WI-based ranging methods could greatly benefit the low-cost AUV community, especially research institutions, where sub-$100k AUVs that rely on lower grades of navigation equipment are commonly used for a variety of missions. WI-based navigation methods could enable such AUVs to spend more time at desired depths within the water column, without being required to frequently expend energy and risk collisions with surface vessels to obtain GPS updates. Depending on the localization accuracy that is required, surface trips for GPS could potentially be eliminated, enabling AUVs to operate deep within the water column as long as batteries allow.

Additionally, users who are interested in the ability to remain submerged for extended periods while traveling great distances might find the benefit of a bounded localization error especially appealing. While such users would likely be employing higher grades of navigation equipment, position errors do still accumulate with time submerged and distance traveled. Thus, even the most advanced AUVs could potentially benefit, at least to a small degree, from incorporating WI-based ranging methods into their navigation systems.

2

WI-based ranging and localization methods

This chapter provides an overview of WI-based range estimation using SOOs for AUV navigation. The math presented in this chapter is relatively minimal compared to the more in-depth analyses provided in Chapters 3 and 4 and is not required for understanding the material presented in later chapters. The content of this chapter is largely drawn from the 2017 work of Young, Soli, and Hickman, which was published in the *IEEE Journal of Oceanic Engineering* [8] and has been adapted and re-formatted for this dissertation.

2.1 Introduction

Navigation is a challenging and expensive capability to provide for AUVs. Equipment ranging from DVLs, sonars, cameras, IMUs, and acoustic beacons are commonly employed for position estimation, with the specific suite of equipment used being heavily dependent on desired system cost and performance [2]. One of the fundamental problems to overcome is the rapidly increasing position uncertainty of the inertial navigation system (INS), which typically grows quadratically as a function of time submerged, as depicted in Figure 2.1. Growth of ranging errors is

unbounded and can reach several kilometers after just one hour, even with relatively high-performance inertial equipment, and this can result in the AUV being required to frequently surface and use a GPS antenna to update its position.

A low-cost solution is now presented that overcomes the limitations of inertial systems by providing a position estimate that does not degrade with time, thus decreasing the frequency of surface trips or possibly eliminating them altogether. Using such a solution, a low-cost AUV could remain submerged indefinitely while maintaining an acceptable position error. Hydrophone-based solutions are preferred due to their comparatively low cost, size, weight, and power consumption and are now examined in greater detail.

In the related problem of target motion analysis (TMA), a source track is estimated with respect to a receiver position, and various bearings-only [9] and range-only [10] techniques have been developed, although such methods typically require an array of hydrophones, prior knowledge of the source spectrum, or require that the source track contains the closest point of approach (CPA). In the AUV localization problem, both the receiver and source positions are unknown. However, if the AUV is receiving AIS data from the SOO, then the source position can be assumed known, and both bearings-only and range-only techniques can be used to estimate the location of the receiver.

AIS data contains a variety of time-stamped information about an SOO, such as its unique identifier, speed over ground (SOG), heading, and GPS coordinates, transmitted every few seconds [11]. This information is typically broadcast via radio frequency (RF) antennas on the SOO for collision avoidance purposes. Cargo ships are required to broadcast AIS data while in transit, and this information can, indirectly, be recovered and exploited by an AUV while submerged. Although the RF broadcasts would not be receivable, previously received AIS data can be projected forward in time due to the predictability of the tracks of large ships, especially while

transiting specified shipping lanes. This leaves only a requirement for periodic, low data rate AIS updates to be received by the AUV, possibly via acoustic communications.

The innovation presented in this chapter is a passive sonar technique by which a submerged AUV can estimate its position using acoustic data from a single hydrophone, combined with knowledge of the track of a transiting SOO. The technique uses a combination of range and bearing estimation methods and does not require prior knowledge of the source spectrum, nor does it require the receiver to maneuver or the source to travel through the CPA. Source range is estimated through spectral analysis of the channel fading pattern, while the source-receiver bearing is estimated through a least squares technique leveraging the Doppler effect. This hybrid technique is herein referred to as "waveguide invariant/Doppler-based localization" (WI-DBL), and it has a position estimation error that does not increase as a function of time submerged, unlike the inertial systems depicted in Figure 2.1, but instead decreases with increased SOO acoustic observation time.

Section 2.2 introduces the signal model, describes the proposed DBL and WI-based range estimation techniques, and ends with a weighted combination of the two methods, which is the WI-DBL technique. Section 2.3 covers the Noise-09 experimental data, the simulation setup, and a discussion of the simulation results. Section 2.4 contains a summary of the key findings regarding the WI-DBL technique as well as brief comments regarding future work.

2.2 WI-DBL method

2.2.1 Signal model

The pressure signal, $s(t)$, received by a single hydrophone from a single SOO is assumed to be a sum of additive Gaussian noise, $n_{\mathrm{p}}(t)$, with K sinusoids characterized by the following unknown parameters: amplitudes $\{a_k\}_{k=1:K}$, phases $\{\phi_k\}_{k=1:K}$, and

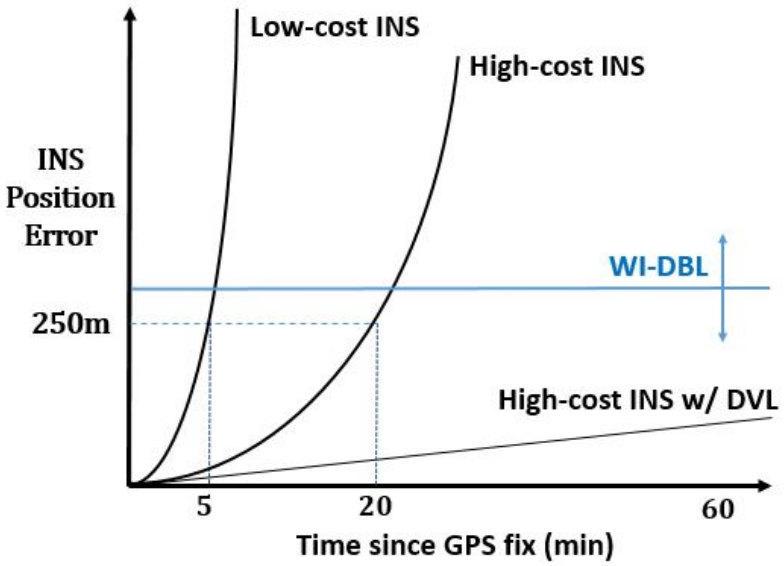

FIGURE 2.1: Notional comparison of typical position errors for low- and high-cost standalone inertial systems, as well as a high-cost INS with external DVL inputs, versus the single-hydrophone WI-DBL technique.

radial frequencies $\{\omega_k\}_{k=1:K}$. The frequencies are multiplied by an unknown, time-varying Doppler factor, $\alpha(t)$, leading to the following equation for the received signal:

$$s(t) = \sum_{k=1}^{K} a_k e^{j(\alpha(t)\omega_k t + \phi_k)} + n_{\mathrm{p}}(t) \tag{2.1}$$

For simplicity, channel fading is ignored for the DBL processing presented in this chapter. However, channel fading could be incorporated through weights applied in the LS algorithm, presented in the following subsection, to improve performance.

The time-varying Doppler factor is determined by the ratio of the source-receiver range rate to the sound speed, c, and is given as follows:

$$\alpha(t) = 1 + \frac{v_{\mathrm{s}}(t)\cos\theta(t)}{c} \tag{2.2}$$

where $\theta(t)$ is the time-varying source-receiver bearing and $v_{\mathrm{s}}(t)$ is the SOG obtained

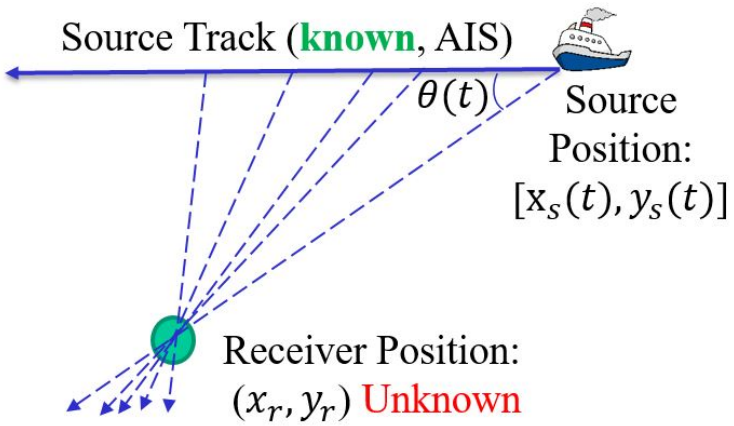

FIGURE 2.2: Geometry under consideration in DBL processing. The time-varying bearing, $\theta(t)$, to a transiting source of opportunity is estimated by exploiting the Doppler effect, and the best-fit receiver position is obtained through linear least squares processing of the projected (dashed) bearing lines.

from the AIS data. The time-varying apparent frequency of the kth tonal component measured at the receiver, $\omega_k(t)$, is modeled as the sum of the true Doppler-shifted source frequency and additive noise:

$$\omega_k(t) = \alpha(t)\omega_k + n(t) \tag{2.3}$$

where $n(t)$ encapsulates all sources of error associated with estimating the true source frequency, including the noisy pressure component, $n_{\mathrm{p}}(t)$. The noise, $n(t)$, is assumed to be Gaussian with zero mean and unknown variance σ_{n}^2:

$$n(t) \sim \mathcal{N}(0, \sigma_{\mathrm{n}}^2) \tag{2.4}$$

2.2.2 Doppler-based localization

The geometry under consideration is depicted in Figure 2.2, in which an SOO travels through a region of the ocean within proximity of a hydrophone-equipped AUV. For simplicity, the AUV is assumed to be stationary throughout this chapter. The source-receiver bearing changes as the source moves, resulting in a time-varying Doppler factor in accordance with (2.2).

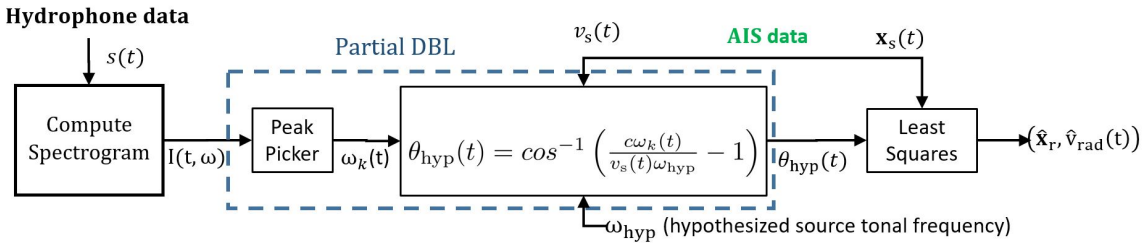

FIGURE 2.3: Block diagram showing the DBL algorithm.

Although the true value of $\alpha(t)$ is not known by the processor, the upper and lower limits of the Doppler factor can be computed by considering the two extremes of $\theta = 0$ and $\theta = \pm\pi$. This effectively bounds α between the following values: $\alpha_{\text{min}} = 1 - \frac{v_s}{c}$ and $\alpha_{\text{max}} = 1 + \frac{v_s}{c}$.

The following steps are repeated for each of the K tonal components in the source signal and are depicted in the block diagram shown in Figure 2.3. First, the apparent frequency, $\omega_k(t)$, of the tonal is estimated by searching for peaks in the time-frequency spectrum of the received acoustic signal. Next, a hypothesized source frequency, ω_{hyp}, is computed by solving (2.3) for ω_k; this is done by substituting a hypothesized Doppler factor, α_{hyp}, in place of the true Doppler factor, $\alpha(t)$. This step is repeated for each hypothesized Doppler factor between α_{min} and α_{max}.

Next, a hypothesized source-receiver bearing, $\theta_{\text{hyp}}(t)$, is computed by plugging (2.3) into (2.2) and solving for θ:

$$\theta_{\text{hyp}}(t) = cos^{-1}\left(\frac{c\omega_k(t)}{v_s(t)\omega_{\text{hyp}}} - 1\right) \tag{2.5}$$

Finally, a series of lines are projected from the known positions along the source track in the hypothesized time-varying direction of the receiver, as depicted in Figure 2.2. For simplicity, only the left-hand portion of the projected lines are drawn, as the other lines are mirrored across the source track. The resulting left/right ambiguity is assumed to be resolvable through one of various conditions being met, such as

having a nonlinear source track or simultaneously analyzing the acoustic signal from multiple sources, assuming their tonals are separable in frequency. For simplicity, the following steps refer only to a single set of either left- or right-hand projected lines and would be repeated for the other set.

The receiver position, $\hat{\mathbf{x}}_{\mathrm{r}} = [\hat{x}_{\mathrm{r}}, \hat{y}_{\mathrm{r}}]^T$, is estimated by finding the LS solution to the over-determined system of equations governing the projected lines:

$$\{y_s(t_n) - m_n x_s(t_n) = b_n\}_{n=1:N} \tag{2.6}$$

where $y_s(t_n)$ and $x_s(t_n)$ refer to the x- and y-coordinates of the SOO on an arbitrary Cartesian plane, N is the number of lines projected, m_n is the slope of the nth projected line, and b_n is the y-intercept of the nth projected line. Equation (2.6) is solved by converting to the form of $\mathbf{Ax} = \mathbf{b}$. The vector $\mathbf{b}$ contains the b_n values while the matrix $\mathbf{A}$ contains the slopes of the projected lines in its first column and a vector of ones in its second column, as follows:

$$\mathbf{A} = \begin{bmatrix} -m_1 & 1 \\ \vdots & \vdots \\ -m_N & 1 \end{bmatrix} \tag{2.7}$$

If the coordinate system is chosen such that the SOO track falls along the x-axis, then $m_n = \tan\theta_{\mathrm{hyp}}(t_n)$, otherwise an adjustment must be made. The LS solution,

$$\hat{\mathbf{x}}_{\mathrm{r}} = (\mathbf{A}^T\mathbf{A})^{-1}\mathbf{A}^T\mathbf{b} \tag{2.8}$$

yields an estimate of the receiver position.

The estimated time-varying source bearing, $\hat{\theta}(t)$, is the $\theta_{\mathrm{hyp}}(t)$ corresponding to the LS position estimate, $\hat{\mathbf{x}}_{\mathrm{r}}$, and is used to provide a source radial velocity estimate, $\hat{v}_{\mathrm{rad}}(t)$, to the WI-based ranging algorithm:

$$\hat{v}_{\mathrm{rad}}(t) = v_{\mathrm{s}}(t)\cos\hat{\theta}(t) \tag{2.9}$$

where $v_{\mathrm{s}}(t)$ is the AIS-provided SOG.

2.2.3 WI-based range estimation

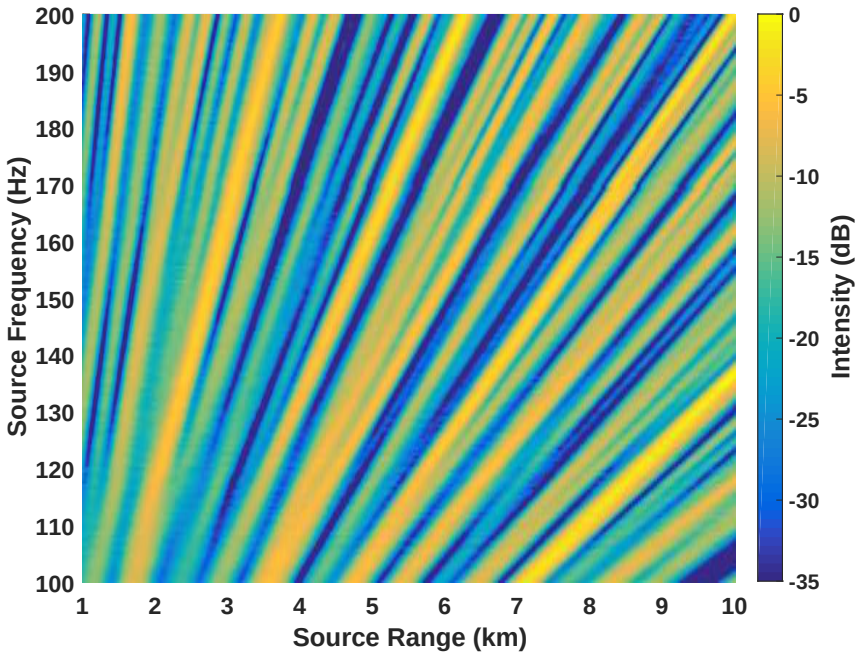

FIGURE 2.4: Typical shallow water striation pattern corresponding to $\beta = 1$

The waveguide invariant, frequently denoted in the literature as β, is a scalar parameter that characterizes the frequency- and range-varying dispersion of acoustic waves in an ocean waveguide. The parameter was first described in [12], where it was presented in the context of striations, or lines of constant intensity, in the channel fading pattern. A clear example of striations is presented in Figure 2.4. The visible striations arise from interference between groups of propagating acoustic modes. This fading pattern, visualized in terms of acoustic intensity as a function of source frequency and range, is referred to as an $I(r, \omega)$ surface. The $I(r, \omega)$ surface shown in Figure 2.4 is a special case of the canonical shallow water WI parameter, $\beta = 1$. The scalar representation of β is a good approximation to shallow water environments, where the acoustic pressure field is typically dominated by higher-order modes that interact with both the surface and the bottom [13].

Multiple techniques have been proposed for estimating β from a broadband $I(r, \omega)$ surface obtained from a single hydrophone. However, SOOs tend to have acoustic emissions spectra that are dominated by narrowband tonals [14]. Motivated by this observation, Harms et al. [15] recently developed a technique to estimate the ML value of β from an $I(r, \omega)$ surface obtained from a single hydrophone measuring the acoustic emissions of a tonal source. Their technique searches over a series of candidate β values, projects striations across the $I(r, \omega)$ surface corresponding to each hypothesized value, β_{hyp}, and selects the β_{hyp} that yields the lowest striation intensity matching error. The projected striations obey the following equation:

$$\frac{\omega}{\omega_0} = \left(\frac{r}{r_0}\right)^{\beta_{\text{hyp}}} \tag{2.10}$$

where (r_0, ω_0) is an initial point along a striation, and (r, ω) is another point along the same striation.

For a given $I(r, \omega)$ surface derived from acoustic measurements of tonal sources corrupted by additive complex Gaussian noise, the minimum variance estimate of β is the following:

$$\hat{\beta} = \arg\min_{\beta_{\text{hyp}}} \frac{1}{KN} \sum_{k=1}^{K} \sum_{n=1}^{N} \left(\hat{I}(n; \beta_{\text{hyp}}) - y_k(n)\right)^2 \tag{2.11}$$

where K is the number of tones analyzed, N is the number of striations projected across the $I(r, \omega)$ surface, $\hat{I}(n; \beta_{\text{hyp}})$ is the ML estimate of noise-free intensity along the nth projected striation parameterized by β_{hyp}, and $y_k(n)$ is the measured intensity of the kth tonal component along the nth striation [15].

Given an estimate of β for an acoustic channel, the range to an SOO can be estimated through a similar spectral analysis technique. The main difference is that a series of candidate source ranges are hypothesized, rather than a series of candidate β values. For each r_{hyp}, the time axis of the spectrogram of the received signal is

mapped to a source range, $r(t)$, by leveraging the source radial velocity estimate, $\hat{v}_{\text{rad}}(t)$, provided by the DBL algorithm:

$$r(t) = r_{\text{hyp}} + \int_{t_0}^{t} \hat{v}_{\text{rad}}(\tau) d\tau \tag{2.12}$$

The process is depicted in the first block of the WI-based ranging portion of the diagram in Figure 2.5, and the output is a hypothesized $I(r, \omega)$ surface. Striations are then projected in accordance with (2.10), and the estimated source range, $\hat{r}(t)$, is chosen in the same manner as $\hat{\beta}$ in (2.11).

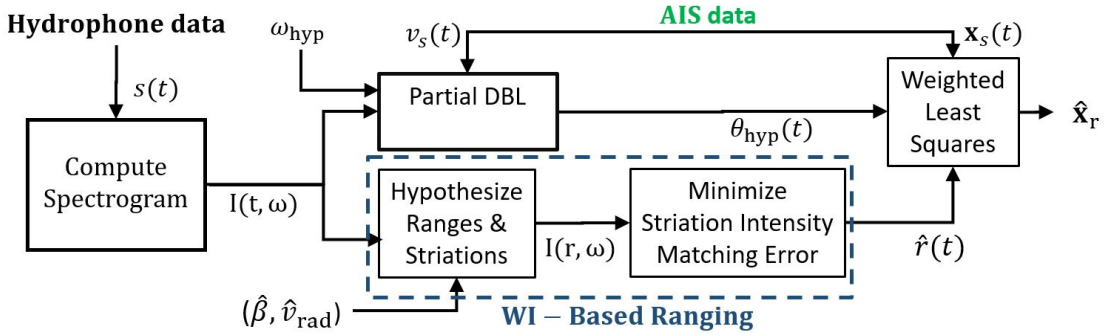

FIGURE 2.5: Block diagram showing the major components in the WI-DBL algorithm, as well as relevant intermediate and final outputs.

The estimated range is modeled as the sum of the true source range, $r(t)$, and an error term, $\epsilon(t)$. The $\epsilon(t)$ term accounts for mismatch between the estimated waveguide invariant parameter for the channel, $\hat{\beta}$, and the true time-varying value, $\beta(t)$. This parameter estimation error, $\Delta\beta(t) \triangleq \beta(t) - \hat{\beta}$, gives rise to the range estimation error $\epsilon(t)$ in accordance with (2.10) for small values of $\Delta\beta(t)$, which is approximated by the following:

$$\epsilon(t) \triangleq r(t) - \hat{r}(t) \approx r(t) \left[1 - \left(\frac{\omega_{\text{H}}}{\omega_{\text{L}}} \right)^{\Delta\beta(t)} \right] \tag{2.13}$$

where ω_{H} and ω_{L} are the processed tonal components with the highest and lowest radial frequencies, respectively. The approximation in (2.13) appears to be valid only for small changes in β near $\beta = 1$, and the relationship between errors in β and errors in range is planned to be investigated more thoroughly in future work. Accordingly, (2.13) should be viewed as a mechanism for generating random range errors, and the reader is cautioned against applying it outside the specific context of this chapter.

Fluctuations in $\beta(t)$ are typically small for SOO tracks in shallow water with slowly-varying bathymetry, and ranges of roughly +/-0.2 were observed by Verlinden et al. [16] for various source tracks from the Noise-09 experiment, which is described in Section 2.3.1. The parameter $\Delta\beta(t)$ is assumed to be normally-distributed with mean μ_β and variance σ_β^2:

$$\Delta\beta(t) \sim \mathcal{N}\left(\mu_\beta, \sigma_\beta^2\right) \tag{2.14}$$

2.2.4 WI-DBL: combining range and bearing estimates

For each hypothesized source frequency, the estimated source range, $\hat{r}(t)$, is combined with hypothesized bearing, $\theta_{\mathrm{hyp}}(t)$, to produce a cluster of point estimates. The variance of the estimates is computed, and the estimate of receiver position, obtained from processing a single tonal, is the center of mass for the minimum variance cluster. The WI-DBL estimate of receiver position is the weighted average of each of the K position estimates, where the weights, w_k, are inversely proportional to the variance of the kth cluster:

$$\hat{\mathbf{x}}_{\mathrm{r}} = \frac{\sum_{k=1}^{K} w_k \mathbf{x}_k}{\sum_{k=1}^{K} w_k} \tag{2.15}$$

Doppler-bearing position estimators are known to suffer from bias issues in noisy environments [17], and the WI-DBL estimator provides reduced bias and variance compared to the DBL estimator, as seen in the following section.

2.3 Simulation and experimental results

A simulation was conducted using data from the Noise-09 experiment to determine realistic values for the signal and environmental parameters. These parameters include the following: the number and frequencies of source tonals, ω_k; the variance, σ_{n}^2, of the frequency estimation noise from (2.4); the mean and variance of the waveguide invariant parameter estimation error, $\Delta\beta(t)$, from (2.14). 300 Monte Carlo trials were conducted comparing the performance of the DBL and WI-DBL techniques, and the results are discussed in Section 2.3.2.

2.3.1 Noise-09 experiment

The Noise-09 experiment took place in shallow water approximately 20 km off the coast of San Diego, California, and represents the acoustic environment of a typical shallow water shipping lane. The experiment geometry is shown in Figure 2.6. The "+" markers indicate the locations of four vertical line arrays, while the arrow indicates the track and heading of a transiting cargo ship.

Data from a single hydrophone on vertical line array (VLA) #2 was processed to obtain the spectrogram shown in Figure 2.6. Six of the tonals within the range of 62 to 100 Hz had a signal-to-noise ratio (SNR) greater than 15 dB. The tonals dominate the frequency spectrum and are caused by fundamental and harmonic oscillations of machinery such as propellers, propulsion engines, and generators [14].

A peak finder with a 1 Hz search window was used to estimate the time-varying apparent frequency, $\omega_k(t)$, of each tone. The output for the 62 Hz source tone, which represents $\omega_1(t)$ for this data set, is shown in Figure 2.6. The standard deviation of the noise component was 0.11 Hz, which was estimated from the first half of the source track when the source range rate was nearly constant. The experimentally derived parameters of interest, K, $\{\omega_k\}_{k=1:K}$, and σ_{n}, were then applied to the simulation.

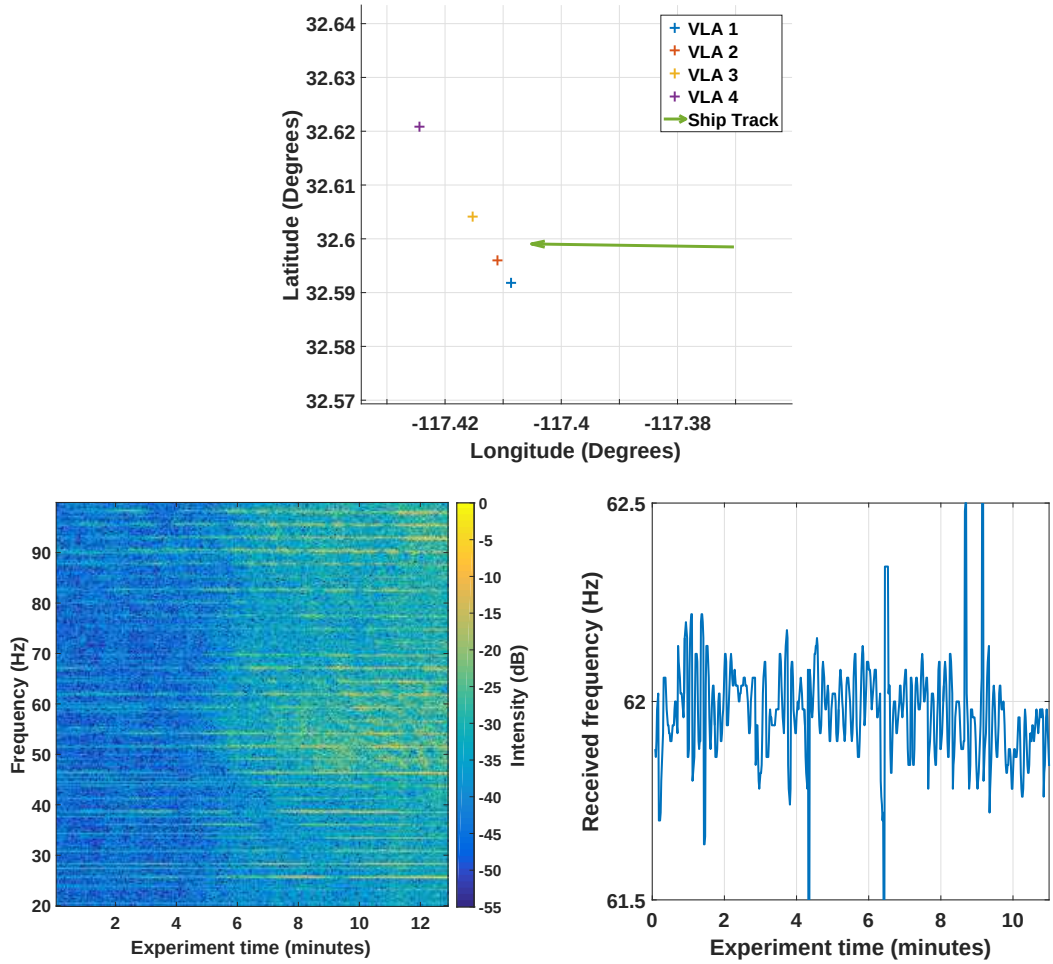

FIGURE 2.6: (Top) Geometry of the Noise '09 experiment and data set. (Left) Spectrogram of acoustic data processed. (Right) Plot of measured time-varying, apparent received frequency, using DBL processing. The data shown correspond to the 62 Hz tonal component of the cargo ship acoustic emissions.

2.3.2 Simulation

Simulations were performed as a proof of concept for the WI-DBL technique. The simulation geometry is shown in Figure 2.7 and is plotted in Cartesian coordinates with the x-axis aligned with the SOO track and the origin at the beginning of the track. The SOO travels a 5 km track with a constant westward heading and a velocity of 12 m/s. The time-varying output of the peak search processing block is modeled

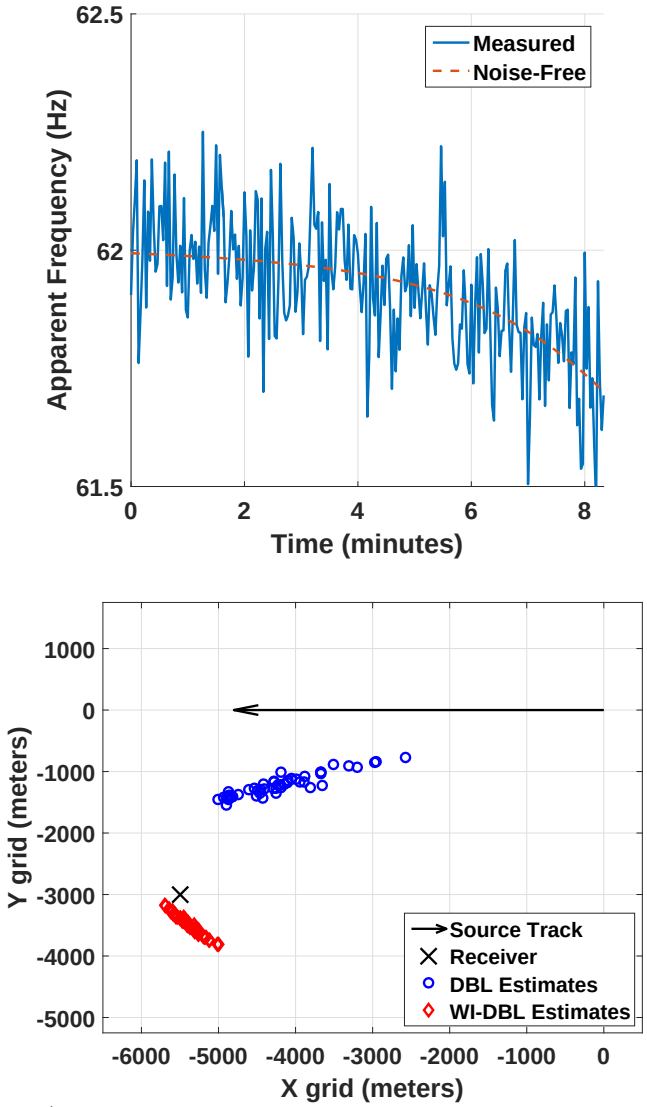

FIGURE 2.7: (Left) Simulation geometry and position estimates from 100 Monte Carlo runs for both DBL and WI-DBL processors. (Right) Plot of one realization of the simulated apparent received frequency, which is the output of the peak search block in the DBL processor. Data shown correspond to the 62 Hz tonal component of the simulated acoustic source emissions.

as the sum of the true Doppler-shifted apparent tonal frequency and additive noise, as previously shown in (2.3). The standard deviation of the noise measured from the experimental data was 0.11 Hz, and six tones evenly spaced between 62 and 100 Hz were simulated. The apparent frequency of the 62 Hz tone, $\omega_1(t)$, is plotted in Figure 2.7, along with the noise-free apparent tonal frequency that is indicated by the dashed line. A comparison of the right-most plots in Figures 2.6 and 2.7 indicates a good match between the simulated noise and the experimental Noise-09 data.

The error in waveguide invariant estimation, $\Delta\beta(t)$, from (2.14) was chosen to have a mean of 0.15 and standard deviation of 0.05. The mean value of $\Delta\beta(t)$ reflects a difference in the large-scale environment between the region in which β was previously estimated and the region transited by the SOO. The value $\mu_\beta = 0.15$ could be plausible if β were estimated from a region several kilometers away from the SOO track. The value of the standard deviation, $\sigma_\beta(t)$, was chosen to reflect a moderately-fluctuating bathymetry comparable to what might be expected in a typical shallow water shipping lane.

The position estimates produced by the DBL estimator are shown in Figure 2.7 for 25 Monte Carlo trials, and the statistics of the estimator were obtained using 300 trials. The DBL estimator, operating without any input from the WI-based range estimator, produced position estimates with a bias of 1200 m and standard deviation of 350 m. The output of the WI-DBL estimator is shown in Figure 2.7 for 25 Monte Carlo experimental trials. In contrast, the WI-DBL technique produced much better position estimates with a greatly improved bias of only 400 m and standard deviation of 125 m.

Overall, the simulation results are favorable for the WI-DBL estimator. By including β in the position estimation process, the standard deviation and bias were each reduced by more than a factor of two. The DBL position standard deviation of 350 m is comparable to the uncertainty corresponding to a low-grade INS after

several minutes, or from a high-grade INS after approximately 20 minutes, as depicted in Figure 2.1. In contrast, the WI-DBL standard deviation of 125 m is on the order of performance that could be expected from a higher-grade INS, possibly with external inputs from equipment such as a low-grade DVL, after a period of 30 to 60 minutes.

2.4 Conclusion

This chapter presented a position estimation technique that leverages both the waveguide invariant and the Doppler effect. The method is intended for AUV navigation and is tailored for exploiting acoustic SOOs that broadcast AIS data. The technique uses acoustic data from a single hydrophone and does not require prior knowledge of source tonal frequencies. The results from the simulations, which were based on parameters derived from the Noise-09 experiment and used imperfect knowledge of β, have promising implications for AUV localization in shallow water environments using WI-based methods. Future work includes a more rigorous validation of the WI-DBL processor using hydrophone data from AUVs; positive results from shallow water environments could pave the way for extensions to deep water environments.

3

Performance bounds for WI-based estimators

This chapter presents a derivation and analysis of the Cramér-Rao bounds for single-hydrophone, passive ranging using broadband sources in shallow water environments. The results for an ideal waveguide are compared to those for a complex shallow water environment characterized by a multiple layer bottom profile and a downward-refracting sound speed profile.

3.1 Introduction

Much work has been done over the past several decades on performance bounds for passive sonar source range estimation. The CRLB, which is the minimum achievable variance for an unbiased estimator, was derived in the 1970s for array processing techniques that exploited wavefront curvature across a horizontal array [18, 19, 20] and in the 1980s for matched field processing (MFP) methods [21], which leverage full-wave propagation models for the signal wavefront across a vertical array [22]. Work on MFP performance bounds continued into the 1990s and 2000s and includes the hybrid Cramér-Rao bound (HCRB) [23], the Barankin bound [24], and Bayesian bounds [25]. In addition to static array geometries, the CRLB has also been derived

for estimating the horizontal field directionality for time-varying arrays [26] and recently for estimating the displacement and rotation of distributed linear arrays [27].

In contrast to sensor arrays, which directly measure the spatial variation of the received signal, single-hydrophone methods typically require source motion [28, 29, 30] or signal bandwidth [31, 32] for localization. Such methods commonly exploit phenomena such as the Doppler effect [33], convergence zones [34], diffraction patterns [35, 36], temporally-distinct multipath arrivals [37], channel fading [38], or combinations thereof [8]. Channel fading due to multipath is a dominant characteristic of shallow water acoustic propagation and is the focus of this work. Such fading is often characterized by striations, or lines of constant intensity, in the time-frequency spectrum of acoustic data recorded by a hydrophone positioned within the water column; Figure 3.1 presents a clear example of striations for the case of an ideal waveguide. Importantly, the slopes of the striations are governed by the WI, β, through the following equation [12, 39, 40]: $\delta\omega/\delta r = \beta\omega/r$, where r is source range and ω is source radial frequency.

Early striation-based ranging methods processed acoustic spectrograms as images and estimated striation slopes using Radon and Hough transforms [41, 38, 42] as well as the 2-D discrete Fourier transform (2D-DFT) [43]. Other WI-based ranging techniques include minimum variance methods [44, 15] and model-based ML parameter estimators [45]. Recent WI-based ranging methods have achieved good localization results in specific contexts, often achieving range estimation root mean square errors (RMSEs) of a few hundred meters for sources at distances of 3 to 7 km [46, 43, 45]. However, it is not currently well understood what the performance bounds are for single-hydrophone ranging methods in shallow water or the relative importance of parameters such as signal-to-noise ratio (SNR), signal bandwidth, or β.

This chapter addresses the theoretical limits of passive, single-hydrophone rang-

ing by presenting a framework that exposes the roles of these parameters and that can account for varying degrees of prior environmental knowledge. The bound is herein derived initially for the case of an ideal waveguide, for which $\beta = 1$, though it can be readily extended to complex, range-independent environments, and this is demonstrated using environmental parameters measured during the SWellEx-96 experiment [47]. Both joint and conditional range estimation CRLBs are derived, corresponding to cases in which β is either unknown or known a priori. The latter case is equivalent to single-sensor MFP in a 2-D, range-independent waveguide with prior knowledge of receiver depth. The bounds presented in this work are validated by a favorable comparison to the asymptotic performance of the ML estimator, which is characterized through Monte Carlo simulations.

The remainder of this chapter is organized as follows: first, the modeling is presented in Section 3.2 and includes a statistical characterization of the received signal, the structure of the signal covariance matrix, and an extension of the standard normal mode model that allows the pressure field magnitude to be expressed directly in terms of β. The CRLB for WI-based range estimators is examined in Section 3.3 and includes a derivation of the Fisher information matrix (FIM), expressions for the conditional and joint parameter estimation bounds, and a derivation of the ML estimators for β and range. Section 3.4 presents plots of the bounds for a variety of signal parameter combinations as well as a comparison of the ML estimator performance to the CRLB. Finally, key findings and a discussion of future work are included in Section 3.5.

3.2 Modeling

This section presents the modeling assumptions employed throughout this chapter and their signal processing implications. The model for the received signal is presented first in Section 3.2.1, followed by an overview of the structure of the corre-

sponding signal covariance matrix in Section 3.2.2 and the range-independent normal mode channel response model in Section 3.2.3.

3.2.1 Signal model

A single broadband source and a single hydrophone at constant depths z_s and z_r, respectively, are considered in a range-independent, shallow water ocean environment. The source and receiver can be stationary or moving, and the time-varying range rate is denoted by $v_\mathrm{r}(t)$. In the time domain, the pressure signal recorded by the receiving hydrophone, $x(t)$, is the sum of two components: one due to the source, $s(t)$, at time-varying range $r(t)$, and another due to a combination of external and internal noise sources, denoted by $\eta(t)$. The time-varying range is given in terms of an initial range r_0 and range rate v_r as follows:

$$r(t) = r_0 + \int_{t_0}^{t} v_\mathrm{r}(\tau) d\tau \tag{3.1}$$

The source signal and noise are generated by independent complex Gaussian random processes. For simplicity, the Doppler effect is ignored in this analysis, though the model can easily be extended to account for the apparent frequency shift in the received signal due to the motion of the source, receiver, and medium. The received signal can be written as follows:

$$x(r,t) = \underbrace{s(t)}_{\text{random}} * \underbrace{h(r,t;z_\mathrm{s},z_\mathrm{r},\mathbf{a})}_{\text{deterministic}} + \underbrace{\eta(t)}_{\text{random}} \tag{3.2}$$

where r is source range; $*$ denotes convolution; $h(r,t;z_\mathrm{s},z_\mathrm{r},\mathbf{a})$ is the channel impulse response at depth z_r due to a point source at depth z_s and range r; and where $\mathbf{a}$ is a vector of relevant environmental parameters such as column depth and sound speed. The parameters z_s, z_r, and $\mathbf{a}$ are constants and will be suppressed in the channel response notation for the remainder of this work.

In the time-frequency domain, the complex-valued received signal is denoted by $x(t_n, \omega_m)$, where m is one of M processed broadband frequency components and n is one of N processed epochs, where epoch refers to the time covered by an individual fast Fourier transform (FFT) block. A slow time-varying approximation is employed in which the channel response and source range are assumed constant over each epoch:

$$x(t_n, \omega_m) \approx \underbrace{s(t_n, \omega_m)}_{\text{random}} \underbrace{H(r_n, \omega_m)}_{\text{deterministic}} + \underbrace{\eta(t_n, \omega_m)}_{\text{random}} \tag{3.3}$$

The source signal and noise are modeled as being generated by independent, circular symmetric complex Gaussian random processes having flat power spectra over a band of frequencies Ω, as follows:

$$s(t, \omega_m \in \Omega) \sim \mathcal{CN}\left(0, \sigma_s^2\right) \tag{3.4}$$

$$\eta(t, \omega_m \in \Omega) \sim \mathcal{CN}\left(0, \sigma_\eta^2\right) \tag{3.5}$$

where σ_s^2 and σ_η^2 are the signal and noise variances, respectively.

3.2.2 Covariance matrix

Let the vector $\mathbf{x}$ contain all the spectral data computed for M frequency components at each of N epochs: $\mathbf{x} \triangleq [\mathbf{x}_1^T \ ... \ \mathbf{x}_N^T]^T$, where $\mathbf{x}_n = [x(t_n, \omega_1) \ ... \ x(t_n, \omega_M)]^T$. The covariance matrix, $\mathbf{R} \triangleq E[\mathbf{x}\mathbf{x}^H]$, is block-diagonal and given as follows: $\mathbf{R} = \text{diag}(\mathbf{R}_1 \ ... \ \mathbf{R}_n \ ... \ \mathbf{R}_N)$, where $\mathbf{R}_n \triangleq E[\mathbf{x}_n \mathbf{x}_n^H] = \text{diag}(R_{1n} \ ... \ R_{mn} \ ... \ R_{Mn})$ and $R_{mn} \triangleq E\left[x(t_n, \omega_m) x(t_n, \omega_m)^*\right] = E\left[|x(t_n, \omega_m)|^2\right]$. Employing the short time-varying approximation used in (3.3), the covariance matrix entries R_{mn} can be expressed as follows:

$$\begin{aligned} R_{mn} &= E\left[\left|s(t_n, \omega_m) H(r_n, \omega_m) + \eta(t_n, \omega_m)\right|^2\right] \\ &= E\left[\left|s(t_n, \omega_m) H(r_n, \omega_m)\right|^2\right] + \sigma_\eta^2 \end{aligned} \tag{3.6}$$

where t_n and r_n are the time and range, respectively, corresponding to the data segment processed during the nth time epoch. Observing that $s(t_n, \omega_m)$ is independent and identically distributed for each epoch, (3.6) can be written as follows:

$$R_{mn} = I(r_n, \omega_m) + \sigma_\eta^2 \tag{3.7}$$

where $I(r_n, \omega_m) \triangleq \sigma_{\mathrm{s}}^2 |H(\omega_m, r_n)|^2$ is the expected received acoustic intensity due to the source at range r_n and radial frequency ω_m.

3.2.3 Modeling channel response using normal modes

By applying a normal mode model, (3.7) can be expressed in a manner that reveals an explicit dependence on the environmental parameter β, allowing the CRLB to be derived for WI-based estimators. First, the channel response, $H(\omega, r)$, is modeled as a sum of P propagating modes:

$$H(\omega_m, r_n) = \frac{1}{\sqrt{r_n}} \sum_{p=1}^{P} A_{pm} e^{j k_{pm} r_n} \tag{3.8}$$

where k_{pm} is the radial wavenumber of the pth propagating mode at frequency ω_m. The modal amplitude term A_{pm} is given by

$$A_{pm} = \frac{\kappa_0 \psi_p(z_{\mathrm{s}}) \psi_p(z_{\mathrm{r}})}{\sqrt{k_{pm}}} \tag{3.9}$$

where κ_0 is a complex constant, and where $\psi_p(z_{\mathrm{s}})$ and $\psi_p(z_{\mathrm{r}})$ denote the mode eigenfunctions evaluated at the source and receiver depths, respectively. The squared magnitude of the complex-valued channel response can be expressed as follows:

$$|H(\omega_m, r_n)|^2 = \frac{1}{r_n} \sum_{p=1}^{P} \sum_{q=1}^{P} A_{pm} A_{qm} e^{-j \Delta k_{pq} r_n} \tag{3.10}$$

where $\Delta k_{pq} \triangleq k_{qm} - k_{pm}$ is the difference in radial wavenumbers between modes p and q. The frequency dependence of Δk_{pq} is suppressed for ease of notation. The

wavenumber difference can be expressed as a function of β as follows [40]:

$$\Delta k_{pq} = \alpha_{pq}(\omega_m^{-1} c^{\gamma_c} D^{\gamma_D})^{1/\beta} \tag{3.11}$$

where α_{pq} is a mode-dependent constant and where γ_c and γ_D are the scalar-valued generalized invariants for sound speed and column depth, respectively. While (3.11) assumes a single value of β characterizes the environment, which is the case for an ideal waveguide, β is more appropriately considered as a distribution in complex environments [48, 49], and the implications of this are explained further in Section 3.4.2. The quantity $(\omega_m^{-1} c^{\gamma_c} D^{\gamma_D})^{1/\beta}$ in (3.11) is herein defined as $\xi_m(\beta)$ with dependence on sound speed and column depth suppressed. The generalized invariants are similar to the waveguide invariant, β, for which the following approximation characterizes the slopes, $\delta\omega/\delta r$ of striations across $I(r, \omega)$ with D and c held constant and where $u = r$ and $\gamma_u = \beta$:

$$\frac{\delta\omega}{\delta u} \approx \gamma_u \frac{\omega}{u} \tag{3.12}$$

For an ideal waveguide, the generalized invariants for sound speed and column depth are as follows [40]: $\gamma_D = -2, \gamma_c = 1$, and the equations for α_{pq} and $\xi_m(\beta)$ are given by:

$$\alpha_{pq} \approx \frac{(q^2 - p^2)\pi^2}{2} \tag{3.13}$$

$$\xi_m(\beta) = \left(D^2 k_m\right)^{-1/\beta} \tag{3.14}$$

where $k_m = \omega_m/c$ is the total wavenumber corresponding to frequency component ω_m. Using this notation, the covariance matrix entries given by (3.7) can be expressed in terms of β as follows:

$$R_{mn} = \frac{\sigma_{\mathrm{s}}^2}{r_n} \sum_{p,q} A_{pm} A_{qm} e^{-j\alpha_{pq}\xi_m(\beta) r_n} + \sigma_\eta^2 \tag{3.15}$$

3.3 Cramér-Rao bounds and ML estimator

This section presents an overview and derivation of the joint and conditional parameter estimation CRLBs, as well as an efficient ML parameter estimator. The bounds are covered first, in Section 3.3.1, followed by the derivation of the ML estimator in Section 3.3.2.

3.3.1 Performance bounds for ideal waveguide

The CRLB is a bound on the minimum variance attainable by an unbiased estimator and is given as follows [50]:

$$\mathrm{var}(\theta_i) \geq \left[\mathbf{J}^{-1}(\boldsymbol{\theta})\right]_{ii} \tag{3.16}$$

where $\mathbf{J}(\boldsymbol{\theta})$ is the FIM and $\boldsymbol{\theta}$ is a vector containing the deterministic, unknown parameters. The FIM is defined as follows:

$$\left[\mathbf{J}(\boldsymbol{\theta})\right]_{ij} = \mathrm{tr}\left(\mathbf{R}^{-1}\frac{\partial \mathbf{R}}{\partial \theta_{\mathbf{i}}}\mathbf{R}^{-1}\frac{\partial \mathbf{R}}{\partial \theta_{\mathbf{j}}}\right) \tag{3.17}$$

Since $\mathbf{R}^{-1}$ is diagonal, (3.17) can be written as follows for the joint parameter estimation case where $\boldsymbol{\theta} = [\beta \;\; r_0]^{\mathrm{T}}$:

$$\mathbf{J}(\boldsymbol{\theta}) = \sum_{m,n}\frac{1}{R_{mn}^2}\begin{bmatrix} \left(\frac{\partial R_{mn}}{\partial \beta}\right)^2 & \left(\frac{\partial R_{mn}}{\partial \beta}\right)\left(\frac{\partial R_{mn}}{\partial r_0}\right) \\ \left(\frac{\partial R_{mn}}{\partial r_0}\right)\left(\frac{\partial R_{mn}}{\partial \beta}\right) & \left(\frac{\partial R_{mn}}{\partial r_0}\right)^2 \end{bmatrix} \tag{3.18}$$

After obtaining partial derivatives and simplifying the result, the elements of the 2x2 FIM can be expressed as follows:

$$J_{11} = \sum_{m,n}\left(\frac{\rho_n r_n \xi_m(\beta)\ln(D^2 k_m)|\chi_{mn}|}{\beta^2(1+\zeta_{mn})}\right)^2 \tag{3.19}$$

$$J_{22} = \sum_{m,n}\left(\frac{\rho_n \xi_m(\beta)\mathrm{Im}(\chi_{mn}) - \zeta_{mn}}{1+\zeta_{mn}}\right)^2 \tag{3.20}$$

$$J_{12} = J_{21} = \sum_{m,n} \left(\frac{\rho_n \xi_m(\beta) \ln(D^2 k_m) \left(\rho_n r_n \xi_m(\beta) |\chi_{mn}|^2 - \zeta_{mn} \mathrm{Im}(\chi_{mn}) \right)}{\beta^2 (1 + \zeta_{mn})} \right) \tag{3.21}$$

where $\rho_n \triangleq \frac{\sigma_s^2}{r_n \sigma_\eta^2}$ is the ratio of source signal power to noise power at the receiver and is herein defined as the SNR, $\mathrm{Im}(\cdot)$ denotes the imaginary part of the argument in parentheses, $\zeta_{mn} \triangleq \frac{I(r_n, \omega_m)}{\sigma_\eta^2}$, and χ_{mn} is defined as follows:

$$\chi_{mn} \triangleq \sum_{p,q} A_{pm} A_{qm} \alpha_{pq} e^{-j \alpha_{pq} \xi_m(\beta) r_n} \tag{3.22}$$

The bounds for conditional parameter estimation are as follows:

$$\mathrm{var}(\hat{\beta}) \geq J_{11}^{-1} \tag{3.23}$$

$$\mathrm{var}(\hat{r}_0) \geq J_{22}^{-1} \tag{3.24}$$

The joint parameter estimation bounds are given by

$$\mathrm{var}(\hat{\beta}) \geq \frac{J_{22}}{J_{11} J_{22} - J_{12}^2} \tag{3.25}$$

$$\mathrm{var}(\hat{r}_0) \geq \frac{J_{11}}{J_{11} J_{22} - J_{12}^2} \tag{3.26}$$

3.3.2 ML parameter estimation

In accordance with (3.3), (3.4), and (3.5), the received signal is circular symmetric complex Gaussian distributed with mean and covariance given as follows:

$$x(\omega_m, t_n) \sim \mathcal{CN}\left(0, I(r_n, \omega_m) + \sigma_\eta^2\right) \tag{3.27}$$

From (3.27), it follows that the magnitude of the received pressure signal is Rayleigh distributed with scale parameter given as follows:

$$|x(\omega_m, t_n)| \sim \mathrm{Rayleigh}\left(\frac{\sqrt{2}}{2} \sqrt{I(r_n, \omega_m) + \sigma_\eta^2} \right) \tag{3.28}$$

Under the single-hydrophone, normal mode-based complex Gaussian signal model presented in Section 3.2.1, the signal magnitude is a sufficient statistic for β and r_0, as the off-diagonal terms in the covariance matrix $\mathbf{R}$ are zero. The ML estimator for the parameter vector $\boldsymbol{\theta}$ can be implemented by searching over a gridded parameter space, as follows:

$$\hat{\boldsymbol{\theta}}_{\mathrm{ML}} = \arg\max_{\boldsymbol{\theta}_{\mathrm{hyp}}} \prod_{m,n} \ell(|x(\omega_m, t_n)|; \boldsymbol{\theta}_{\mathrm{hyp}}) \tag{3.29}$$

where the likelihood function, derived from the Rayleigh density, is given by [51]:

$$\ell(|x(\omega_m, t_n)|; \boldsymbol{\theta}_{\mathrm{hyp}}) = \frac{|x(\omega_m, t_n)| \exp\left(-|x(\omega_m, t_n)|^2 / (I(r_n, \omega_m; \boldsymbol{\theta}_{\mathrm{hyp}}) + \sigma_\eta^2)\right)}{2(I(r_n, \omega_m; \boldsymbol{\theta}_{\mathrm{hyp}}) + \sigma_\eta^2)} \tag{3.30}$$

where $I(r_n, \omega_m; \boldsymbol{\theta}_{\mathrm{hyp}})$ is obtained by evaluating $I(r_n, \omega_m)$, as defined in Section 3.2.2, using the hypothesized parameter values $\boldsymbol{\theta}_{\mathrm{hyp}}$. ML parameter estimation results are obtained using Monte Carlo methods and are compared to the corresponding CRLBs in Section 3.4.1.

3.4 Results

This section presents numerical results and plots of the CRLBs for joint and conditional range and β estimation in both ideal and complex environments. The bounds corresponding to a range-independent, ideal waveguide are presented first in Section 3.4.1 and are compared to the ML estimator that was derived in Section 3.3.2. The extension to complex environments is presented in Section 3.4.2, in which the bounds corresponding to an ideal waveguide are compared to those for the complex SWellEx-96 experimental environment.

3.4.1 CRLB analysis

The sensitivity of the joint and conditional parameter estimation CRLBs to SNR, source range, and time-bandwidth product (TBP) is now examined, beginning with

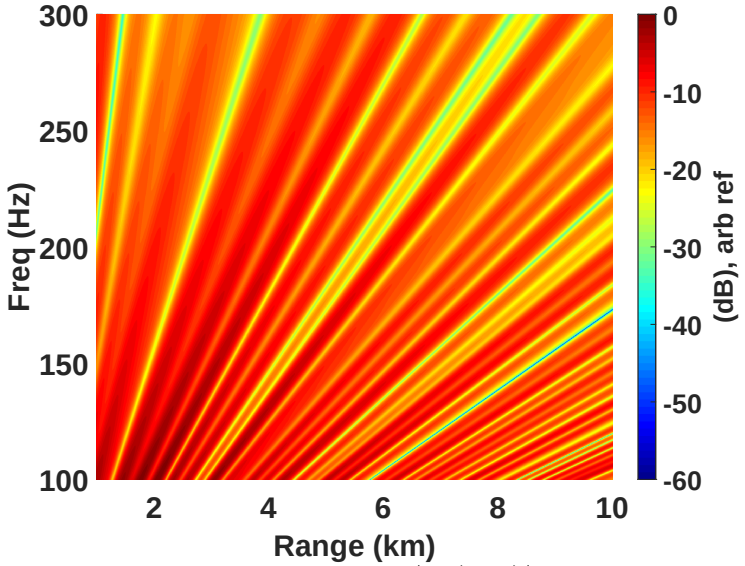

FIGURE 3.1: Channel response magnitude, $|H(r, \omega)|$, plotted as a function of frequency and source range for the ideal waveguide utilized in this work. The response shown was computed using the following parameters: column depth $D = 200$ m, sound speed $c = 1500$ m/s, $\beta = 1$, $P = 10$ propagating modes.

the case of an ideal waveguide with column depth 200 m and sound speed of 1500 m/s. The source and receiver depths are fixed at 9 m and 25 m, respectively. The channel response magnitude for this setup is depicted in Figure 3.1 and was computed using (3.10) and (3.11), in which $\beta = 1$ was used to solve for the mode wavenumber differences, Δk_{pq}, for the first 10 propagating modes. A single acoustic source moves at a steady rate $v_{\mathrm{r}} = 5$ m/s relative to the receiver and emits a band-limited white noise signal. The receiver processes the band from 150 to 250 Hz in successive 1-sec time epochs.

Figure 3.2 depicts the joint and conditional parameter estimation bounds for this scenario, plotted as a function of SNR and source range using a TBP of 1000, and Figure 3.3 shows the CRLB plotted as a function of SNR for a variety of source ranges and TBPs. The curves corresponding to a TBP of 1000 can be interpreted as slices through the plots shown in Figure 3.2. A few points are worth noting:

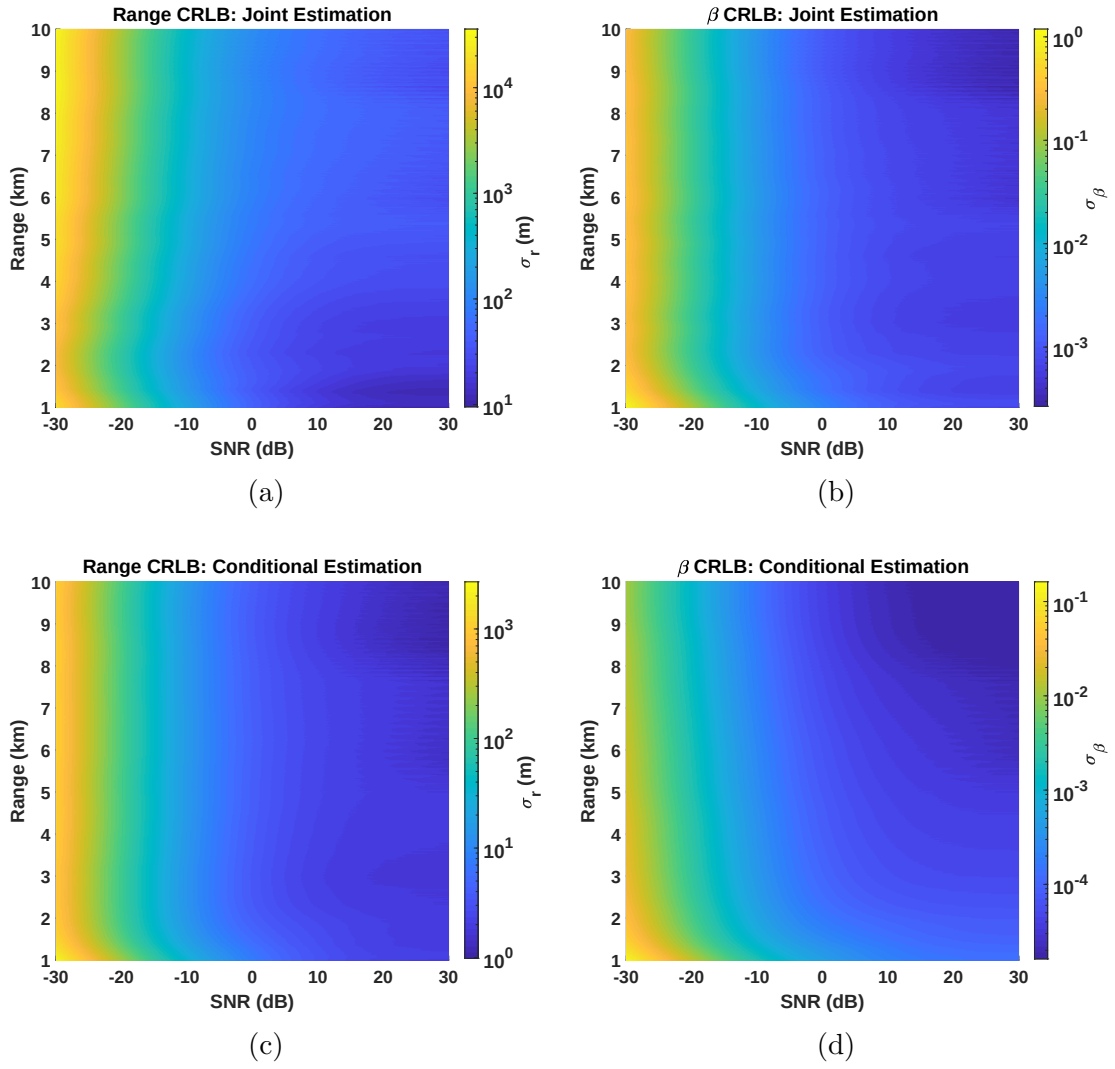

FIGURE 3.2: Joint and conditional CRLBs for an ideal waveguide, plotted as a function of SNR and source range with a TBP of 1000. Source range estimation bounds are shown at left, and CRLBs for β estimation are shown at right. The top row compares joint parameter estimation bounds, and the bottom row examines conditional bounds.

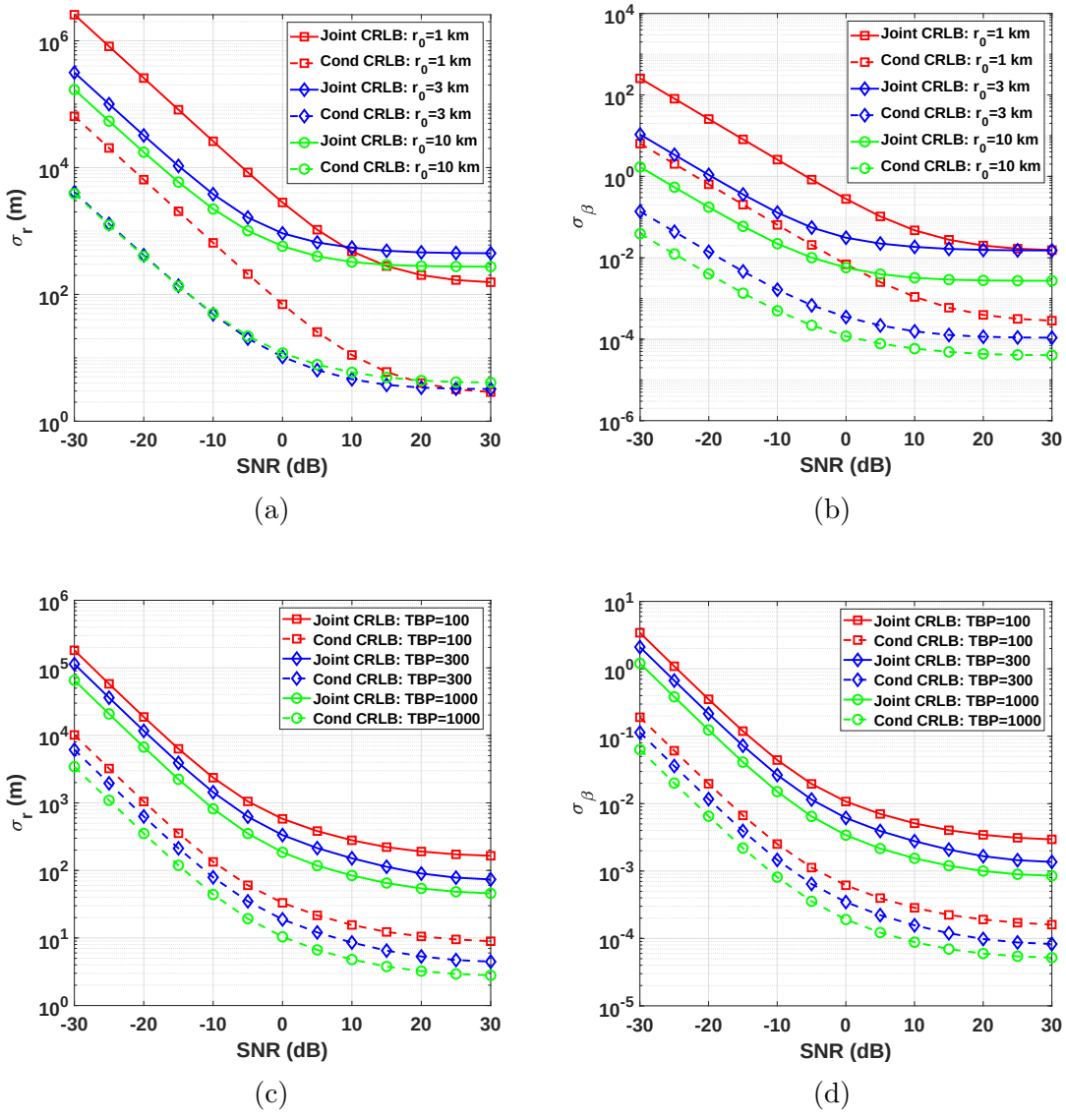

FIGURE 3.3: Joint and conditional CRLBs for an ideal waveguide plotted as a function of SNR. Source range estimation bounds are shown in the left column, and CRLBs for β estimation are shown at right. The top row compares the bounds using different source ranges, and the bottom row examines sensitivity to TBP.

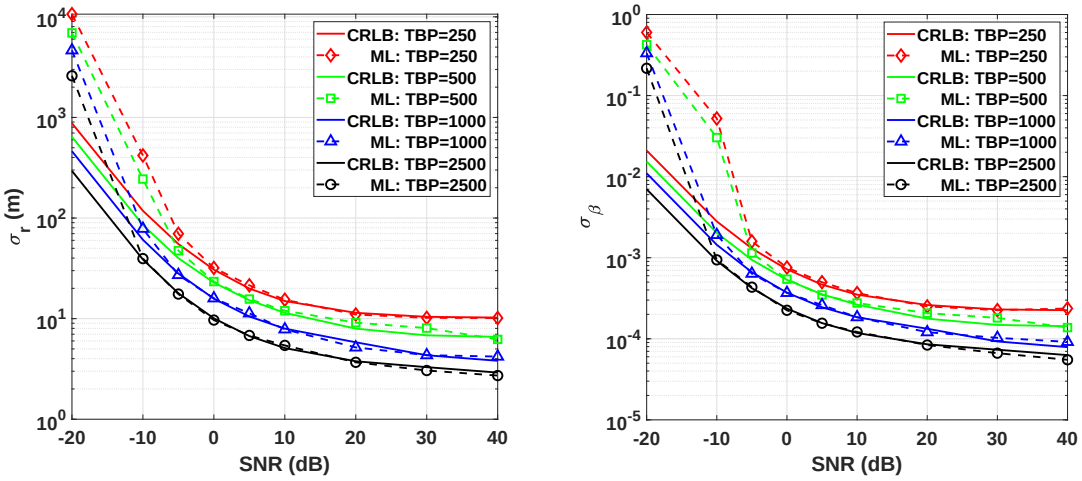

(a) (b)

FIGURE 3.4: Comparison of joint ML parameter estimation results to the CRLBs for various TBPs using an ideal waveguide with $P = 10$ propagating modes and source range $r_0 = 3.5$ km. Plots indicate RMSE of (a) range estimates and (b) β estimates obtained over 100 Monte Carlo trials.

first, there is generally between one and two orders of magnitude separation between the joint and conditional bounds for any given combination of parameters. Thus, for source ranging applications, prior knowledge of β could prove especially useful. Second, while the bounds decrease monotonically with increasing SNR, there are diminishing returns above 0 dB SNR, with the curves flattening out around 20 to 30 dB SNR. Third, as observed in prior work by the authors [45], the bounds decrease monotonically with increasing processed signal bandwidth, and Figure 3.3 shows a consistent trend across all combinations of parameters examined. This follows from the assumption that the spectral Fourier coefficients are independent, which is generally the case for sufficiently long observation times [52], and thus the bound on estimator variance decreases in proportion to the number of independent time-frequency spectral data points processed. Finally, it is observed that the conditional bound for β is strongly range-dependent, decreasing with increasing range, which

follows from a close inspection of the FIM element J_{11} in (3.19). However, the joint bound for β and the conditional bound for range estimation do not strictly increase or decrease with range when SNR is held constant. The apparent range-related trends observed in the joint range estimation bounds are much weaker than those observed for the conditional β estimation bound. Those bounds increase with range at SNRs above -10 to 0 dB, though they exhibit a fair degree of fluctuation due to the local structure of the computed channel response at particular ranges.

The performance of the ML estimator derived in Section 3.3.2 is compared to the joint estimation CRLB for both β and source range in Figure 3.4. Asymptotic convergence of the estimator performance to the CRLB is attained around -5 to 0 dB SNR with a TBP of 250 and at -10 to -5 dB SNR with larger TBPs. The ML estimator performance was characterized using Monte Carlo methods with 100 trials conducted at each combination of parameters.

In practical applications, however, precise knowledge of mode shape functions and wavenumbers might not be readily available, and the uncertainty in such parameters would lead to higher performance bounds. Similarly, an ML estimator that operates using an estimate of β in lieu of precise environmental knowledge, such as that used in [45], would exhibit higher variance than the ML estimator performance depicted in Figure 3.4. Thus, for striation-based range estimators that utilize the scalar parameter β to succinctly represent the entirety of their prior environmental knowledge, the range estimation bounds would be significantly higher than those shown in Figure 3.4, and a more thorough investigation of that particular case remains for future work.

3.4.2 Performance bounds for complex environments

The bounds are now extended to the complex environment depicted in Figure 3.5, which has a 198 m column depth, a downward-refracting sound speed profile (SSP),

and a three-layer bottom. The parameter values indicated in the figure correspond to environmental measurements taken during the SWellEx-96 experiment [47]. The first step is to obtain mode shape functions and wavenumbers, and this was done numerically using KRAKEN [53]. This allows the mode-dependent α_{pq} values in (3.11) to be computed using β and the numerically-obtained mode wavenumber differences Δk_{pq}. However, as noted in Section 3.2.3, a single value of β does not perfectly describe complex acoustic environments. To this end, β can either be treated as mode-dependent or as a scalar approximation. The latter approach is used in this work, and the value $\hat{\beta} = 1.10$ was obtained using the ML β estimation technique presented in Chapter 4 and demonstrated using a similar environment.

A comparison of joint and conditional CRLBs for range and β estimation for the ideal waveguide and complex SWellEx-96 environments is presented in Figure 3.7. The comparison uses a TBP of 1500, a source range of 2.5 km, and 10 propagating modes. More modes can be used for such analyses, especially with higher source frequencies or deeper water columns. However, the effective number of propagating modes is typically low for shallow water environments in which higher-order modes with steeper grazing angles are heavily attenuated by the bottom. The CRLBs are seen to increase significantly for the complex environment, and this is due to the environment not being well characterized by a scalar β, as was the case for the ideal waveguide. This effectively causes the striations in $I(r, \omega)$ to become blurred, reducing the sensitivity of the measured acoustic intensities to the parameters of interest and thereby decreasing the information content of each measurement.

3.5 Conclusions

This work presented the CRLBs for passive ranging and β estimation using a single hydrophone in a multipath environment with a single, broadband source. The bounds were derived using a normal mode model for the case of a range-independent ideal

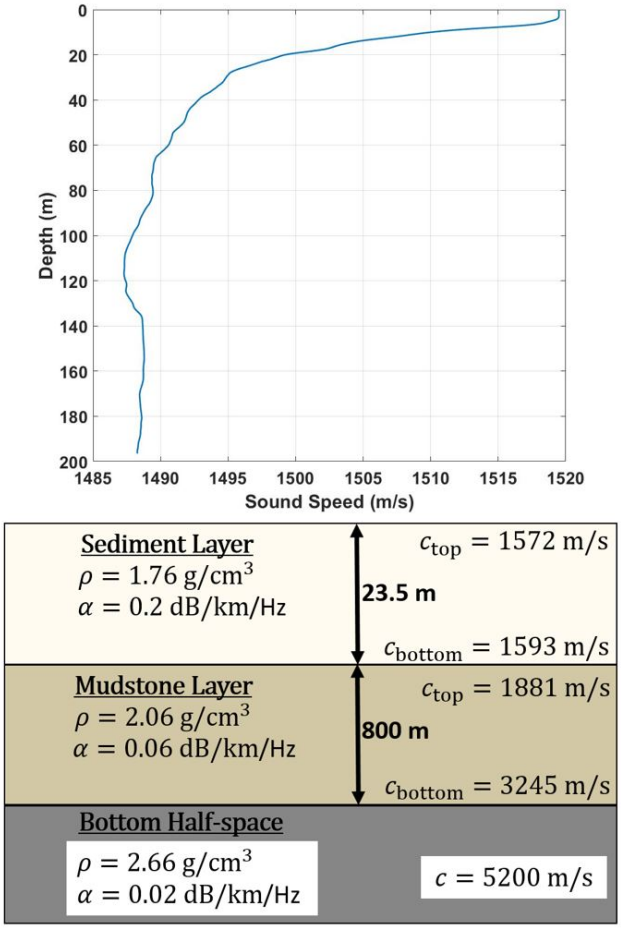

FIGURE 3.5: SSP and bottom properties measured during the shallow water SWellEx-96 experiment. The parameters depicted were used to compute mode shape functions and wavenumbers for the complex environment using KRAKEN.

waveguide and were extended to a more complex environment, which was modeled after the SWellEx-96 experiment using KRAKEN to compute mode shape functions and wavenumber differences. The bounds were observed to decrease linearly with increasing SNR up to about 0 dB SNR before flattening out around 20 to 30 dB SNR due to the stochastic nature of the unknown source signal. The bounds were also seen to be proportional to the time-bandwidth product of the processed signal, which agrees with observations made in Chapter 4 using WI-based ranging for tonal sources. An ML parameter estimator was also presented, which used acoustic intensity as a sufficient statistic for β and source range and was seen to asymptotically achieve the

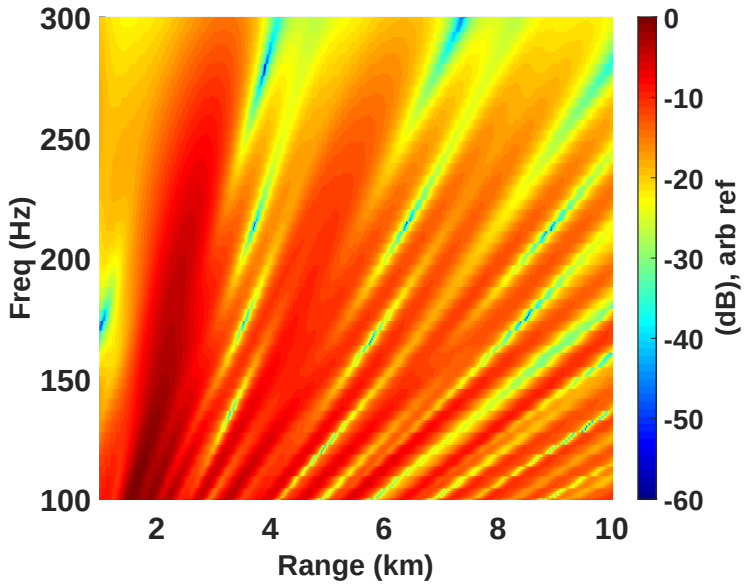

FIGURE 3.6: Channel response magnitude plotted as a function of frequency and source range for the complex shallow water environment measured during the SWellEx-96 experiment and computed using $P = 10$ propagating modes.

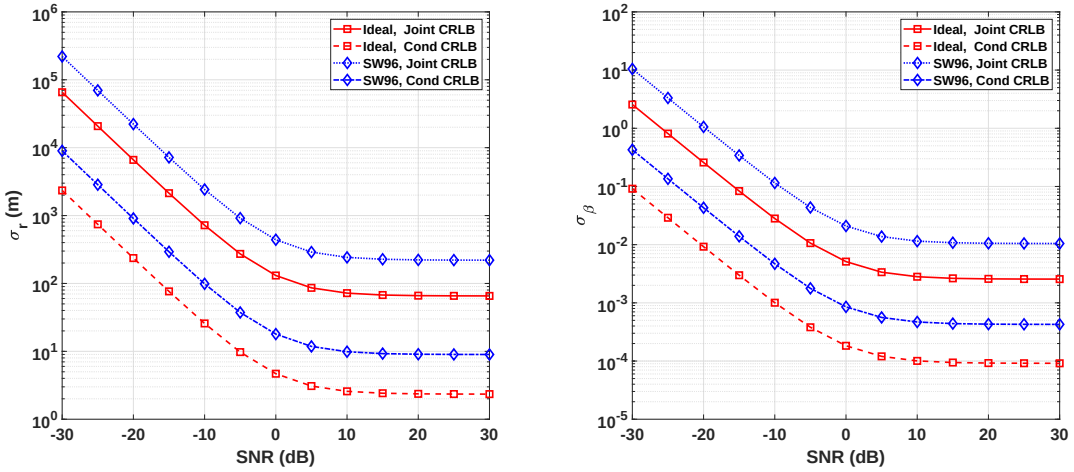

(a) (b)

FIGURE 3.7: Comparison of CRLBs for both joint and conditional source range (left) and β estimation (right) in ideal and complex environments. Parameters used: $P = 10, r_0 = 2.5$ km, TBP $= 1500$.

CRLB at high SNR and with a large time-bandwidth product.

Future work in this area may include extensions to account for limited prior knowledge of parameters such as β or source range. Additionally, a tonal source model may be used to provide insight regarding the performance bounds for single-hydrophone ranging methods that optimally process the full acoustic spectra of sources of opportunity such as commercial shipping vessels.

4

ML WI-based estimators with experimental validation

This chapter provides an in-depth introduction to WI-based range estimation using tonal sources of opportunity as well as a rigorous derivation of the physics- and statistics-based modeling employed to obtain optimal parameter estimators. Results obtained from experimental data (SWellEx-96) are also presented. The content of this chapter was largely drawn from the 2019 work of Young, Harms, Hickman, Rogers, and Krolik, which was published in the *IEEE Journal of Oceanic Engineering* [45] and has been adapted and re-formatted for this dissertation.

4.1 Introduction

For a broadband source in shallow water, interference patterns can be readily observed in a plot of the acoustic intensity at a single hydrophone as a function of source-receiver range, r, and radial frequency, ω. A clear example is provided in Figure 4.1a for a broadband source in a shallow water environment characterized by $\beta = 1$. When the time-varying range to a transiting broadband source is known, the $I(r, \omega)$ surface is easily obtained by first computing the squared magnitude of

a spectrogram of hydrophone data and subsequently mapping time to source range. For sources of opportunity such as cargo ships, this mapping can be performed using the AIS data they are required to broadcast while transiting coastal waterways [54].

Multiple techniques have been developed to leverage the striations observed in time-frequency spectrograms to estimate source range, beginning in 2000 with Thode [41], who used a Radon transform technique applied to data from a vertical hydrophone array. When using only a single hydrophone to estimate source range, however, an estimate of the range rate is also required, and in 2007 Tao et al. [38] proposed a Hough-transform-based method for estimating the ratio of source velocity to range in cases where the source track exhibits the CPA. Alternatively, the 2D-DFT can be employed to estimate the slope, $\frac{\Delta\omega}{\Delta r}$, of striations locally across the spectrogram when source range rate is known, as in the 2010 work by Cockrell and Schmidt [43] that does not require the CPA to be exhibited in the source track. Striation-based range estimation techniques require estimates of β, and although the $\beta = 1$ approximation is commonly employed in shallow water environments, more accurate estimates of β for a particular environment can improve range estimation results, as noted by Turgut et al. [42] in their 2010 work that utilized striations observed in beam data from a horizontal line array to estimate source range.

When source range is known, β can be estimated by applying the same types of techniques used for range estimation. Early examples include the 2-D DFT-based techniques employed by Rouseff and Spindel [48] in 2002 and Yang [55] in 2003, the normalized striation slope estimation technique of Heaney [56] in 2004 and the minimum variance technique proposed by Brooks et al. [44] in 2006. Such image-processing-based techniques have been shown to work well for broadband sources in shallow water environments, but their performance can be significantly degraded when applied to tonal sources.

Acoustic SOOs tend to have emissions spectra that are dominated by narrowband

tonals [14], and the resulting $I(r, \omega)$ surface does not exhibit broadband striations as it does for the case shown in Figure 4.1a but is instead more likely to resemble Figure 4.1b, which was obtained from hydrophone measurements of the acoustic emissions of a cargo ship transiting a shallow water shipping lane off the coast of San Diego, California. The mixture of narrowband and broadband components significantly reduces the effectiveness of image processing techniques that inherently assume a uniform, broadband source spectrum. Motivated in part by the ubiquity of powerful, tonal acoustic radiators in the ocean, Verlinden et al. [16] have recently proposed a technique for mitigating the impact of the tonal components in SOO spectra; the tones are first removed in the Radon transform domain, allowing β to be estimated from striations in the filtered $I(r, \omega)$ surface. This was shown to improve the ability to estimate striation slopes using the broadband spectral content, but it dismisses a wealth of environmental information encoded in the tonal components.

In this chapter, a complementary β estimation technique is presented in which the tonal components are viewed as the signal, rather than as noise, and the processor only considers striations in the loudest tones. A general framework for estimating β from tones was introduced by Harms, Odom, and Krolik in 2014 [15], and this chapter extends the signal model they developed to a maximum likelihood (ML) framework for estimation of both β and source range. Range estimation using SOOs has a potentially significant application to AUV navigation, a concept which has been introduced in recent work by Young, Soli, and Hickman in 2017 [8]. In their work, the authors investigated the feasibility of exploiting the waveguide invariant for AUV localization and proposed a simple, LS-based algorithm that utilizes WI-based source range estimates, AIS data, and the Doppler effect. In this chapter, a similar technique, although one that does not utilize the Doppler effect, is presented. Results obtained using real data from the SWellEx-96 experiment highlight the potential for this technique to be used for localizing AUVs that have incurred substantial position

uncertainty during the interval between deployment and recovery, either in real time or post-mission.

Derivations of the tonal-based techniques for ML estimation of β and source range are presented in Section 4.2 along with a validation of the β estimator using a simulated Pekeris waveguide [57]. The performance of the estimators is evaluated using real data from the SWellEx-96 experiment, which is presented in Section 4.3 and compared to simulation results obtained using KRAKEN. The application to AUV navigation, as well as receiver localization results obtained from processing SWellEx-96 data, are presented in Section 4.4, and key findings are summarized in Section 4.5.

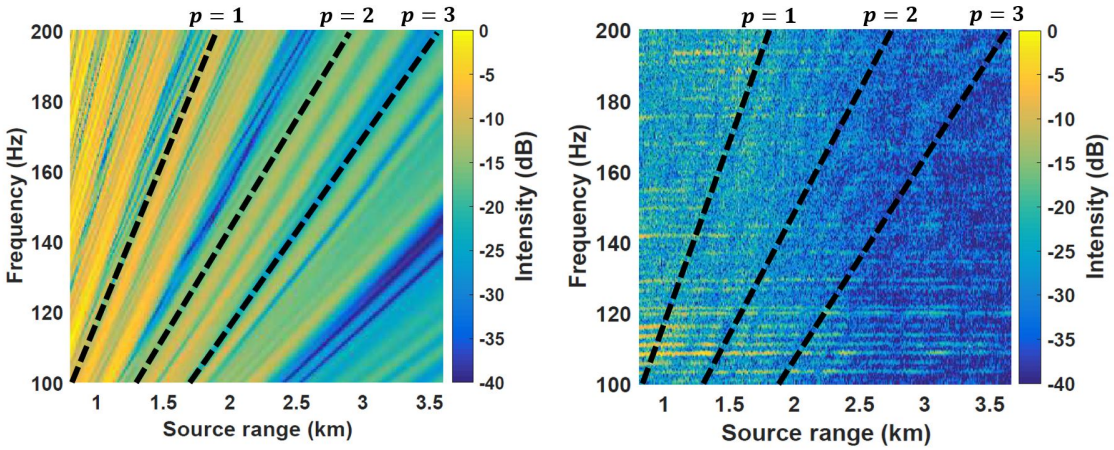

(a) (b)

FIGURE 4.1: Acoustic intensity at a single receiver plotted as a function of frequency and range to a transiting source. (a) Simulated broadband source in a Pekeris waveguide. (b) Real, tonal source (cargo ship) in a shallow water environment from the Noise-09 experiment. In both cases, the striations, or lines of constant intensity, in the plots are generally characterized by $\beta = 1$, as seen by the agreement between the slopes of the striations and those of the three dashed lines obeying (4.7) and identified by $p = 1, 2, 3$ labels overlaid on each plot. The fading pattern is more difficult to see in (b) due to the mixture of strong tonal components with weaker, broadband components in the cargo ship acoustic emissions spectrum.

4.2 Signal model and derivation of estimators

This section begins with an introduction of the signal model that is used throughout this chapter and then moves into specific derivations of the estimators for β, source range, and receiver position. The signal model described in Sections 4.2.1 and 4.2.2 borrows heavily from Harms et al. [15] but also extends the authors' prior work by adjusting for unequal tonal source levels and including an ML estimator for frequency-dependent noise variance.

4.2.1 Received signal model

The acoustic emissions spectra of cargo ships are generally dominated by narrowband tonals corresponding to fundamental and harmonic oscillations of rotary mechanical devices and structures such as onboard diesel generators, propulsion engines, and propellers [14]. Accordingly, the source signal, $s(t)$, is modeled as a sum of K tones:

$$s(t) = \sum_{k=1}^{K} A_k e^{j(\omega_k t + \phi_k)} \tag{4.1}$$

where k is the index of each tonal component, in ascending order according to radial frequency, and A_k is the amplitude of the kth tonal. The values A_k and ϕ_k correspond to pressure field magnitudes and phases, respectively, and are assumed constant, but unknown, over the observation interval. However, the phases ϕ_k do not have to be perfectly stable, as the processor only considers acoustic intensity, which is proportional to the square of the pressure magnitude, and discards the phase measurement of the received signal.

In the frequency domain, the signal received at a hydrophone due to a transiting, tonal SOO at range r can be expressed as follows:

$$Z(r,\omega) = \underbrace{S(\omega)H(r,\omega)}_{X(r,\omega)} + N(\omega) \tag{4.2}$$

where $S(\omega)$ represents the source spectrum, $H(r,\omega)$ is the channel response expressed as a function of frequency and source range, and $N(\omega)$ represents the frequency-dependent contribution from background noise sources. $X(r,\omega)$, which is the product of the channel response and the source spectrum, represents the source signal received at the hydrophone. The noise component, $N(\omega)$, is modeled as a circularly-symmetric Gaussian random variable consisting of independent real and imaginary components as follows:

$$\begin{aligned} N(\omega) &= N_{\mathrm{R}}(\omega) + jN_{\mathrm{I}}(\omega) \\ N_{\mathrm{R}}(\omega), N_{\mathrm{I}}(\omega) &\sim \mathcal{N}(0, \sigma_{\mathrm{n}}^2(\omega)) \end{aligned} \tag{4.3}$$

where $\sigma_n^2(\omega)$ is a frequency-dependent noise variance. Let $Y(r,\omega)$ be defined as the ratio of the intensity of the received signal at a specific source range and frequency, $|Z(r,\omega)|^2$, to the noise variance, as follows:

$$\begin{aligned} Y(r,\omega) &\triangleq \frac{|Z(r,\omega)|^2}{\sigma_{\mathrm{n}}^2(\omega)} \\ &= \left(\frac{X_{\mathrm{R}}(r,\omega)}{\sigma_{\mathrm{n}}(\omega)} + \frac{N_{\mathrm{R}}(\omega)}{\sigma_{\mathrm{n}}(\omega)}\right)^2 + \left(\frac{X_{\mathrm{I}}(r,\omega)}{\sigma_{\mathrm{n}}(\omega)} + \frac{N_{\mathrm{I}}(\omega)}{\sigma_{\mathrm{n}}(\omega)}\right)^2 \end{aligned} \tag{4.4}$$

where $X_{\mathrm{R}}(r,\omega)$ and $X_{\mathrm{I}}(r,\omega)$ denote the real and imaginary parts of $X(r,\omega)$, respectively. As a result of assuming constant, non-random source tone amplitudes A_k in (4.1), $Y(r,\omega)$ is noncentral chi-squared distributed [58] with two degrees of freedom and will be represented by the random variable Y for ease of notation. The density function of Y is as follows [59]:

$$f_Y(y;\lambda) = \frac{1}{2} I_0\left(\sqrt{\lambda y}\right) \mathrm{e}^{-\frac{1}{2}(y+\lambda)} \tag{4.5}$$

where $I_0(\cdot)$ denotes a modified Bessel function of the first kind. The noncentrality

parameter, λ, is as follows:

$$\begin{aligned}\lambda &= \frac{X_{\mathrm{R}}(r,\omega)^2}{\sigma_{\mathrm{n}}^2(\omega)} + \frac{X_{\mathrm{I}}(r,\omega)^2}{\sigma_{\mathrm{n}}^2(\omega)} \\ &= \frac{I(r,\omega)}{\sigma_{\mathrm{n}}^2(\omega)}\end{aligned} \tag{4.6}$$

where $I(r,\omega)$ is the intensity of the received acoustic signal due to the tonal source at range r and frequency ω and is represented as the squared magnitude of $X(r,\omega)$: $I(r,\omega) = |X(r,\omega)|^2$.

4.2.2 Modeling intensity along striations

The statistical signal modeling presented in Section 4.2.1 allows for the fading observed in measured data to be attributed to channel effects, rather than source generation, which is often the case in multipath environments. For multipath environments that are well-characterized by a single value of β, the loci of points along striations in the fading pattern obey the following relationship [40]:

$$\frac{\omega}{\omega_0} = \left(\frac{r}{r_0}\right)^{\beta} \tag{4.7}$$

Evaluation of the likelihood function from (4.5) for measurements along the loci given by (4.7) requires $\sigma_{\mathrm{n}}^2(\omega)$ and $I(r,\omega)$, and methods for obtaining ML estimates of these parameters are now presented.

To estimate $\sigma_{\mathrm{n}}^2(\omega)$, we begin by observing that under the commonly-employed assumption of complex Gaussian additive ambient noise [60, 61, 62, 26], the magnitude of $N(\omega)$ is Rayleigh distributed with scale parameter $\sigma_{\mathrm{n}}(\omega)$ [51]. The parameter $\sigma_{\mathrm{n}}^2(\omega)$ can be estimated directly from samples of the $Z(r,\omega)$ surface taken at frequencies that are adjacent to the source tonals, yet with sufficient separation to have negligible contribution to the measured intensity, such that $|Z(r,\omega)| \approx |N(\omega)|$. In

practice, there will also be a non-zero contribution from the broadband source emissions spectrum, and this is not explicitly accounted for under the model. Although such broadband noise has been noted to be approximately log-normal in distribution [63], rather than effectively having the Rayleigh distribution that is assumed under this signal model, the environmental noise arising from a multitude of point sources spread throughout the channel is herein assumed to dominate the broadband vessel noise. Notable exceptions could include scenarios in which the source vessel is at close range, as noted by Urick [64], when the signal contains very weak tonals, or when processing array data steered in the source direction. Broadband models might, therefore, be profitably incorporated into this technique in future work to account for such cases.

The unbiased ML estimate [65] of $\sigma_{\mathrm{n}}^2(\omega)$ is computed as follows:

$$\widehat{\sigma_{\mathrm{n}}^2}(\omega) = \frac{1}{4M} \sum_{m=1}^{M} \left(|Z(r_m, \omega + \delta\omega)|^2 + |Z(r_m, \omega - \delta\omega)|^2 \right) \tag{4.8}$$

where ω corresponds to one of the tonal frequencies, $\delta\omega$ is a small frequency offset, and M is the number of short-time Fourier transform (STFT) frames in $Z(r, \omega)$. For an environment well-characterized by a scalar β, any striation projected through frequency and range using (4.7) using the correct value of β will have a constant value of $H(r, \omega)$ from (4.2). Therefore, the received intensities due to the signal, $I(r, \omega)$, at each tonal frequency along a striation are related as follows:

$$\frac{I(r_k, \omega_k)}{I(r_l, \omega_l)} = \left(\frac{A_k}{A_l} \right)^2 \tag{4.9}$$

where A_k and A_l are the magnitudes of the kth and lth tones in the source signal described in (4.1), and r_k and r_l are the ranges along the striation corresponding to the kth and lth tones. Let α_k be defined as the ratio of the amplitude of the kth

tone to the largest tonal amplitude, $A_{\max} \triangleq \max_k A_k$:

$$\alpha_k \triangleq \frac{A_k}{A_{\max}} \tag{4.10}$$

The received signal intensities along a striation can then be written as follows:

$$I(r_k, \omega_k) = \alpha_k^2 I_{\max} \tag{4.11}$$

where $I_{\max} \triangleq \max_k I(r_k, \omega_k)$. Along with the frequency-dependent noise variance estimates, $\widehat{\sigma_n^2}(\omega)$, the signal intensities given by (4.11) allow the noncentrality parameter λ to be computed using (4.6), which enables (4.5) to be evaluated for the measured data. Given estimates of α_k and $I_{\max}$, the received signal intensities $I(r_k, \omega_k)$ along a striation can be estimated using (4.11), and methods for obtaining those parameters are now covered, beginning with α_k.

Since the tonal amplitudes are assumed constant, the parameter α_k can be estimated for each tonal component by averaging the magnitudes of the corresponding spectral components over all M frames, as follows:

$$\hat{\alpha}_k = \frac{\sum_{m=1}^{M} |Z(r_m, \omega_k)|}{\max\limits_{\omega_l \in \Omega} \sum_{m=1}^{M} |Z(r_m, \omega_l)|} \tag{4.12}$$

where Ω represents the set of all K tonal frequencies processed.

With α_k estimated, the ML estimate of $I_{\max}$ for each striation is obtained as follows. First, let p be an index corresponding to a particular striation projected across the $|Z(r, \omega)|$ surface, and let $\mathbf{y}(p, \beta_{\text{hyp}})$ be a K-vector of scaled intensity measurements taken along the pth striation, projected using a hypothesized value of β, with components defined as follows:

$$y_k(p, \beta_{\text{hyp}}) \triangleq \frac{|Z(r_k, \omega_k; p, \beta_{\text{hyp}})|^2}{\widehat{\sigma_n^2}(\omega_k)} \tag{4.13}$$

where the notation $Z(r_k, \omega_k)$ has been expanded to $Z(r_k, \omega_k; p, \beta_{\text{hyp}})$ to indicate a particular locus of points obtained from applying (4.7) to the $|Z(r, \omega)|$ surface using specific values of p and β_{hyp}. It is assumed that noisy intensity measurements along a striation are statistically independent, which is in accordance with the source model in (4.2) given a linear channel and independent additive noise. Therefore, the likelihood of a hypothesized maximum striation value I_{hyp} is the joint density of the scaled measurements $\mathbf{y}(p, \beta_{\text{hyp}})$ along the striation and is written as follows:

$$\ell\left(I_{\text{hyp}} | \mathbf{y}(p, \beta_{\text{hyp}})\right) = \prod_{k=1}^{K} f_Y\left(y_k(p, \beta_{\text{hyp}}); \lambda_k(I_{\text{hyp}})\right) \tag{4.14}$$

where λ_k is parameterized by the hypothesized striation intensity as follows:

$$\lambda_k(I_{\text{hyp}}) = \frac{\hat{\alpha}_k^2 I_{\text{hyp}}}{\widehat{\sigma_n^2}(\omega_k)} \tag{4.15}$$

The ML estimate of maximum received signal intensity along a particular striation is obtained through an iterative search process and is expressed as follows:

$$\hat{I}_{\text{ML}}(p, \beta_{\text{hyp}}) = \arg\max_{I_{\text{hyp}}} \ell\left(I_{\text{hyp}} | \mathbf{y}(p, \beta_{\text{hyp}})\right) \tag{4.16}$$

The ML intensity estimator derived here is central to both the β estimator presented in Section 4.2.3 and the range estimator in Section 4.2.4.

4.2.3 Maximum likelihood β estimation

The ML estimate of β is obtained through a parameter search process, assuming source range is known, as outlined in Figure 4.2. Let β_{hyp} denote one of L hypothesized β values under consideration at a given step of the search. For each hypothesized β, a series of P curves are projected through frequency and range across the $Z(r, \omega)$ surface, which is obtained by computing a spectrogram of the measured hydrophone data and subsequently mapping time to source range. The striations are

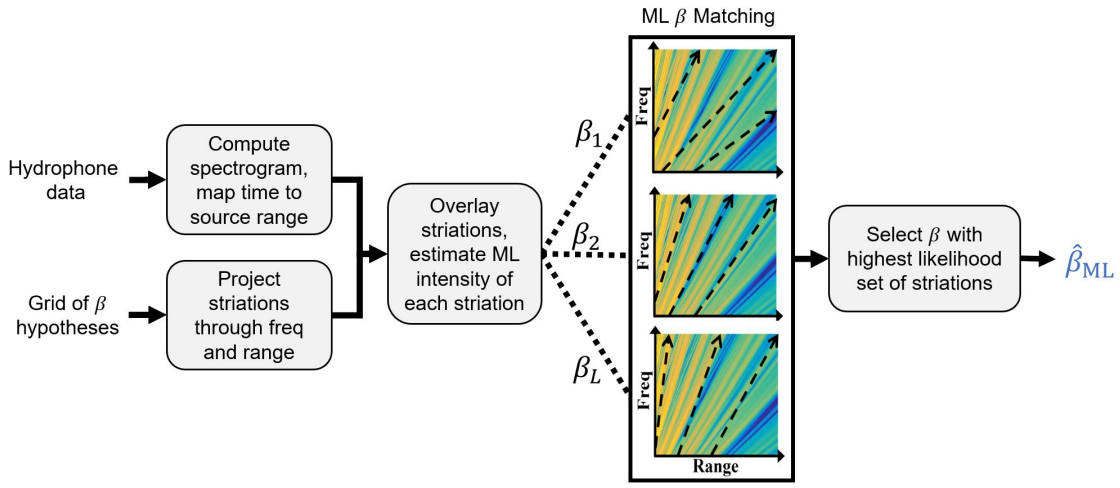

FIGURE 4.2: Block diagram showing an overview of the β estimation process. First, a spectrogram is computed from the hydrophone data, and the resulting time axis is mapped to source range. Striations are computed using (4.7) for each of L hypothesized β values and are overlaid on the spectrogram. The ML intensity along each striation is calculated using (4.16), and the likelihood of each set of striations, corresponding to a particular hypothesized β, is obtained using (4.17). Finally, the hypothesized β with the highest likelihood is selected. In the example shown in the figure, the second hypothesized β yields a set of projected striations that match closely with those in the spectrogram and would have a relatively high likelihood compared to mismatched hypotheses.

projected in accordance with (4.7), using β_{hyp} in place of β. For each projected striation, the ML estimate of noise-free intensity is estimated using (4.16), and the likelihood of a particular β_{hyp} is the product of likelihoods of the P curves:

$$\ell\left(\beta_{\mathrm{hyp}}\right) = \prod_{p=1}^{P} \ell\left(\hat{I}_{\mathrm{ML}}(p, \beta_{\mathrm{hyp}}) | \mathbf{y}(p, \beta_{\mathrm{hyp}})\right) \tag{4.17}$$

The ML estimate of β is obtained by maximizing this likelihood:

$$\hat{\beta}_{\mathrm{ML}} = \arg\max_{\beta_{\mathrm{hyp}}} \ell\left(\beta_{\mathrm{hyp}}\right) \tag{4.18}$$

4.2.4 Maximum likelihood range estimation

In the previous section, a method was presented by which β can be estimated from the time-frequency spectrum of measured hydrophone data when the time-varying

source range is known. In this section, however, it is instead assumed that the time-varying source range is unknown, but the source range rate and β are known. Using knowledge of those two parameters, source range can be estimated using a method similar to the β estimation technique described previously. The range estimation technique is now presented, beginning with the process by which a spectrogram magnitude surface, $|Z(t,\omega)|$, is mapped to a $|Z(r,\omega)|$ surface without knowledge of the source range.

With an estimate of the time-varying source range rate, $\hat{v}_{\mathrm{rs}}(t)$, a time-range mapping can be constructed by hypothesizing an initial source range, r_0, at time t_0. The mapping is computed as follows:

$$r_{\mathrm{hyp}}(t, r_0) = r_0 + \int_{t_0}^{t} \hat{v}_{\mathrm{rs}}(\tau) d\tau \tag{4.19}$$

Using AIS data, which provides time-varying source position, $\mathbf{x}_{\mathrm{s}}(t)$, and velocity, $\mathbf{v}_{\mathrm{s}}(t)$, and an initial estimate of the receiver position relative to the source, $\hat{\mathbf{x}}_{\mathrm{rs}}(t)$, the source range rate is computed as follows:

$$\hat{v}_{\mathrm{rs}}(t) = \frac{\hat{\mathbf{v}}_{\mathrm{rs}}(t) \cdot \hat{\mathbf{x}}_{\mathrm{rs}}(t)}{||\hat{\mathbf{x}}_{\mathrm{rs}}(t)||_2} \tag{4.20}$$

where $\hat{\mathbf{x}}_{\mathrm{rs}}(t) \triangleq \mathbf{x}_{\mathrm{s}}(t) - \hat{\mathbf{x}}_{\mathrm{r}}(t)$, $\hat{\mathbf{v}}_{\mathrm{r}}(t)$ is the time-varying receiver velocity estimate provided by on-board equipment such as an IMU, $\hat{\mathbf{v}}_{\mathrm{rs}}(t) \triangleq \mathbf{v}_{\mathrm{s}}(t) - \hat{\mathbf{v}}_{\mathrm{r}}(t)$, and $||\cdot||_2$ indicates the Euclidean norm. The time-varying receiver position, $\hat{\mathbf{x}}_{\mathrm{r}}(t)$, is the sum of two parts: an initial position, $\hat{\mathbf{x}}$, and a time-varying displacement, $\hat{\mathbf{s}}(t)$, given as follows:

$$\hat{\mathbf{s}}(t) = \int_{t_0}^{t} \hat{\mathbf{v}}_{\mathrm{r}}(\tau) d\tau \tag{4.21}$$

Other methods can also be used to obtain $\hat{v}_{\mathrm{rs}}(t)$ without the requirement of AIS data or estimates of the receiver position and velocity. One such example is the

WI-based "source differencing" technique proposed by Rakatonarivo and Kuperman [46] in which the source velocity in the same SWellEx-96 data set analyzed in this chapter was estimated with an accuracy of ± 0.3 m/s. Alternatively, if the source track exhibits the CPA, then Hough-transform-based techniques can be applied to the $|Z(t,\omega)|$ surface to estimate the ratio of source velocity to range at CPA, as in the work of Tao et al. [38].

Once the time-range mapping has been performed, P striations are projected across the corresponding $|Z(r_{\text{hyp}}(t,r_0),\omega)|$ surface in accordance with (4.7) for each hypothesized initial source range, r_0. The measured intensities at each point along the pth projected striation are scaled using estimated noise variance, $\widehat{\sigma_n^2}(\omega)$, and are denoted by the K-vector $\mathbf{y}(p,\beta,r_0)$. The ML estimate of maximum striation intensity is computed as in (4.16), and the likelihood of a particular range hypothesis, r_0, is the product of likelihoods for each of the P corresponding striations:

$$\ell\left(r_{\text{hyp}}(t,r_0)\right) = \prod_{p=1}^{P} \ell\left(\hat{I}_{\text{ML}}(p,\beta_{\text{hyp}},r_0)|\mathbf{y}(p,\beta_{\text{hyp}},r_0)\right) \tag{4.22}$$

The ML estimate of source range at time t is as follows:

$$\hat{r}_{\text{ML}}(t) = \arg\max_{r_0} \ell(r_{\text{hyp}}(t,r_0)) \tag{4.23}$$

4.2.5 Simulation

The KRAKEN normal mode ocean acoustic simulation program [53] was used to model a shallow water Pekeris environment with range-independent bathymetry, 200 m column depth, and an isovelocity sound speed profile. This environment was chosen because it is known to be well-characterized by $\beta = 1$ [40], and the mean $\hat{\beta}_{\text{ML}}$ obtained by the estimator is expected to be near unity.

The channel response magnitude was computed for a mid-column hydrophone at frequencies from 100 to 200 Hz and at ranges from 2.5 to 7 km, similar to the

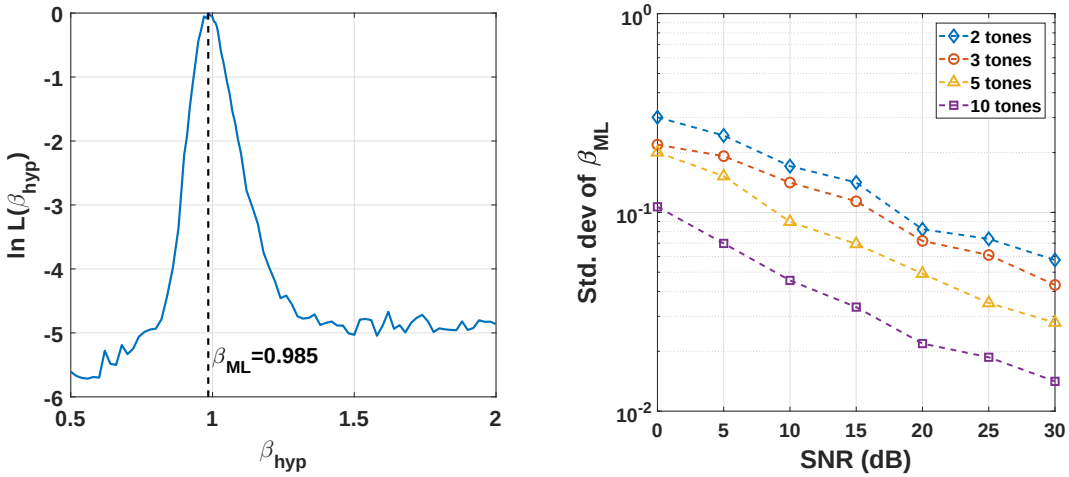

(a) (b)

FIGURE 4.3: β estimation results for a simulated shallow water Pekeris environment: (a) Log-likelihood of hypothesized β values for a single realization at 20 dB SNR using 5 tones (b) Standard deviation of the ML estimate of β, computed from 175 Monte Carlo trials at each combination of SNR and number of tones processed.

experimental setup described in Section 4.3.1. β was estimated using the method presented in 4.2.3, and a representative plot of the log-likelihood of various hypothesized β values is shown in Figure 4.3a; this corresponds to a particular realization at an SNR of 20 dB, defined here as the mean value of λ_k for each tonal component. The distribution of β is sharply peaked near $\beta = 1$, as expected, and the mean value of β obtained from repeated trials was 1.003. This indicates excellent agreement with the canonical $\beta \approx 1$ shallow water value and lends credibility to the estimator.

To investigate the impact of SNR and number of tones processed on estimator performance, 175 Monte Carlo trials were conducted at each of seven SNRs evenly spaced between 0 and 30 dB using 2, 3, 5, and 10 tones. 0 to 5 dB is the approximate SNR corresponding to typical tones above 200 Hz in the received spectrum of a fast-moving ship, while 10 to 30 dB SNR is more representative of the lower-frequency tones between 20 and 100 Hz of a slow-moving ship [14]. Similarly, a typical ship generates about 10 tones in the 20 to 100 Hz spectrum, but only 3 to 7 tones per 100

Hz at higher frequencies [63]. A minimum of two tones are required for β and range estimation, and performance improves with SNR and number of tones processed, as seen in Figure 4.3b. For the Pekeris environment, the standard deviation of $\hat{\beta}$ varies from about 0.02 for an optimistic scenario using 10 tones at an SNR of 25 dB to a standard deviation of 0.2 when only three tones are processed at an SNR of 5 dB.

To put the β estimation performance into perspective, a standard deviation of 0.02 in $\hat{\beta}$ corresponds to an average receiver position error of around 200 m (using the range estimator presented in Section 4.2.4 and the position estimator in 4.2.6 with source parameters set to mirror those from the experiment described in Section 4.3.1), while a standard deviation of 0.2 produced a position error of about 1.3 km. A conservative assumption of processing five tones at an SNR of 10 dB results in a standard deviation of 0.09, which corresponds to a position error of roughly 700 m. In real environments, however, the standard deviation of $\hat{\beta}$ is likely to be slightly higher for a given SNR and number of tones processed, due to the more diffuse underlying distribution of β values, as discussed in greater detail in Section 4.3.3.

4.2.6 NLLS-based receiver localization

The ML estimates of time-varying range to a transiting cargo ship, described in Section 4.2.4, can be combined with knowledge of the source track, obtained from AIS data, to localize the receiver using a nonlinear least squares technique. In practice, this could be used for AUV localization, where the receiver is co-located with the AUV. Let $\hat{\mathbf{x}}_\mathrm{r} = [\hat{x}_\mathrm{r}, \hat{y}_\mathrm{r}]^T$ represent the estimated AUV position vector in 2-D, defined as follows:

$$\hat{\mathbf{x}}_\mathrm{r} = \underset{\mathbf{x}_\mathrm{hyp}}{\arg\min} \, ||\mathbf{f}(\mathbf{x}_\mathrm{hyp})||_2 \tag{4.24}$$

where $\mathbf{f}(\mathbf{x}) = [f_1(\mathbf{x}), ..., f_Q(\mathbf{x})]^T$ is a Q-vector of residuals defined as follows:

$$f_q(\mathbf{x}) = ||\mathbf{x}_\mathrm{s}(t_q) - (\mathbf{x} + \hat{\mathbf{s}}(t_q))||_2 - \hat{r}_\mathrm{ML}(t_q) \tag{4.25}$$

Geometrically, the output of the f_q function is the distance from a hypothesized AUV position, $\mathbf{x}_\mathrm{hyp} + \hat{\mathbf{s}}(t)$, to a circle of radius $\hat{r}_\mathrm{ML}(t)$ centered at the source position $\mathbf{x}_\mathrm{s}(t)$ at time t_q. The LS solution, $\hat{\mathbf{x}}_\mathrm{r}$, can be obtained using a variety of techniques and will not generally be computationally expensive for small values of Q, such as $Q = 19$ used in this chapter.

If the source track is linear over the observation interval, (4.24) will yield two solutions that are symmetric with respect to the track axis. However, it is assumed that one of the two solutions will be significantly closer to an initial estimate of the AUV position, provided by an on-board IMU, and the closer of the two solutions would be chosen in such cases. Receiver localization results from the SWellEx-96 experiment, presented in the context of AUV navigation, are provided in Section 4.4.

4.3 Experiment and results

The time-varying range from a stationary hydrophone to a transiting tonal source was estimated by processing acoustic data from Event S5 of the SWellEx-96 experiment. Estimating β is a critical part of this process, and while there are several means by which this parameter could be obtained by an AUV, only two are investigated in this section. One method, similar in concept to that employed by Bonnel et al. [66], is to use prior knowledge of the environment to estimate β via simulation using a normal mode program, and this is covered in 4.3.3. The other method investigated is to estimate β from $|Z(r, \omega)|$, as in 4.2.3, which requires knowledge of source range. With access to AIS data and an estimate of its position, such as could be obtained when surfacing periodically for GPS, the range to a nearby SOO could be computed, allowing β to be accurately estimated. However, due to the speed at

which SOOs typically transit shipping lanes, a different SOO track would likely be used for receiver localization than was used for β estimation. For this reason, the source track in Figure 4.4 is partitioned into two sub-tracks, with the first being used to estimate β and the second being used to estimate source range and subsequently localize the receiver.

Sections 4.3.1 and 4.3.2 cover the experimental geometry, measured environmental parameters, and source characteristics. Following that, simulation results are presented for β and range estimation for the SWellEx-96 environment in Sections 4.3.3 and 4.3.4. Finally, experimental results are presented in Section 4.3.5 and are shown to be in close agreement with those obtained through simulation for the second track.

4.3.1 Experiment environment and geometry

Event S5 of the SWellEx-96 experiment took place on the afternoon of 10 May 1996 in shallow water about 12 km off the tip of Point Loma, California [47]. A cross-section of the environment is depicted in Figure 4.5 along with parameters of interest such as SSP, which is downward refracting, as well as various bottom properties. The SSP shown was measured at Station #5, which was selected for its spatial and temporal proximity to Event S5.

During Event S5, which was approximately 75 minutes in duration, the GPS-equipped research vessel R/V Sproul traveled northeast along the roughly 10 km track shown in Figure 4.4 at a rate of 2.5 m/s. The vessel towed a shallow source at a depth of 9 m and a deep source at a depth of 54 m, but the deep source was not utilized for β or range estimation. Although the track of the tow ship was known from GPS data, the track of the shallow source was not recorded. Based on matched field processing and other spectral analysis of the hydrophone data, which are not described in this chapter, it was determined that the shallow source lagged behind

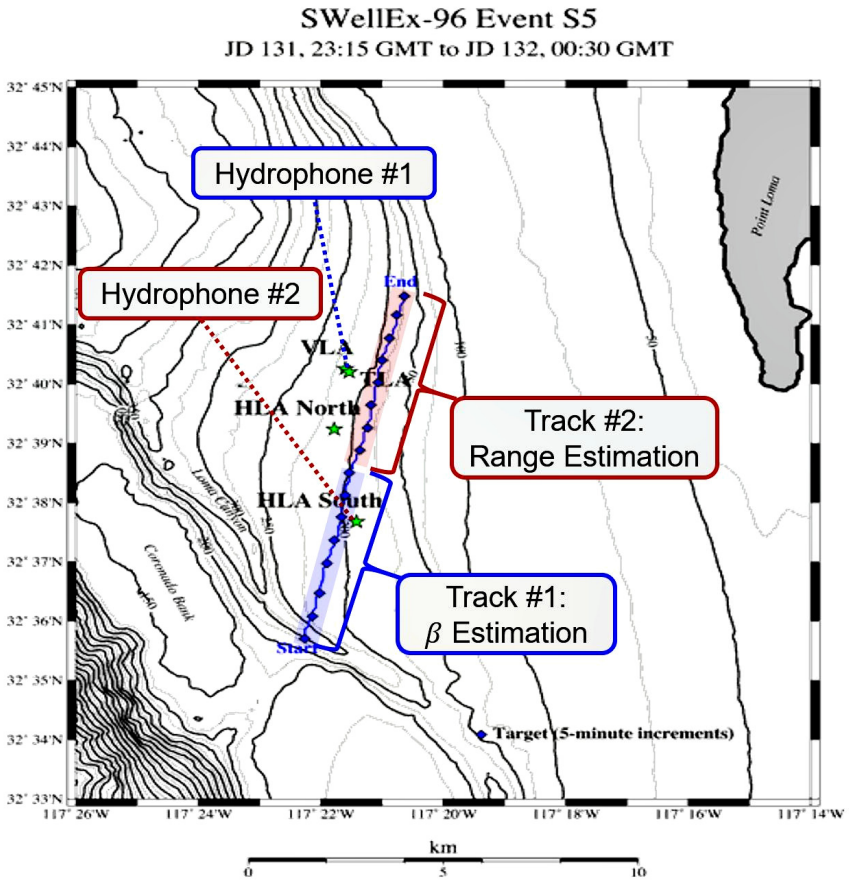

FIGURE 4.4: Overview of source track, hydrophone positions, and bathymetry for Event S5 of the SWellEx-96 experiment. Bathymetry isolines, drawn every 25 meters, are indicated by the alternating thick black and thin gray curves. The source track is indicated by the blue diamonds and is marked in 5-minute intervals. The hydrophones utilized for processing data from Tracks #1 and #2 were located within the arrays labeled TLA and HLA South, respectively, and each of the four arrays that were present during the experiment is marked with green stars. The source track was partitioned into two sub-tracks: the first (shaded blue) is used to estimate β, and the second (shaded red) is used to estimate source range and receiver position. Image credit: Murray and Ensberg [47], original online at http://swellex96.ucsd.edu/s5.htm.

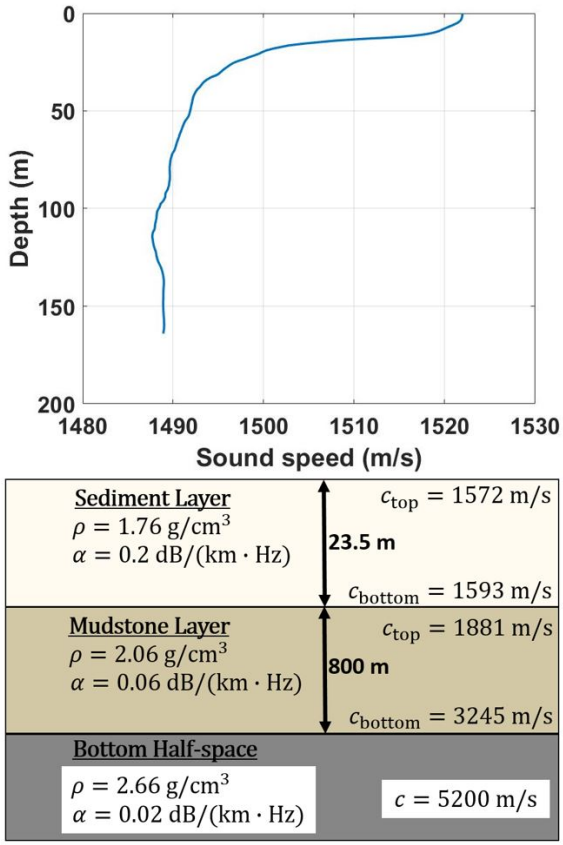

FIGURE 4.5: Graphical depiction of a cross-section of the simulated SWellEx-96 environment. Sound speed profile is shown at top and was obtained using Station #5 CTD data. Bottom properties include layer depth, density, attenuation, and sound speed. Parameters shown were obtained from the SWellEx-96 website [47].

the tow ship by approximately 13 seconds; this offset was applied to the GPS data to estimate the time-varying source position.

The bathymetry over the first half of the total track, herein referred to as Track #1, varies between roughly 275 m to 200 m, while Track #2 aligns reasonably well with the 180 m isobath. Although four fixed arrays of 16 hydrophones recorded the event, only the data from the last hydrophone in the Tilted Line Array (TLA) and the first hydrophone in the Horizontal Line Array South (HLAS) were processed; these hydrophones are herein referred to as Hydrophone #1 and Hydrophone #2, respectively. Hydrophone #1 was located at a depth of 67 m, and Hydrophone

#2 at a depth of 198 m. β is known to vary in response to changes in bathymetry between source and receiver [13], as well as receiver depth [67]; splitting the track and data in this manner thus presents a significant challenge to employing the waveguide invariant for range estimation and receiver localization.

4.3.2 Source signal

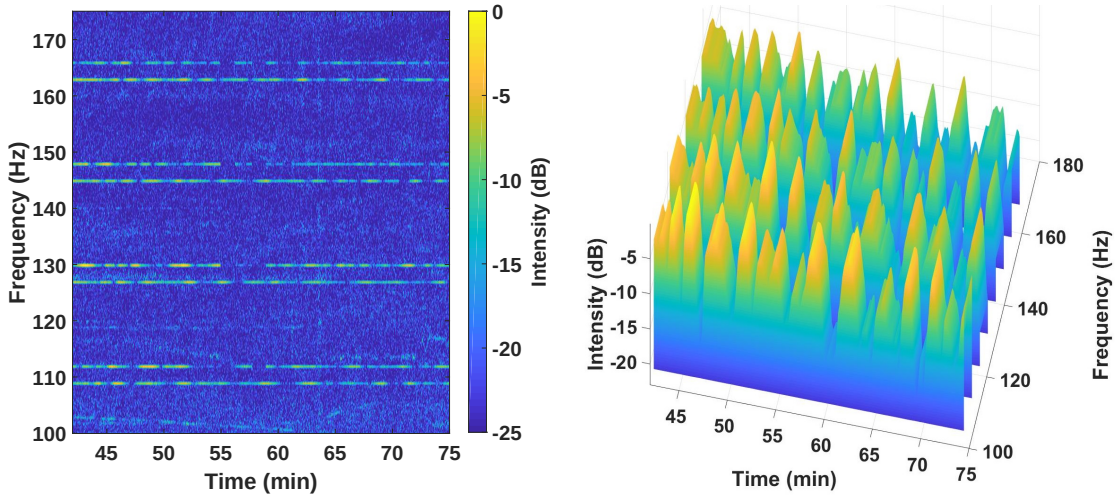

(a) (b)

FIGURE 4.6: (a) Spectrogram of data recorded by Hydrophone #2 during Track #2 of Event S5 of the SWellEx-96 experiment, normalized to 0 dB. The plot shows four pairs of tones between 110 and 170 Hz. The lower frequency tone in each pair corresponds to the shallow source, and the upper tone corresponds to the deep source. (b) Cuts from the spectrogram at left plotted in 3-D to emphasize the fading pattern in the shallow source tones at [109, 127, 145, 163] Hz used for range estimation.

The shallow source emitted a set of 9 tones ranging from 109 to 385 Hz. The time-frequency spectrum of the signal received at Hydrophone #2 during the second half of the source tow is shown in Figure 4.6a, for 100 to 175 Hz. Four pairs of tones are distinctly visible in the spectrogram, with a 3 Hz spacing between tones in each pair. The higher-frequency tone in each pair was transmitted by the deep source and the lower-frequency tone by the shallow source. Unlike the shallow source, which

transmitted tones continuously throughout the experiment, the deep source ceased its tonal emissions for approximately one minute at both 55 and 58 minutes into the experiment; the corresponding portions of the spectrogram in Figure 4.6a thus resemble nulls in the fading pattern.

Only the four lowest-frequency tones present in the shallow source signal were used for WI-based range estimation, and the fading pattern observed in these tones is shown in Figure 4.6b. The lowest-frequency tones were chosen primarily because SOOs are known to exhibit strong tonal emissions at lower frequencies [63], especially when traveling at lower speeds [14].

4.3.3 Simulation: β estimation

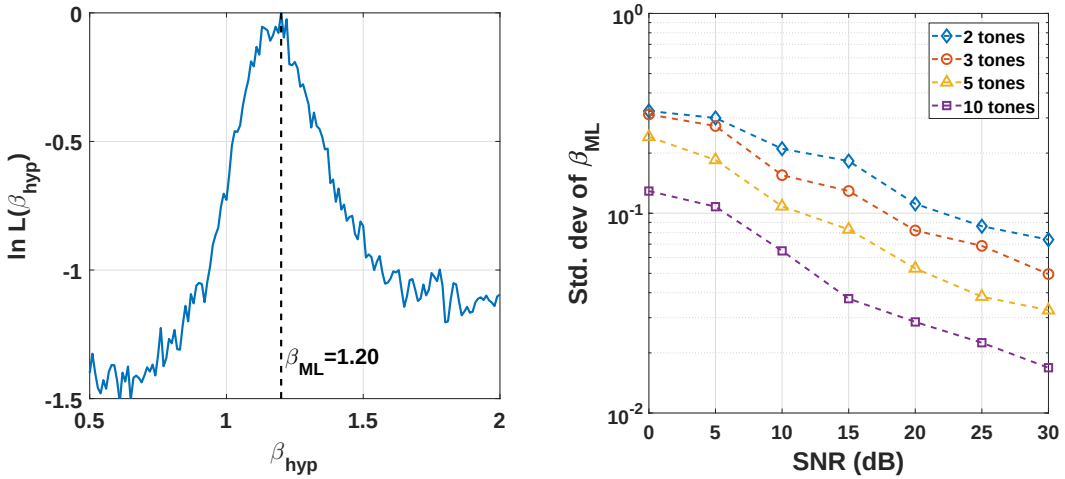

(a) (b)

FIGURE 4.7: β estimation results for the simulated SWellEx-96 shallow water environment, with 163 m column depth and experimentally-measured SSP and bottom properties: (a) Log-likelihood of hypothesized β values for a single realization at an SNR of 20 dB. (b) Standard deviation of $\hat{\beta}_{\mathrm{ML}}$, computed from 175 Monte Carlo trials at each combination of SNR and number of tones processed.

In addition to the isovelocity channel used in Section 4.2.5, a more realistic environment was also simulated in which the SSP and bottom properties used in

KRAKEN matched those that were measured during Event S5 of the SWellEx-96 experiment [47]. In this environment, the receiver was located below the thermocline at the bottom of the water column, at a depth of 163 m. Note that the approximate depth of the hydrophones belonging to HLAS was 198 m, but 163 m was used in simulation as that was the depth of the water column at which the Station #5 conductivity, temperature, depth (CTD) cast took place. This environment was used to separately estimate both β and source range, although in practice the same track would not generally be used to estimate both parameters, as knowledge of one is required to obtain the other.

To estimate β, a 4.5 km source tow was simulated at 5 frequencies evenly spaced between 110 and 170 Hz, which is approximately the span of source frequencies utilized from the SWellEx-96 data. With a simulated shallow source at 9 m depth, β is estimated to be 1.20, as shown in Figure 4.7a. In comparison to Figure 4.3a, the peak in Figure 4.7a is broader, and this corresponds to a more diffuse distribution of β values, as noted by Rouseff [67] and Turgut et al. [49] for environments in which the receiver is located below the thermocline. However, as noted in [49], the broadening of the peak is moderated when the source is located above the thermocline, as it would be in the case of SOOs such as cargo ships, and the mode of the distribution does not tend to shift far from unity. For AUVs operating near shipping lanes, the relative stability of the distribution could potentially allow for range estimation and receiver localization to be performed without requiring the vehicle to maintain a constant depth.

The performance of the estimator was analyzed using various numbers of tones and SNRs, as in Section 4.2.5, and the sample standard deviation for each set of 175 Monte Carlo trials is plotted in Figure 4.7b. Across all combinations of parameters tested, an average increase of 23% was observed in the standard deviation of $\hat{\beta}$ compared to the results obtained for the Pekeris environment (Figure 4.3b). Thus,

despite the moderate broadening of the β distribution compared to the Pekeris environment, a fairly low variance in β estimates should be seen when processing portions of the SWellEx-96 data for which the environment is relatively range-independent, as it was in simulation.

4.3.4 Simulation: range estimation

Prior to analyzing the experimental data, source range was estimated using the same, simulated SWellEx-96 environment that was used previously for β estimation. The previously-obtained mean ML estimate of the waveguide invariant parameter over the entire 4.5 km source track, $\hat{\beta} = 1.20$, was used for range estimation. However, to facilitate a more direct comparison of the simulation results to those obtained from processing the real data, the source track was shortened to 2.1 km; this corresponds to a 15-minute time interval with an average source range rate of 2.3 m/s, approximately matching the typical data segment processed from Track #2 of the experimental data.

For the selected range estimation trial shown in Figure 4.8a, the actual source range was 2.5 km, and the ML range estimate at an SNR of 20 dB is 2.57 km, an error of about 3%. The standard deviation of the range estimator as a function of SNR is shown in Figure 4.8b and is approximately 120 m at 20 dB SNR using 5 tones. At an SNR of 13.7 dB, which is the average from the SWellEx-96 experiment, the standard deviation increases to just over 200 m.

4.3.5 SWellEx-96 range estimation results

In this section, real data from the SWellEx-96 experiment is used to produce ML estimates of the time-varying source range. The noise variance parameter, $\sigma_{\mathrm{n}}^2(\omega)$, was estimated using the following frequency components in the spectrograms: [107 125 143 161] Hz. The average SNR for the processed data was 13.7 dB, with a peak of 14.8 dB and a minimum of 10.8 dB for the last portion of the track. The $\hat{\alpha}_k$ values

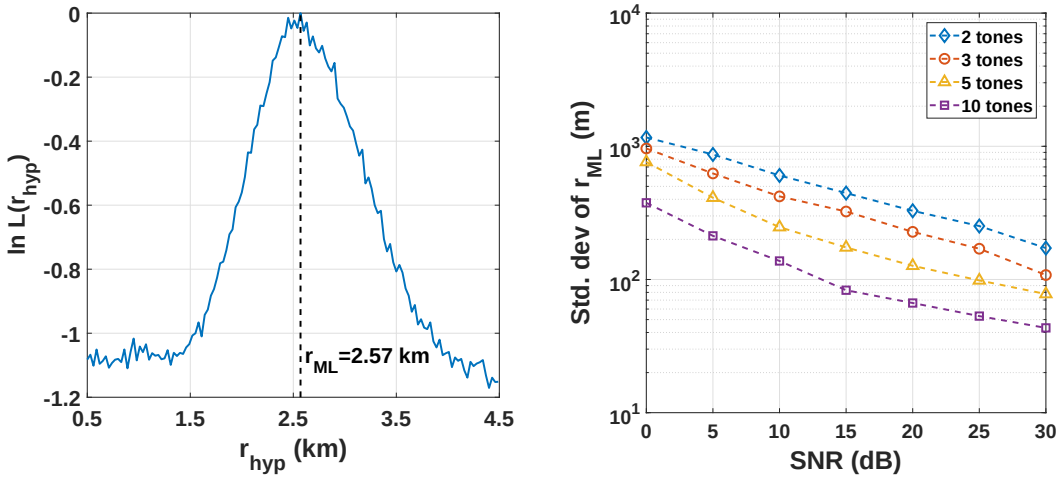

(a) (b)

FIGURE 4.8: (a) Log-likelihood of hypothesized initial source range, r_{hyp}, for a simulated 2.1 km track in the SWellEx-96 environment. True initial source range was 2.5 km, and estimated range is 2.57 km. (b) Standard deviation of ML estimate of initial source range, computed from 175 Monte Carlo trials at each combination of SNR and number of tones processed.

computed using (4.12) ranged from -0.1 to 0 dB, which is not surprising given that all tones in the source signal that were selected for processing were transmitted at the same level of 158 dB re 1 uPa [47].

There are multiple ways to obtain the requisite estimate of β, and the method employed here utilizes data acquired from Hydrophone #1 to estimate β over Track #1 and subsequently uses this value for range estimation over Track #2. The mean value of the waveguide invariant estimated over the 40-minute track, $\hat{\beta}_1$, was 1.26. The log-likelihood of various hypothesized β values for a 20-minute portion of data covering the middle of Track #1 is plotted in Figure 4.9a. The distribution of β values is much less concentrated near the mode than it was in simulation, and this is likely due to the rapidly-varying bathymetry over the track.

Source range was estimated using data from Hydrophone #2 assuming $\beta = 1.26$,

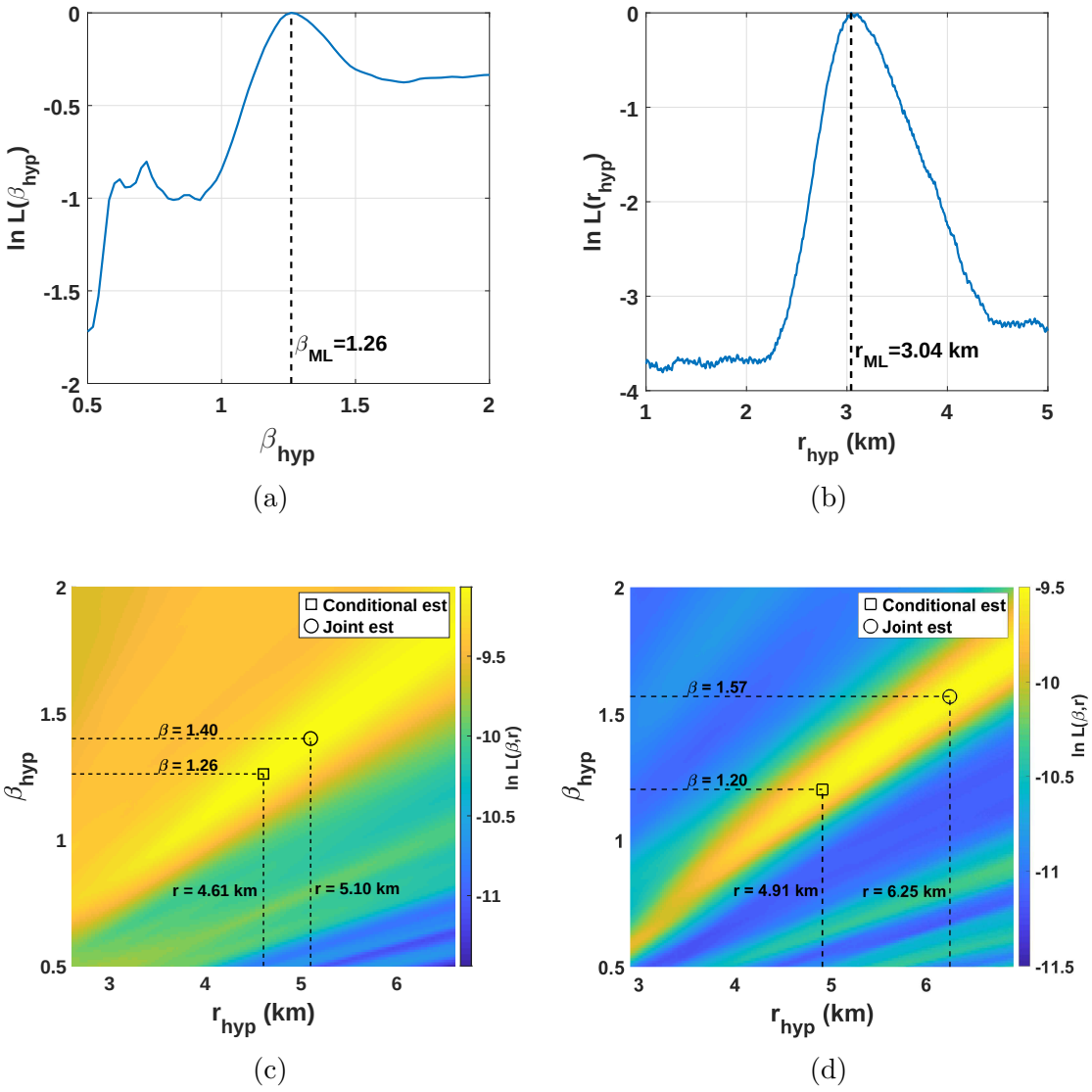

FIGURE 4.9: Log-likelihood of hypothesized parameters obtained from processing selected segments of the SWellEx-96 data. (a) Hypothesized β values for a 20-minute segment of data from Hydrophone #1 over Track #1 for which β is estimated to be 1.26 (b) Hypothesized source ranges for a 15-minute segment of data recorded by Hydrophone #2 from Track #2. (c) Joint likelihood surface for β and range over Track #1. (d) Joint likelihood surface for β and range over Track #2.

and the log-likelihood of various hypothesized source ranges for a 15-minute window of data beginning at 46 minutes is plotted in Figure 4.9b. Additionally, data from Hydrophone #2 was used to estimate β over Track #2, using knowledge of source range, and this yielded a mean estimate $\hat{\beta}_2 = 1.20$, which is identical to the value obtained through simulation using KRAKEN in Section 4.3.3. Joint likelihood surfaces for β and range estimation are also shown in Figure 4.9c and Figure 4.9d for Tracks #1 and #2, respectively. Note that the joint ML parameter estimates, which correspond to the case in which both source range and β are unknown, are quite different from the conditional ML parameter estimates. It is therefore important to obtain and employ an accurate estimate of β for the environment to have a low range estimation RMSE.

The ML range estimates obtained from processing Track #2 in overlapping 15-minute blocks are overlaid in Figure 4.10 for both estimates of β. The mean error in range estimates using $\hat{\beta}_1$ was 240 m, compared to only 9 m when using $\hat{\beta}_2$. The impact of an error in $\hat{\beta}$ is thus a shift in the range estimates, which follows from (4.7). The standard deviation of range estimation error was 115 m using $\hat{\beta}_2$ and 140 m using $\hat{\beta}_1$. These results are lower than the value of 200 m predicted from simulations, and the difference could be due to the small sample size of the experimental data. The RMSE of range estimates over Track #2 obtained using $\hat{\beta}_1$ and $\hat{\beta}_2$ are only 6% and 3%, respectively, of the average source range of 5 km; this level of accuracy is remarkable for a passive ranging method that uses a single hydrophone with minimal environmental knowledge. Overall, the results indicate this environment is reasonably well-characterized by a single value of β, even though the receiver was located below the thermocline and the bathymetry fluctuated by nearly 50 m from the middle of Track #1 to the end of Track #2.

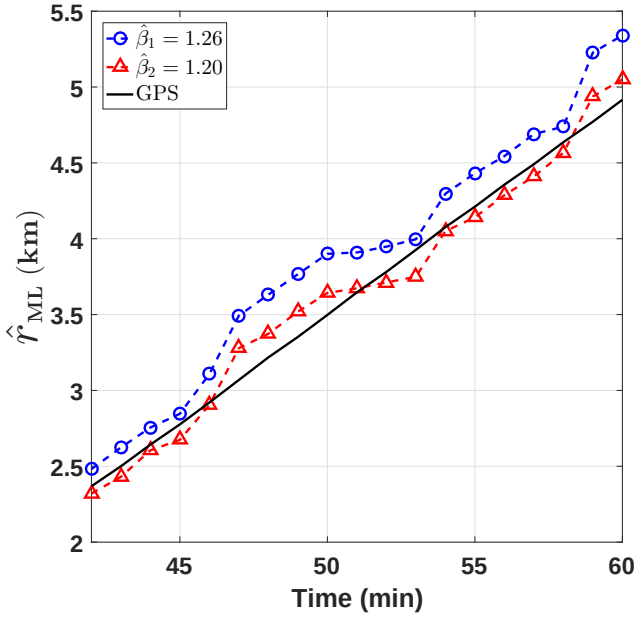

FIGURE 4.10: Maximum likelihood source range over Track #2 plotted against the true, GPS-derived range to the shallow source as a function of experiment time. The blue circles correspond to range estimates obtained using the value of β estimated from processing acoustic data from Track #1, and the red triangles correspond to using the value of β estimated from Track #2. Acoustic data was processed independently in 15-minute blocks, and estimated range corresponds to the source-receiver range at the beginning of a block.

4.4 AUV localization

In this section, the source range estimates obtained from processing acoustic data from Track #2 in Section 4.3.5 are applied to AUV navigation by demonstrating the potential to localize a simulated submerged AUV using a combination of hydrophone, AIS, and IMU data. To this end, Hydrophone #2 is considered to be located inside a submerged AUV, and the data it recorded during the SWellEx-96 experiment will be used to estimate the position of the vehicle. Furthermore, the IMU located inside the simulated AUV is assumed to have a velocity estimation error, due to factors such as underwater currents and accelerometer drift, despite the real hydrophone

actually being moored to ocean floor during the experiment.

For real-time AUV localization, the method would be contingent upon a processor onboard the AUV having access to time-varying source position information, such as that contained in AIS data. This can be accomplished by having a surface buoy receive radio frequency AIS broadcasts from nearby transiting cargo ships and then relay the data acoustically to submerged assets using the JANUS protocol; this was demonstrated during the REP15-Atlantic and REP16-Atlantic sea trials with successful AIS data transmissions at distances up to 5.5 km [5], and recently up to 7.5 km during REP18-Atlantic [6]. Another potential application is post-mission AUV localization, or reconstruction analysis, in which the objective is to estimate the track that was transited by an underwater vehicle between deployment and recovery. For that application, the AIS data can be readily obtained from various online databases after recovery, without the need for real-time AIS-relaying mechanisms.

4.4.1 Localization algorithm and scenario

The process by which the AUV position is estimated is as follows: first, the source range rate is computed using (4.20) based on data provided by the IMU. Next, the WI-based range estimation processor uses an estimate of β for the environment, combined with the source range rate estimates, to produce a sequence of time-varying ML range estimates using (4.23). Finally, the AUV position hypothesis is updated using the estimate obtained from (4.24), and the process is repeated. After several iterations, the mean position estimate begins to converge, and the AUV position can be estimated once a desired change threshold has been met.

A scenario is now presented in which an AUV has been submerged for over an hour, and the on-board IMU provides an erroneous position estimate 3 km southeast of its actual location, as shown in Figure 4.11b, in addition to a velocity estimate with an error of 0.25 m/s. A position error of this magnitude is consistent with what

could be expected for a low-cost, standalone IMU [2], and the velocity error would, in reality, be scaled higher by a factor roughly equal to the ratio of average cargo ship speed to the speed of the source towed in the SWellEx-96 experiment, which is about 5. Thus, the 0.25 m/s velocity estimation error assumed in this scenario would produce a similar effect to an error of 1.25 m/s when using a cargo ship SOO.

4.4.2 Results: AUV localization scenario

The erroneous AUV position and velocity estimates obtained from the IMU lead to an error in source range rate, $\hat{v}_{\mathrm{rs}}(t)$, as shown by the plot corresponding to the first iteration in Figure 4.12a. The WI-based range estimator subsequently produces the series of range estimates corresponding to the first iteration in Figure 4.12b. The NLLS estimate of receiver position, indicated by the red '1' in Figure 4.11b is about 800 m east of the true AUV position. This updated position estimate is 2.8 km away from the initial position estimate provided by the IMU, as indicated by the red circle corresponding to the first iteration in Figure 4.11c. At this point, the first iteration is completed, and the AUV position hypothesis is updated. The first iteration yields range and range rate hypotheses that are much closer to ground truth than those computed directly from the IMU data, as indicated by the plots corresponding to Iteration #2 in Figures 4.12a and 4.12b. Successive iterations produce progressively smaller changes in estimated position, as seen in Figure 4.11c, with a distance of only one meter separating subsequent runs beyond Iteration #8 for this scenario. The final position estimate is 0.43 km southwest of the true AUV position, which is a marked improvement over the error of 3 km in the estimate provided by the IMU. Results obtained using other source velocity errors are overlaid in Figure 4.11 and include an error of 0.64 km when correctly assuming a stationary AUV and an error of 0.9 km when assuming a velocity of 0.25 m/s due west ($\hat{v}_{\mathrm{rx}} = -0.25$ m/s).

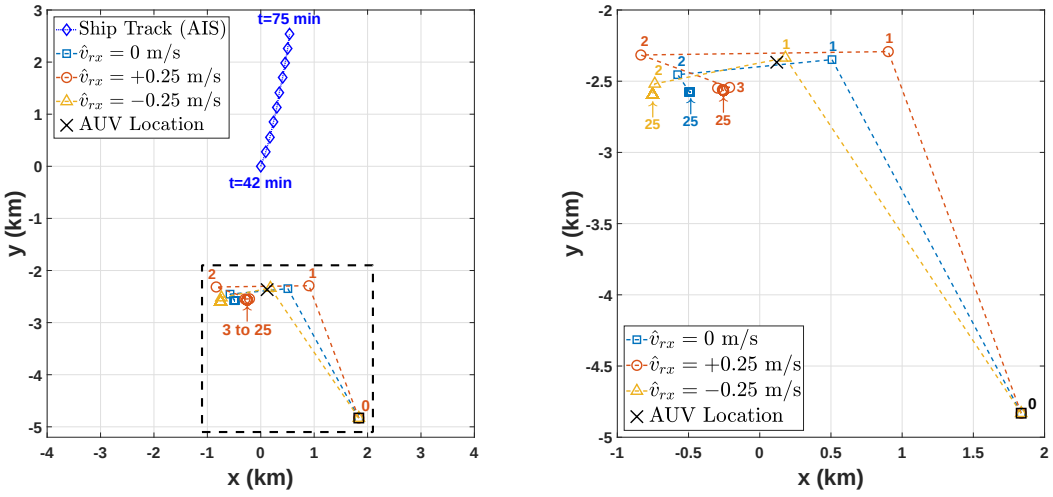

(a) (b)

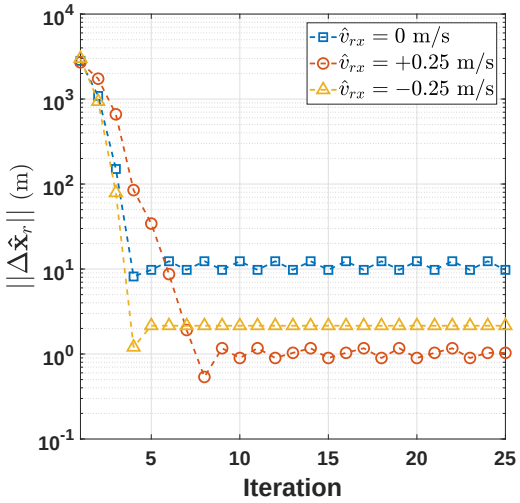

(c)

FIGURE 4.11: Results for the first 25 iterations of the NLLS-based receiver localization algorithm using various estimates of the x-component of the receiver velocity, $\hat{v}_{\text{rx}}$. (a) Localization results shown relative to ship track, indicated by the blue diamonds, and initial location estimate provided by the IMU, indicated by the solid black square labeled "0" at (1.8, -4.8) km. The portion of the figure bounded by the dashed box is enlarged in (b), with points indicating the location estimates obtained at the end of the iterations specified by accompanying color-coded numerical labels. (c) Plot of the distance, in meters, between subsequent NLLS estimates of AUV position.

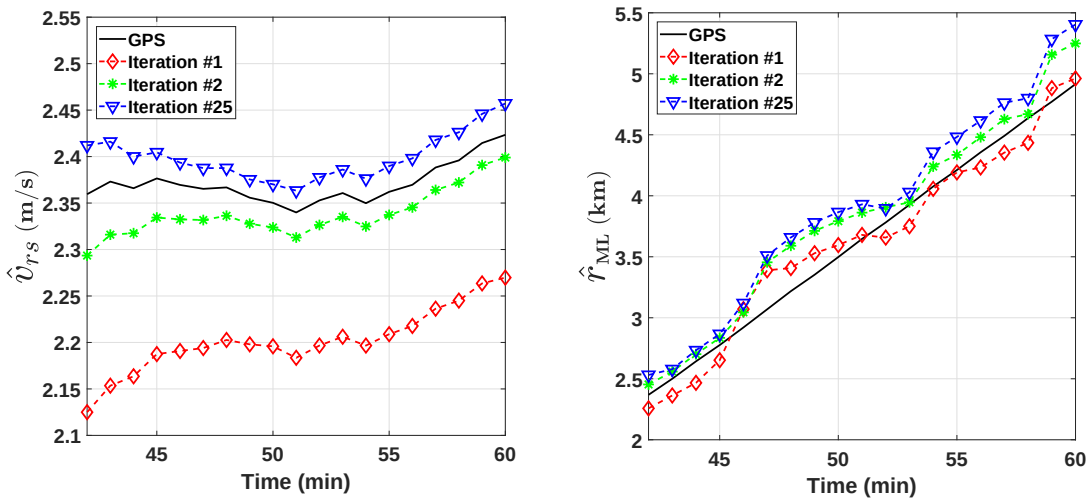

(a) (b)

FIGURE 4.12: (a) Estimated source range rate and (b) source range as a function of experiment time for various NLLS iterations using $\hat{\beta}_1 = 1.26$ and assuming a stationary receiver. The first iteration begins with an IMU estimate 3 km southeast of the true AUV position.

4.4.3 Discussion of results

This result shows promise for AUV navigation applications, in which the IMU position error grows quadratically with time submerged due to accelerometer drift. In contrast to this, the WI-based localization accuracy can be expected to improve with additional measurements of the channel fading pattern as the source transits through an area, assuming the AUV can receive periodic AIS updates. In a high-traffic environment, in which one or more cargo ships transit per hour, an AUV could potentially remain submerged indefinitely while maintaining a position uncertainty of less than 1 km using this localization technique.

The experimental results obtained in this chapter used data from hydrophones that were located below the thermocline, due to being moored to the ocean floor, and the more diffuse distribution of β values caused a higher variance in range esti-

mates than would otherwise be obtained for a receiver located closer to the surface. Thus, AUVs that have the mission flexibility to operate above the thermocline could potentially benefit from much lower position estimation error. However, as noted in Section 4.3.3, the detrimental impact to AUV localization when operating below the thermocline will be somewhat mitigated by the fact that the propellers and hulls of SOOs are near the top of the water column, and the excitation of higher-order, surface-interacting modes helps to anchor the distribution of β values near unity. In principle, an SOO located beneath the thermocline could also be utilized for AUV localization, but β would be much more sensitive to receiver depth, as noted in [48].

4.4.4 Application considerations

The accuracy of the localization method depends on several factors such as SNR, source range, and the number of tones processed. As mentioned previously, SNR is likely to be relatively constant at close ranges but will degrade at longer ranges as the background noise sources overpower the tones of the ship. From examining spectrograms of ship data obtained during the Noise-09 experiment, ranges up to 5 km seem reasonable for applying WI-based methods on the tonal components of the source signal. However, the method also requires the source to be at least several column depths away from the receiver due to the Lloyd's mirror effect.

The primary advantage of this AUV localization technique over others that are commonly employed is that it requires minimal equipment to be added to the AUV. A single hydrophone could presumably be incorporated at relatively low cost and complexity, and many AUVs are already equipped with one or more hydrophones for signal collection purposes. Furthermore, this technique is passive and does not require any signal transmission by the AUV, thus minimizing its acoustic footprint. In contrast to this, other types of navigation equipment such as DVLs or acoustic transponders can be costly to equip, require acoustic transmissions by the AUV,

and also come with operational limitations. For example, DVLs require the AUV to maintain proximity to the ocean floor, and acoustic transponders require the AUV to remain within a predetermined region of the ocean where the equipment has been previously deployed. In contrast, this technique allows the AUV to transit at a variety of depths within the water column and only requires it to be in proximity to shipping lanes, which translates to a vast potential operating area throughout the world.

The primary impediments to employing this technique are having the infrastructure in place by which AIS data can be relayed to the AUV, as mentioned previously, and in initially characterizing an environment with an estimate of β. The former is not an issue if real-time AUV localization is not a requirement, as in the case of post-mission processing mentioned previously. The latter could potentially be mitigated through prior knowledge of the environment, such as bathymetry and sound speed, or by employing β maps, as proposed by Verlinden et al. [16], while also accounting for range dependencies using the method of Sell and Culver [68]. Further validation using measured acoustic data from cargo ships in shallow water shipping lanes might help to identify additional advantages and disadvantages relative to conventional localization techniques.

4.5 Summary

This chapter presented maximum likelihood estimators for β and source range, along with potential applications to real-time AUV navigation and post-mission AUV localization. The β estimator extended prior work by Harms et al. [15] and was validated in multiple ways, beginning with a simulation of a Pekeris environment using KRAKEN and moving on to a simulation of the SWellEx-96 environment, for which the resulting estimate of β matched closely with those obtained from processing the experimental data over two separate tracks. A performance analysis was conducted

to examine the impact of SNR and number of tones processed, and the results look promising using parameters that are typical for acoustic emissions of cargo ships. The source range estimator was an extension of the ML β estimator and required an estimate of range rate. The range estimates obtained from the real data had a standard deviation of under 150 m when processing a source track from 2.5 km to 7 km in range. The estimator was further validated by employing an estimate of β obtained from one source track to estimate both source range and receiver position using data recorded from a different track on a hydrophone located 5 km away.

Most importantly, it was shown that AUV localization could potentially be performed using WI-based range estimates combined with knowledge of the source track obtained from AIS data, in either real-time or post-mission settings. Furthermore, the localization technique presented can be performed without knowledge of the source range rate, as this parameter can instead be estimated iteratively from an initial position estimate provided by an instrument such as a low-grade, on-board IMU. The experimental data suggest that a hydrophone-equipped AUV could use the proposed localization technique to reduce its position estimation error from 3 km to less than 1 km through an iterative nonlinear LS-based technique using just four tones from the acoustic emissions of a transiting SOO.

The results presented bode well for applications to AUV navigation in high-traffic, shallow water environments such as coastal shipping lanes. With an extension to incorporate broadband striations for increased performance, and with the necessary AIS-relaying infrastructure in place, the technique could potentially enable AUVs to remain submerged indefinitely while maintaining an acceptable position uncertainty in real time. In addition to the broadband extension, future work in this area could include a derivation of the Cramér-Rao bounds for these estimators, field validation using AUVs operating near coastal shipping lanes, and extensions to exploit multiple sources of opportunity simultaneously.

5

Conclusion

This dissertation presented model-based signal processing methods and performance bounds for passive ranging using the waveguide invariant. The models exploit the physics of multipath acoustic propagation in shallow water, as described by the scalar parameter β, and they also account for both tonal and broadband sources. Results were examined in both a statistical context and within an application framework designed specifically for AUV navigation.

The AUV application was presented first as a motivation for the mathematical modeling and statistical characterizations that followed. The results showed that under reasonable assumptions regarding parameters such as source range, number of tones processed, and variability in β, WI-based methods can yield localization RMSEs on the order of a few hundred meters. These findings were further supported by the derivation of the Cramér-Rao bounds for passive ranging with a single hydrophone using broadband SOOs, for which the minimum achievable standard deviation was shown to be on the order of tens of meters for various sets of parameters considered.

Finally, ML estimators for both β and range were presented using tonal SOOs.

The simulation and experimental results were seen to be in close agreement and matched the trends observed from the CRLBs in terms of SNR and time-bandwidth product. Furthermore, the proposed WI-based AUV localization algorithm was employed for a simulated AUV using experimental hydrophone data; the results provided additional validation that position estimation errors on the order of hundreds of meters can be attained in practice, particularly if the source spectrum contains many narrowband tones.

Future work

Much work remains to be done before WI-based ranging is likely to be implemented for underwater localization in practice. First, one could examine localization performance using hydrophone data acquired by AUVs operating near busy, shallow water shipping lanes. With favorable results in such settings, further experiments could be performed that align more closely with the concept of operations outlined in Chapter 1.

Second, although recent work has focused on shallow water ranging using β, the CRLB presented in Chapter 3 suggests that range estimation performance in deep water could be favorable compared to shallow water environments. An extension of the algorithms presented in this dissertation to deep water environments could be pursued following field validation of the proposed methods in shallow water; this would significantly increase the portion of the world's oceans in which the proposed ranging and localization methods could be used.

Finally, improvements to the AIS-relaying infrastructure mentioned in this dissertation could stimulate further research on WI-based localization. Although recent experimental work has made significant progress in this area by achieving AIS-relaying distances of up to 7 km, longer transmission ranges may help to minimize the number of relaying buoys required to cover large operating areas. To this end, experiments

involving the use of submerged assets as AIS relay points could also be particularly helpful.

Appendix A

Supplemental information

This appendix provides supplemental information regarding the waveguide invariant, the automatic identification system, and related passive range estimation and localization works in the literature. Appendices A.1, A.2, and A.3 borrow heavily from prior work by the author [69] and have been adapted and re-formatted for this dissertation.

A.1 The waveguide invariant

The waveguide invariant, commonly denoted as β, is a compact, scalar parameter that characterizes the frequency- and range-varying fluctuations of received acoustic intensity in a ducted environment. Early work on the foundation for understanding the parameter was laid by Weston and Stevens in 1972 [70], and β was formally described a decade later in works by Chuprov [12] and Grachev [39] before being applied more directly to range estimation in the early 2000s by Thode [41] and others whose work is described in Section A.3. Chuprov presented the parameter in the context of the readily-observable interference structures that result from the coherent

addition of propagating modes in a ducted channel. He noted that, without having to obtain a multitude of precise, spatially- and temporally-varying measurements of environmental parameters that are required to compute exact phase differences between all propagating modes, the interference structure of the total pressure field can be obtained by leveraging β, even at ranges of tens of kilometers. Interference structures can be observed visually by plotting the magnitude of a channel's frequency response as a function of source-receiver range, as shown in Figure A.1. With an appropriate offset to account for source transmit level, this can be viewed as a plot of the received spectral intensity of a radiated broadband, band-limited white noise signal as a function of source-receiver range, or $I(r, \omega)$.

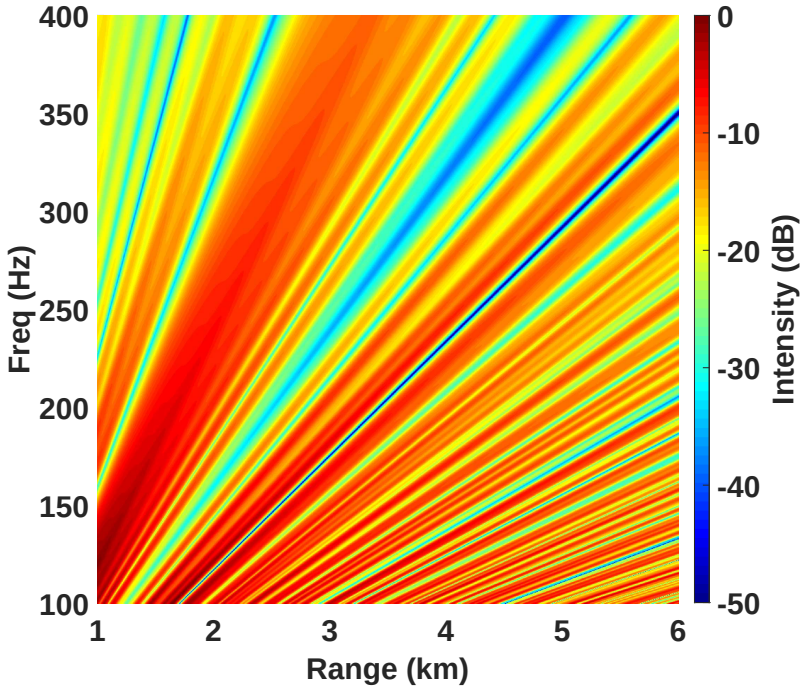

FIGURE A.1: Received acoustic intensity from a broadband source as a function of frequency and range in an ideal waveguide, computed using the first 20 propagating modes. The striations, or lines of constant intensity, are defined by (A.4) and satisfy (A.6) with $\beta = 1$.

Traditionally, waveguide invariance has been analyzed in terms of the patterns

that emerge in intensity plots derived from the spectrograms of acoustic data obtained from transiting sources with continuous spectral levels [46]. The superposition of direct path and multipath arrivals within the waveguide results in the appearance of lines of constant intensity in range and frequency, which are commonly referred to as striations. The general character of this type of interference structure is governed by the relationship between group and phase velocities of propagating modes within the medium [12], and the spacing between striations in the $I(r, \omega)$ surface can also be computed using the value of β that characterizes the environment [46]. The parameter β is formally defined as the negative ratio of the change in phase slowness to that of group slowness between a pair of modes [40]:

$$\beta \triangleq \frac{-dS_p^{mn}}{dS_g^{mn}} = \frac{-(S_p^n - S_p^m)}{S_g^n - S_g^m} \tag{A.1}$$

This can be rewritten to show a linear relationship with β^{-1} as:

$$S_g^n = S_g^m - \frac{1}{\beta} dS_p \tag{A.2}$$

Here, S_g^n is the group slowness (inverse group velocity) and S_p^n is phase slowness (inverse phase velocity) for the nth mode, which is adjacent to the mth mode. The linear relationship between group and phase slowness across an entire group of propagating modes, which is implied by a constant β, can be expressed as follows [40]:

$$S_g^n = S_g - \frac{1}{\beta}(S_p^n - S_p) \tag{A.3}$$

where S_g and S_n refer to average phase and group slowness for a group of modes. Equation (A.3) can be viewed as a requirement that must approximately hold for β to be considered stable within a particular acoustic environment.

In the Pekeris model, β is approximately constant across all propagating modes [15]. However, this is not generally the case, and in complex environments β is approximately constant when contributions from reflected paths dominate the modal

sum [40]. This means that non-constant, highly-variable β values are possible, particularly in deeper water regions or areas with rapidly changing bathymetry or sound speed profiles [46]. This leads to an understanding that β is not only mode-dependent but can also be frequency- and range-dependent in complex environments, and care should be taken before applying the scalar β approximation.

In terms of range r and frequency ω, β can be applied through examination of the lines of constant intensity through $I(r, \omega)$, which are described by the following differential equation:

$$\frac{\partial I}{\partial \omega}\delta\omega + \frac{\partial I}{\partial r}\delta r = 0 \tag{A.4}$$

By taking partial derivatives of the modal sum equation with respect to frequency and range, the slope $d\omega/dr$ along the isolines in $I(r, \omega)$ surface given by (A.4) is:

$$\frac{d\omega}{dr} = -\frac{\frac{\partial I}{\partial r}}{\frac{\partial I}{\partial \omega}} = -\frac{\omega}{r}\frac{dS_p}{dS_g} = \frac{\omega}{r}\beta \tag{A.5}$$

Readers interested in a full derivation of this result are referred to [40]. Equation (A.5) can be integrated to reveal the following relation that holds between β, frequency, and range along striations in the $I(r, \omega)$ surface:

$$\frac{\omega}{\omega_0} = \left(\frac{r}{r_0}\right)^{\beta} \tag{A.6}$$

After isolating ω in (A.6), differentiating with respect to range, and setting $\beta = 1$, the slope can be written as $d\omega/dr = \omega_0/r_0$. That is, when $\beta = 1$, each isoline has constant slope throughout the entire $I(r, \omega)$ surface, which can be verified visually by examining Figure A.1. When $\beta > 1$, the striations are curved, with slopes that strictly increase with range; when $\beta < 1$, the slopes strictly decrease with range. Importantly, by applying (A.6), a striation can be extrapolated in frequency and range from any point, (r_0, ω_0), given β. Striation patterns are generally noticeable

at source-receiver ranges exceeding several water column depths but are obscured by the Lloyd's mirror effect at closer ranges [46]. In shallow water environments, this means the interference structure could potentially be utilized for WI-based range estimation at distances from a few hundred meters to tens of kilometers [12].

Since its discovery, the stability of the parameter β in real environments has been investigated with great interest. Chuprov noted a diversity of β values in deep water environments, but relative stability near $\beta \approx 1$ in shallow water. Later, Rouseff and Spindel [48] noted that β is perhaps best modeled as a distribution; the distribution is often sharply peaked in shallow water environments where surface-interacting modes dominate, while being more diffuse in deep water environments where ducted modes have greater expression. Recently, Turgut et al. [49] have noted that the apparent distribution of β values can also be strongly dependent on the depth of both the source and receiver in the water column relative to the thermocline. As the experimental results show in Chapter 4, a scalar β can be adequate for passive ranging purposes in coastal regions with relatively flat bathymetry, especially when the source is located near the surface.

A.2 Automatic identification system data

This section provides an overview of the automatic identification system (AIS), which is central to the WI-based localization method presented in this dissertation. AIS equipment includes devices such as GPS receivers, very high frequency (VHF) transceivers, and chart plotters. The GPS receivers are typically located at well defined positions on commercial and passenger vessels for collision avoidance purposes. Such ships continuously broadcast a variety of data about their tracks to other ships in the area as well as to satellites and shore-based stations; this information includes parameters such as speed, heading, and GPS location and is commonly broadcast at intervals from 2 to 10 seconds using the VHF antenna at power levels of 12.5

Watts [11]. Since 2002, AIS has been required for large sea-going vessels and all passenger ships as part of an international effort to reduce maritime collisions. In the United States, AIS has also been required for all commercial vessels transiting inland waterways and ports since 2005 as part of increased port security measures [54, 71].

Both real-time and delayed AIS data can be retrieved by various means, including querying the United States Coast Guard database [71]. As Figure A.2 shows, AIS data is concentrated along coastlines and throughout trans-ocean shipping lanes. It was estimated in 2009 that more than 40,000 ships worldwide carry AIS equipment [54], and the increasing density of AIS data has been leveraged in recent work by Harms et al. [15], Verlinden et al. [72], and Young et al. [8, 45, 73] through the development of methods that use AIS-broadcasting ships as acoustic SOOs for estimating various parameters of interest.

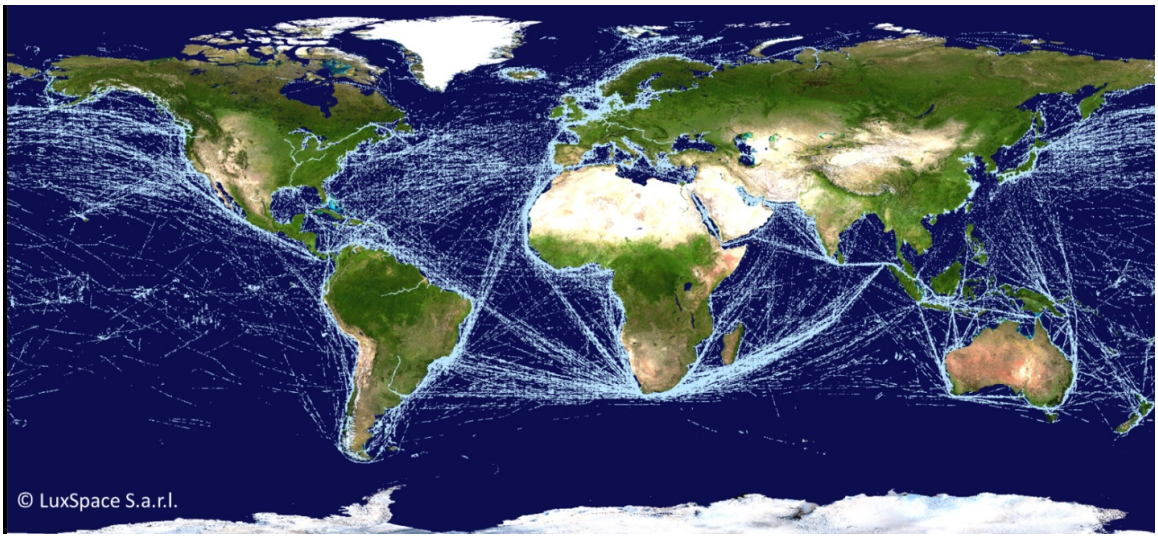

FIGURE A.2: World map with an overlay showing AIS tracks of commercial ships over a 24-hour period. Image Credit: European Space Agency (ESA), "Satellite-AIS-based map of global ship traffic." Copyright 2016, LuxSpace.

A.3 Review of related passive ranging methods

A review of passive, acoustics-based range estimation work related to the proposed AUV localization technique is presented. This review is not intended to be comprehensive; rather, the author has chosen to emphasize works that were found to be especially helpful while formulating and conducting the research presented in this dissertation. In accordance with the concept of operations outlined in Chapter 1, this review focuses on techniques that can be used in shallow water marine environments, especially those that involve the waveguide invariant. For ease of comparison to the proposed WI-based localization technique, this review categorizes each work into one of two areas: techniques that use a single hydrophone, and those that use multiple hydrophones. Most single hydrophone techniques are more akin to image processing algorithms than model-based processors and typically assume a broadband, spectrally flat source signal, although a few notable exceptions are covered, particularly the work by Harms et al. [15] that paved the way for this research. Passive techniques requiring multiple hydrophones include the following: matched field processing, machine learning, and transponders that incorporate chip-scale atomic clocks. CSAC-based methods enable passive, one-way travel time (OWTT) computations to be used instead of active, two-way travel time (TWTT) for ranging.

A.3.1 Single hydrophone methods

Several methods have been proposed in recent years for either estimating β, or for using β to estimate source range. In many cases, the same striation-based techniques used to estimate β can also be used to estimate range, with minor modifications. This review begins with one of the earliest techniques published on the matter.

Waveguide invariant estimation

In 2000, Thode developed a method [41] that uses the Radon transform to estimate β using a controlled broadband source in a shallow water environment. The method effectively views the $I(r, \omega)$ surface as an image and estimates striation slopes through analysis of tomographic projections. A decade later in 2010, Turgut et al. [42] demonstrated using the Hough transform to estimate Beta through a method involving line integrals taken over parameterized projections across the $I(r, \omega)$ surface that obey (A.6).

However, a downside of these image processing methods is their reliance on obtaining a finely-sampled grid of $|H(r, \omega)|$ estimates derived from a broadband source signal. Although the flat spectrum approximation has been shown to work well with controlled sources, Arveson and Vendittis [14] noted that modern, high-tonnage cargo ships produce radiated noise spectra that are dominated by narrowband tones, which are commonly referred to as tonals. As Figure A.3 shows, the tonals are typically spaced a few Hz apart with a concentration of energy below 100 Hz. This is significantly different from the white noise spectrum implicitly assumed by image processing methods, and it has motivated the development of new techniques for estimating β that do not require broadband sources.

In 2014, Harms, Odom, and Krolik [15] derived a minimum mean-square error estimator for β using a tonal signal model. Under their model, the source consists of pure tones with known amplitudes and unknown phases, and the received acoustic signal is corrupted by additive complex Gaussian noise. Monte Carlo simulations were run using a tonal source with three equal-amplitude tones corrupted by varying levels of additive noise in a Pekeris environment. The results showed an average estimate of $\beta = 0.93$, which was close enough to the canonical value of 1.0 for the Pekeris environment to conclude that the model warranted further evaluation.

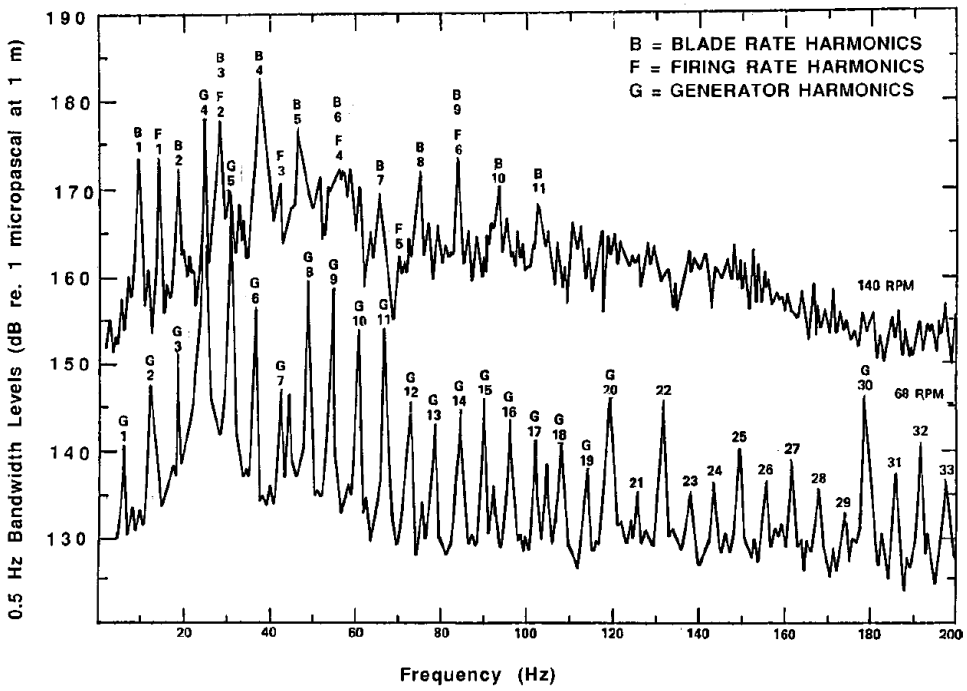

FIGURE A.3: Example of high-speed (top) and low-speed (bottom) cargo ship emission spectrum. Note that the spectrum is dominated by closely-spaced, narrowband tonals, especially at lower speeds. Reprinted with permission from [14]. Copyright 2000, Acoustical Society of America.

Encouraged by this initial result, the research presented in this dissertation effectively picked up where Harms et al. [15] left off by using their model to derive maximum likelihood estimators for both β and source range and by validating the estimators using data obtained from the SWellEx-96 experiment [47, 73, 45].

Range estimation using the waveguide invariant

The discussion now moves to work involving the application of the waveguide invariant to passive ranging. As previously mentioned, Thode presented a method [41] for estimating β using the Radon transform, given a broadband source, in 2000. In that work, Thode also presented a Radon-transform-based method to estimate source range using β; the method achieved an error of about 10% of source range using

data from SWellEx-3. In that experiment, the source transmitted a pseudo-random noise (PRN) sequence with 150 Hz bandwidth and relatively high SNR. Although the Radon-transform-based method, like many other WI-based ranging techniques, requires minimal prior environmental knowledge, it does require the environment to have a relatively flat bathymetry and a flat source spectrum to yield a stable estimate of β.

In 2007, Tao et al. [38] described a striation-based single hydrophone method for estimating the range and time of the CPA of a moving surface ship, as well as the ratio of velocity to range at the time of CPA, $\frac{v}{r_{\text{CPA}}}$. Experimental results showed their method to be robust to interfering sources, given sufficiently high SNR, and they were able to separately identify a pontoon boat from a speedboat and estimate the range and velocity of both sources at their respective CPAs. A key assumption made in their processing is that β is approximately unity, which is a common assumption to make in shallow water environments [46], although their method does allow for other values of β to be used. Their results showed the ability to estimate r_{CPA} with an error of about 4% at close range. Overall, this result demonstrated the waveguide invariant can be useful for determining the range to transiting surface vessels in shallow water environments using only a single hydrophone.

In 2010, Cockrell and Schmidt [43] described another image-processing-based, passive range estimation method utilizing a 2D-DFT of the $I(r, \omega)$ surface. They employed limited prior environmental knowledge to apply a low-pass filter based on maximum and minimum group velocities expected for propagating modes in the environment. They tested their method using a hydrophone-equipped AUV that proceeded on a course at a fixed radial velocity toward a stationary source transmitting a PRN sequence, and they were able to estimate source range with an error of 25%. This result presented an alternative to Radon- and Hough-transform-based methods and helped pave the way for subsequent passive ranging and localization methods

for AUV applications.

Also in 2010, Zhen-Dong et al. [74] proposed a method for estimating the range to a broadband source, using only a single hydrophone and the waveguide invariant. Their approach was unique in that it attempted to calculate a distinct value of β for each pair of propagating modes, rather than estimating a single value of β that covers a range of modes. To separate the modes, the authors used the MUSIC (MUltiple SIgnal Classification) algorithm. Their method relies on having a broadband guide source at a known range, which they can use to estimate the range to other broadband sources. They conducted two experiments in the Yellow Sea and Laoshan Bay using underwater explosions produced by energy exploration teams as guide sources. Although they were able to estimate the range to several explosions with errors of only 5 to 10% at ranges up to 20 km, the authors expect ranging results to be degraded when either the guide sources or unknown sources to be localized do not have flat emissions spectra. Overall, this result provided further confirmation of the ability to use WI-based methods for passive ranging of distant sources in shallow water, even at ranges of tens of kilometers.

In 2012, Rakatonarivo and Kuperman [46] introduced a WI-based ranging method that included an estimator for source range rate. They employed a field differencing technique that leverages sinusoidal variations in the DFT of the cross-correlation of the received pressure field with a subtracted measurement corresponding to various time lags to estimate range rate. They were able to estimate the range of a tonal source in the SWellEx-96 experiment with approximately 10% error using the same data set presented in Chapter 4 of this work. Their results demonstrated the ability to leverage the waveguide invariant for estimating the range to a tonal source (pure tones) in a shallow water environment without prior knowledge of source speed.

Most recently, Verlinden et al. [16] proposed a modified Radon-transform-based technique for estimating source range using β. Their approach begins by transform-

ing the $I(r, \omega)$ surface to the Radon transform domain (sinogram). Spectral content from projections near 0-degrees is subsequently removed, which corresponds to tones in the spectrogram. After taking an inverse transform, the filtered $I(r, \omega)$ surface is used to estimate source range using broadband striation-based methods. Thus, Verlinden's work is complementary to the one proposed in Chapter 4, as it uses only the broadband portion of the received signal to estimate range; in principle, both broadband and tonal-based methods could be employed together for improved ranging performance.

A.3.2 Multi-hydrophone and array-based methods

Multi-hydrophone techniques

In 2015, Verlinden et al. [72] described a method for localizing sources by utilizing a cross-correlation library that is seeded using acoustic data obtained from pairs of hydrophones, which are spatially separated by several hundred meters, when AIS-broadcasting surface ships transit through the local area. The waveguide invariant is used to interpolate and create replica vectors corresponding to positions (latitude and longitude) that fill out a gridded search space. Their approach for populating the library leverages the availability of AIS data for surface ships, and it locates unknown sources by searching for peaks in the cross-correlation of the cross-correlations of the received acoustic signals (using hydrophone pairs) with the library replica vectors corresponding to the grid positions. Their method was shown to work well with tonal sources (cargo ships) and was also remarkably robust; the library that was constructed using data from the first day of the Noise '09 experiment was used to localize transiting cargo ships five days later with an error of only 500-m for selected tracks.

Hydrophone array-based techniques

The discussion of array-based source ranging and receiver localization techniques begins with matched field methods. Bucker [22] is credited with the seminal work on MFP in 1976, in which he introduced the concept of the ambiguity surface for the source localization problem and showed that the acoustic field generally exhibits enough complexity to facilitate inversion for source depth and range [75]. However, the main drawback to MFP methods is their reliance on precise knowledge of environmental parameters, as small changes to water column depth, sound speed, or bottom properties can dramatically alter the shape of the wavefront across the array elements. Efforts have been made to overcome this by judiciously incorporating prior knowledge, including the 1998 and 2002 works by Tantum, Nolte, and Krolik [76, 77].

More recently, Worthmann et al. [78] introduced frequency-difference MFP, a non-linear array signal processing technique that incorporates frequency difference beamforming and effectively shifts the matching computations to a lower-frequency regime, in which the results are notably less sensitive to environmental mismatch. However, one of the drawbacks to this technique, as noted by the authors, is a high sensitivity to model parameters including, but not limited to, difference frequency bandwidth and the number of modes to include in replica field calculations.

Machine learning techniques seek to improve upon MFP methods by effectively deducing information about the environment directly from the pressure field data, thus allowing them to overcome some, but not all, of the problems that arise from having insufficient prior environmental knowledge to adequately perform a model-based inversion for source depth and range. Recent contributions in this area include the 2017 works of Gemba et al. [79] and Niu et al. [80]. In [79], a Bayesian learning approach was applied to the same SWellEx-96 data set examined in Chapter 4 to estimate source range and depth through a robust MFP procedure. In [80], the

authors present a technique for estimating the range to cargo ships transiting through the Santa Barbara Channel, which is located off the coast of southern California, using data from a fixed, 77-m aperture VLA consisting of 28 hydrophones. Their technique used both feed-forward neural network (FNN) and support vector machine (SVM) processing methods with tuned parameters. Array data from three transiting ships were arranged into training and test sets, and the results showed the ability to estimate source range out to 10 km with very low error. The authors also showed that traditional MFP methods failed to localize the transiting ships beyond 4 km range without employing precise environmental knowledge.

A recent AUV localization technique that was proposed by Rypkema et al. [3] in 2017 involves a USBL transponder setup. The method is passive on the part of the submerged AUV, but it requires transmission of a linear frequency-modulated (LFM) chirp waveform by a controlled source at a known location. The clocks on the source and receiver are synchronized prior to the mission, and timing accuracy is maintained by employing chip-scale atomic clocks. The AUV, equipped with an internal four-element hydrophone array, applies beamforming and graphical model methods to estimate the bearing to the transmitter. The bearing estimates are subsequently combined with range estimates obtained through measurements of the OWTT of the acoustic signal from the transmitter to the AUV. Initial results showed a localization error of about 2-3% of source range after 20 minutes submerged. This technique appears promising for both its accuracy at close range and for its applicability to low-cost AUVs, though the authors note that performance is degraded at longer ranges.

The last ranging technique to be reviewed, and perhaps the most relevant to the proposed research, is using the array invariant. As implied by its name, array-invariant-based techniques utilize an array of hydrophones and leverage the physics of multipath propagation in much the same way as the waveguide invariant [81].

The array invariant was first proposed for source ranging in 2005 by Lee and Makris [82], and in 2017 it was used by Byun et al. [83] to estimate the time-varying range to a transiting research vessel in a shallow water experiment. Array-invariant-based ranging exploits the linear relationship between a trigonometric function of grazing angle (which varies depending on the array orientation) and the time delay of multipath arrivals in shallow water environments. The method does not require prior environmental knowledge; in practice, however, a good estimate of the local sound speed profile is helpful when the source signal is unknown. A distinct advantage that array-invariant-based range estimation has over WI-based techniques is that it provides instantaneous range estimation, as it does not require the collection of an $I(r, \omega)$ surface representing the channel fading pattern over a diversity of ranges. However, the requirement for an AUV to tow a potentially large array is significantly more restrictive than having just a single hydrophone equipped.

A.3.3 Summary

A variety of methods have been proposed by which one or more hydrophones can be used for passive ranging. Recent developments using hydrophone arrays are promising in specific contexts, but they are not broadly applicable to the low-cost AUV navigation problem addressed in this dissertation due to a variety of issues, which include the following: unsatisfactory performance at long ranges; requiring extensive prior environmental or source knowledge; degraded performance in dynamic environments; towing large sensor arrays. In contrast, WI-based methods work at long ranges, require just a single parameter to characterize the environment, can work in dynamic environments without a cooperative source, and come with relatively minimal operational or equipment burdens. With the necessary AIS-relaying infrastructure in place, satisfactory single-hydrophone-based AUV localization may be within reach in the near future.

Bibliography

[1] L. Brekhovskikh and Y. Lysanov, *Fundamentals of Ocean Acoustics*. New York: Springer, 2003.

[2] L. Paull, S. Saeedi, M. Seto, and H. Li, "AUV navigation and localization: A review," *IEEE Journal of Oceanic Engineering*, vol. 39, pp. 131–149, Jan 2014.

[3] N. Rypkema, E. Fischell, and H. Schmidt, "One-way travel-time inverted ultra-short baseline localization for low-cost autonomous underwater vehicles," *IEEE International Conference on Robotics and Automation*, pp. 4920–4926, 2017.

[4] G. Rui and M. Chitre, "Cooperative positioning using range-only measurements between two AUVs," *Proc. IEEE OCEANS Conf.*, 2010.

[5] R. Petroccia, J. Alves, and G. Zappa, "JANUS-based services for operationally relevant underwater applications," *IEEE Journal of Oceanic Engineering*, vol. 42, pp. 994–1006, Oct 2017.

[6] F. Ferreira, R. Petroccia, and J. Alves, "Increasing the operational safety of autonomous underwater vehicles using the JANUS communication standard," in *AUV 2018 - Portugal*, pp. 1–6, 2018. accepted for publication.

[7] "Marine traffic: Live map." `https://www.marinetraffic.com/en/ais/home/`, 2018. Accessed 2018-06-01.

[8] A. Young, J. Soli, and G. Hickman, "Self-localization technique for unmanned underwater vehicles using sources of opportunity and a single hydrophone," in *OCEANS 2017 - Anchorage*, pp. 1–6, Sept 2017.

[9] J. Passerieux, D. Pillon, P. Blanc-Benon, and C. Jaufret, "Target motion analysis with bearings and frequencies measurements," in *Signals, Systems and Computers, 1988. Twenty-Second Asilomar Conference on*, vol. 1, pp. 458–462, IEEE, 1988.

[10] A. Pignol, C. Jauffret, and D. Pillon, "Properties of range-only target motion analysis," in *Proceedings of the 16th International Conference on Information Fusion*, pp. 1693–1698, July 2013.

[11] J. M. Mou, C. V. Tak, and H. Ligteringen, "Study on collision avoidance in busy waterways by using AIS data," *Ocean Engineering*, vol. 37, no. 5-6, pp. 483–490, 2010.

[12] S. Chuprov, "Interference structure of a sound field in a layered ocean," *Ocean Acoustics: Current State*, pp. 71–91, 1982.

[13] G. L. D'Spain and W. A. Kuperman, "Application of waveguide invariants to analysis of spectrograms from shallow water environments that vary in range and azimuth," *The Journal of the Acoustical Society of America*, vol. 106, no. 5, pp. 2454–2468, 1999.

[14] P. T. Arveson and D. J. Vendittis, "Radiated noise characteristics of a modern cargo ship," *The Journal of the Acoustical Society of America*, vol. 107, no. 1, pp. 118–129, 2000.

[15] A. Harms, J. L. Odom, and J. L. Krolik, "Ocean acoustic waveguide invariant parameter estimation using tonal noise sources," in *2015 IEEE International Conference on Acoustics, Speech and Signal Processing (ICASSP)*, pp. 4001–4004, April 2015.

[16] C. M. A. Verlinden, J. Sarkar, B. D. Cornuelle, and W. A. Kuperman, "Determination of acoustic waveguide invariant using ships as sources of opportunity in a shallow water marine environment," *The Journal of the Acoustical Society of America*, vol. 141, no. 2, pp. EL102–EL107, 2017.

[17] N. H. Nguyen and K. Doğançay, "Single-platform passive emitter localization with bearing and doppler-shift measurements using pseudolinear estimation techniques," *Signal Processing*, vol. 125, pp. 336–348, 2016.

[18] W. J. Bangs and P. M. Schultheiss, "Space-time processing for optimal parameter estimation," in *Signal Processing* (J. W. R. Griffiths, P. L. Stocklin, and C. van Schooneveld, eds.), pp. 577–590, Academic, 1973.

[19] W. R. Hahn, "Optimum signal processing for passive sonar range and bearing estimation," *The Journal of the Acoustical Society of America*, vol. 58, no. 1, pp. 201–207, 1975.

[20] G. C. Carter, "Variance bounds for passively locating an acoustic source with a symmetric line array," *The Journal of the Acoustical Society of America*, vol. 62, no. 4, pp. 922–926, 1977.

[21] A. B. Baggeroer, W. A. Kuperman, and H. Schmidt, "Matched field processing: Source localization in correlated noise as an optimum parameter estimation problem," *The Journal of the Acoustical Society of America*, vol. 83, no. 2, pp. 571–587, 1988.

[22] H. P. Bucker, "Use of calculated sound fields and matched-field detection to locate sound sources in shallow water," *The Journal of the Acoustical Society of America*, vol. 59, no. 2, pp. 368–373, 1976.

[23] S. Narasimhan and J. L. Krolik, "Fundamental limits on acoustic source range estimation performance in uncertain ocean channels," *The Journal of the Acoustical Society of America*, vol. 97, no. 1, pp. 215–226, 1995.

[24] J. Tabrikian and J. L. Krolik, "Barankin bounds for source localization in an uncertain ocean environment," *IEEE Transactions on Signal Processing*, vol. 47, pp. 2917–2927, Nov 1999.

[25] W. Xu, A. B. Baggeroer, and C. D. Richmond, "Bayesian bounds for matched-field parameter estimation," *IEEE Transactions on Signal Processing*, vol. 52, pp. 3293–3305, Dec 2004.

[26] J. S. Rogers and J. L. Krolik, "Time-varying spatial spectrum estimation with a maneuverable towed array," *The Journal of the Acoustical Society of America*, vol. 128, no. 6, pp. 3543–3553, 2010.

[27] A. Ganti, "Calibration and direction of arrival performance of sonar arrays composed of multiple sub-arrays," in *OCEANS 2018 MTS/IEEE Charleston*, pp. 1–6, Oct 2018.

[28] M. D. Collins, L. T. Fialkowski, W. A. Kuperman, and J. S. Perkins, "Environmental source tracking," *The Journal of the Acoustical Society of America*, vol. 94, no. 6, pp. 3335–3341, 1993.

[29] M. D. Collins, L. E. Tinker, J. S. Perkins, N. C. Makris, and W. A. Kuperman, "Single-frequency matched-field processing with a single hydrophone," *Journal of the Acoustical Society of America*, vol. 90, 1998.

[30] J. Unpingco, W. A. Kuperman, W. S. Hodgkiss, and R. Hecht-Nielsen, "Single sensor source tracking and environmental inversion," *The Journal of the Acoustical Society of America*, vol. 106, no. 3, pp. 1316–1329, 1999.

[31] C. S. Clay, "Optimum time domain signal transmission and source location in a waveguide," *The Journal of the Acoustical Society of America*, vol. 81, no. 3, pp. 660–664, 1987.

[32] L. N. Frazer and P. I. Pecholcs, "Single-hydrophone localization," *The Journal of the Acoustical Society of America*, vol. 88, no. 2, pp. 995–1002, 1990.

[33] W. C. Dixon and J. R. McGrath, "Method to estimate surface ship range from a stationary hydrophone," *The Journal of the Acoustical Society of America*, vol. 62, no. S1, pp. S52–S52, 1977.

[34] W. A. Kuperman, G. L. D'Spain, and K. D. Heaney, "Long range source localization from single hydrophone spectrograms," *The Journal of the Acoustical Society of America*, vol. 109, no. 5, pp. 1935–1943, 2001.

[35] J. S. Rogers, C. A. Rohde, M. D. Guild, C. J. Naify, T. P. Martin, and G. J. Orris, "Demonstration of acoustic source localization in air using single pixel compressive imaging," *Journal of Applied Physics*, vol. 122, no. 21, p. 214901, 2017.

[36] J. Ramirez, J. S. Rogers, and G. F. Edelmann, "A performance metric for screen selection with the acoustic single pixel imager," *The Journal of the Acoustical Society of America*, vol. 143, no. 6, pp. 3829–3837, 2018.

[37] S. M. Jesus, M. B. Porter, Y. Stephan, X. Demoulin, O. C. Rodriguez, and E. M. M. F. Coelho, "Single hydrophone source localization," *IEEE Journal of Oceanic Engineering*, vol. 25, pp. 337–346, July 2000.

[38] H. Tao, G. Hickman, J. L. Krolik, and M. Kemp, "Single hydrophone passive localization of transiting acoustic sources," in *OCEANS 2007 - Europe*, pp. 1–3, June 2007.

[39] G. Grachev, "Theory of acoustic field invariants in layered waveguides," *Acoust. Phys.*, vol. 39, no. 1, pp. 33–35, 1993.

[40] F. B. Jensen, W. A. Kuperman, M. B. Porter, and H. Schmidt, *Computational Ocean Acoustics*. New York: Springer, 2011. pp. 133-136.

[41] A. M. Thode, "Source ranging with minimal environmental information using a virtual receiver and waveguide invariant theory," *The Journal of the Acoustical Society of America*, vol. 108, no. 4, pp. 1582–1594, 2000.

[42] A. Turgut, M. Orr, and D. Rouseff, "Broadband source localization using horizontal-beam acoustic intensity striations," *The Journal of the Acoustical Society of America*, vol. 127, no. 1, pp. 73–83, 2010.

[43] K. L. Cockrell and H. Schmidt, "Robust passive range estimation using the waveguide invariant," *The Journal of the Acoustical Society of America*, vol. 127, no. 5, pp. 2780–2789, 2010.

[44] L. Brooks, M. Kidner, A. Zander, C. Hansen, and Z. Zhang, "Techniques for extraction of the waveguide invariant from interference patterns in spectrograms," in *ACOUSTICS 2006*, pp. 1–8, Nov 2006.

[45] A. H. Young, H. A. Harms, G. W. Hickman, J. S. Rogers, and J. L. Krolik, "Waveguide-invariant-based ranging and receiver localization using tonal sources of opportunity," *IEEE Journal of Oceanic Engineering*, pp. 1–14, 2019.

[46] S. T. Rakotonarivo and W. A. Kuperman, "Model-independent range localization of a moving source in shallow water," *The Journal of the Acoustical Society of America*, vol. 132, no. 4, pp. 2218–2223, 2012.

[47] J. Murray and D. Ensberg, "Swellex-96: S5 event." `http://swellex96.ucsd.edu/s5.htm`, 1996. Accessed 2017-02-01.

[48] D. Rouseff and R. C. Spindel, "Modeling the waveguide invariant as a distribution," *AIP Conference Proceedings*, vol. 621, no. 1, pp. 137–150, 2002.

[49] A. Turgut, L. T. Fialkowski, and J. A. Schindall, "Measured depth-dependence of waveguide invariant in shallow water with a summer profile," *The Journal of the Acoustical Society of America*, vol. 139, no. 6, pp. EL184–EL189, 2016.

[50] S. Kay, *Fundamentals of Statistical Signal Processing: Estimation Theory*. Englewood Cliffs, NJ: Prentice Hall PTR, 1993.

[51] A. Papoulis, *Probability, Random Variables, and Stochastic Processes, Third Edition*. New York: McGraw-Hill, 1991. pp. 140.

[52] W. S. Hodgkiss and L. W. Nolte, "Covariance between fourier coefficients representing the time waveforms observed from an array of sensors," *The Journal of the Acoustical Society of America*, vol. 59, no. 3, pp. 582–590, 1976.

[53] M. B. Porter, "The acoustics toolbox." `http://oalib.hlsresearch.com/Modes/AcousticsToolbox/index.html`, 2017. Accessed 2017-09-07.

[54] H. M. Perez, R. Chang, R. Billings, and T. L. Kosub, "Automatic Identification Systems (AIS) Data Use in Marine Vessel Emission Estimation," *18th Annual International Emission Inventory Conference*, pp. 1–25, 2009.

[55] T. C. Yang, "Beam intensity striations and applications," *The Journal of the Acoustical Society of America*, vol. 113, no. 3, pp. 1342–1352, 2003.

[56] K. D. Heaney, "Rapid geoacoustic characterization using a surface ship of opportunity," *IEEE Journal of Oceanic Engineering*, vol. 29, pp. 88–99, Jan 2004.

[57] C. L. Pekeris, "Theory of propagation of explosive sound in shallow water," *Geological Society of America*, 1948.

[58] M. Abramowitz and I. Stegun, *Handbook of Mathematical Functions*. Dover Publications, 1972.

[59] S. Kay, *Fundamentals of Statistical Signal Processing, Vol. 2*. New Jersey: Prentice Hall PTR, 2011.

[60] N. C. Makris, "The statistics of ocean-acoustic ambient noise," in *Sea Surface Sound* (T. Leighton, ed.), pp. 1–9, Kluwer Academic Publishers, 1997.

[61] R. Urick and W. A. Kuperman, "Ambient noise in the sea," *The Journal of the Acoustical Society of America*, vol. 86, no. 4, pp. 1626–1626, 1989.

[62] M. Bouvet and S. C. Schwartz, "Underwater noises: Statistical modeling, detection, and normalization," *The Journal of the Acoustical Society of America*, vol. 83, no. 3, pp. 1023–1033, 1988.

[63] S. C. Wales and R. M. Heitmeyer, "An ensemble source spectra model for merchant ship-radiated noise," *The Journal of the Acoustical Society of America*, vol. 111, no. 3, pp. 1211–1231, 2002.

[64] R. J. Urick, "Models for the amplitude fluctuations of narrow-band signals and noise in the sea," *The Journal of the Acoustical Society of America*, vol. 62, no. 4, pp. 878–887, 1977.

[65] M. Evans, N. Hastings, and B. Peacock, *Statistical Distributions, Third Edition*. New York: John Wiley and Sons, Inc, 2000. pp. 169.

[66] J. Bonnel, B. Nicolas, J. I. Mars, and D. Fattaccioli, "Source localisation in deep water using waveguide invariant distribution," in *10th European Conference on Underwater Acoustics*, (Istanbul, Turkey), July 2010.

[67] D. Rouseff, "Effect of shallow water internal waves on ocean acoustic striation patterns," *Waves In Random Media*, vol. 11, pp. 377–393, 2001.

[68] A. W. Sell and R. Lee Culver, "Waveguide invariant analysis for modeling time-frequency striations in a range-dependent environment," *The Journal of the Acoustical Society of America*, vol. 130, no. 5, pp. EL316–EL322, 2011.

[69] A. Young, "Passive ranging of tonal sources in shallow water using the waveguide invariant," Master's thesis, Duke University, 2017. Retrieved from http://hdl.handle.net/10161/15234.

[70] D. Weston and K. Stevens, "Interference of wide-band sound in shallow water," *Journal of Sound and Vibration*, vol. 21, no. 1, pp. 57 – 64, 1972.

[71] "United states coast guard navigation center: Nais data sharing categories and requirements." `http://www.navcen.uscg.gov/?pageName=NAISdisclaimer`, 2016. Accessed 2016-02-01.

[72] C. M. Verlinden, J. Sarkar, W. S. Hodgkiss, W. A. Kuperman, and K. G. Sabra, "Passive acoustic source localization using sources of opportunity.," *The Journal of the Acoustical Society of America*, vol. 138, no. 1, pp. EL54–9, 2015.

[73] A. Young and A. Harms, "Single hydrophone, passive ranging of tonal sources in shallow water using the waveguide invariant," *The Journal of the Acoustical Society of America*, vol. 139, no. 4, pp. 2225–2225, 2016.

[74] Z. Zhen-Dong, W. Ning, G. Da-Zhi, and W. Hao-Zhong, "Broadband source ranging in shallow water using the omega-interference spectrum," *Chinese Physics Letters*, vol. 27, pp. 064301–1–4, June 2010.

[75] A. B. Baggeroer, W. A. Kuperman, and P. N. Mikhalevsky, "An overview of matched field methods in ocean acoustics," *IEEE Journal of Oceanic Engineering*, vol. 18, 1993.

[76] S. L. Tantum and L. W. Nolte, "Tracking and localizing a moving source in an uncertain shallow water environment," *The Journal of the Acoustical Society of America*, vol. 103, no. 1, pp. 362–373, 1998.

[77] S. L. Tantum, L. W. Nolte, J. L. Krolik, and K. Harmanci, "The performance of matched-field track-before-detect methods using shallow-water pacific data," *The Journal of the Acoustical Society of America*, vol. 112, no. 1, pp. 119–127, 2002.

[78] B. M. Worthmann and D. R. Dowling, "High frequency source localization in a shallow ocean sound channel using frequency-difference matched field processing," *The Journal of the Acoustical Society of America*, vol. 137, no. 4, pp. 2240–2240, 2015.

[79] K. L. Gemba, S. Nannuru, P. Gerstoft, and W. S. Hodgkiss, "Multi-frequency sparse bayesian learning for robust matched field processing," *The Journal of the Acoustical Society of America*, vol. 141, no. 5, pp. 3411–3420, 2017.

[80] H. Niu, E. Ozanich, and P. Gerstoft, "Ship localization in santa barbara channel using machine learning classifiers," *The Journal of the Acoustical Society of America*, vol. 142, no. 5, pp. EL455–EL460, 2017.

[81] H. C. Song and C. Cho, "The relation between the waveguide invariant and array invariant," *The Journal of the Acoustical Society of America*, vol. 138, no. 2, pp. 899–903, 2015.

[82] S. Lee and N. C. Makris, "The array invariant," *The Journal of the Acoustical Society of America*, vol. 119, no. 1, pp. 336–351, 2006.

[83] G. Byun, J. S. Kim, C. Cho, H. C. Song, and S.-H. Byun, "Array invariant-based ranging of a source of opportunity," *The Journal of the Acoustical Society of America*, vol. 142, no. 3, pp. EL286–EL291, 2017.

Biography

Andrew H. Young received the Bachelor of Science degree in Electrical Engineering from the University of Colorado at Colorado Springs in 2008. He received the Master of Science in Electrical Engineering from Duke University in Durham, NC in 2017 and the Ph.D. in 2019. During his first four years at Duke University, he was a research assistant in the Sensor Array and Multipath (SAM) Signal Processing Lab under the guidance of Prof. Jeffrey Krolik. Since 2018, he has been employed with the Acoustics Division at the Naval Research Laboratory in Washington, DC under the supervision of Dr. Jeffrey Rogers. His research interests include signal processing for radar and sonar applications.

During the course of his graduate studies, he had two conference publications [8, 73], a published Master's thesis [69], and a refereed publication in the *IEEE Journal of Oceanic Engineering* [45]. Additionally, the CRLB work presented in Chapter 3 has recently been submitted for publication.